Analysis of Mathematical Models with Different Aspects of Heat Transfer

By

Faisal Shah

Department of Mathematics
Quaid-I-Azam University
Islamabad, Pakistan
2021

Analysis of Mathematical Models with Different Aspects of Heat Transfer

By

Faisal Shah

Supervised by

Prof. Dr. Tasawar Hayat

Department of Mathematics
Quaid-I-Azam University
Islamabad, Pakistan
2021

Analysis of Mathematical Models with Different Aspects of Heat Transfer

By

Faisal Shah

A THESIS SUBMITTED IN THE PARTIAL FULFILLMENT OF THE REQUIREMENT FOR THE DEGREE OF

DOCTOR OF PHILOSOPHY

IN

MATHEMATICS

Supervised by

Prof. Dr. Tasawar Hayat

Department of Mathematics
Quaid-I-Azam University
Islamabad, Pakistan

2021

Author's Declaration

I **Faisal Shah** hereby state that my PhD thesis titled **Analysis of Mathematical Models with Different Aspects of Heat Transfer** is my own work and has not been submitted previously by me for taking any degree from the Quaid-I-Azam University Islamabad, Pakistan or anywhere else in the country/world.

At any time if my statement is found to be incorrect even after my graduate the university has the right to withdraw my PhD degree.

Name of Student: **Faisal Shah**

Date: **26-05-2021**

Plagiarism Undertaking

I solemnly declare that research work presented in the thesis titled "**Analysis of Mathematical Models with Different Aspects of Heat Transfer**" is solely my research work with no significant contribution from any other person. Small contribution/help wherever taken has been duly acknowledged and that complete thesis has been written by me.

I understand the zero tolerance policy of the HEC and **Quaid-I-Azam University** towards plagiarism. Therefore, I as an Author of the above titled thesis declare that no portion of my thesis has been plagiarized and any material used as reference is properly referred/cited.

I undertake that if I am found guilty of any formal plagiarism in the above titled thesis even afterward of PhD degree, the University reserves the rights to withdraw/revoke my PhD degree and that HEC and the University has the right to publish my name on the HEC/University Website on which names of students are placed who submitted plagiarized thesis.

Student/Author Signature: ____________

Name: **Faisal Shah**

Analysis of Mathematical Models with Different Aspects of Heat Transfer

By

Faisal Shah

CERTIFICATE

A THESIS SUBMITTED IN THE PARTIAL FULFILLMENT OF THE REQUIREMENTS FOR THE DEGREE OF THE

DOCTOR OF PHILOSOPHY IN MATHEMATICS

We accept this dissertation as conforming to the required standard

1. ____________________
Prof. Dr. Sohail Nadeem
(Chairman)

2. ____________________
Prof. Dr. Tasawar Hayat
(Supervisor)

3. ____________________
Dr. Nasir Ali
Associate Professor
Department of Mathematics & Statistics
International Islamic University,
Sector, H-10 Islamabad
(External Examiner)

4. ____________________
Dr. Muhammad Awais
Assistant Professor
Department of Mathematics, COMSATS,
University Islamabad, Attock Campus
(External Examiner)

Department of Mathematics
Quaid-I-Azam University
Islamabad, Pakistan
2021

Certificate of Approval

This is to certify that the research work presented in this thesis entitled **Analysis of Mathematical Models with Different Aspects of Heat Transfer** was conducted by Mr. **Faisal Shah** under the kind supervision of **Prof. Dr. Tasawar Hayat**. No part of this thesis has been submitted anywhere else for any other degree. This thesis is submitted to the Department of Mathematics, Quaid-i-Azam University, Islamabad in partial fulfillment of the requirements for the degree of Doctor of Philosophy in field of Mathematics from Department of Mathematics, Quaid-i-Azam University Islamabad, Pakistan.

Student Name: **Faisal Shah** Signature:__________

External committee:

a) **External Examiner 1**: Signature:__________
Name: **Dr. Nasir Ali**
Designation: Associate Professor
Office Address: Department of Mathematics & Statistics International Islamic University, Sector H-10 Islamabad.

b) **External Examiner 2**: Signature:__________
Name: **Dr. Muhammad Awais**
Designation: Assistant Professor
Office Address: Department of Mathematics, COMSATS, University Islamabad, Attock Campus.

c) **Internal Examiner** Signature:__________
Name: **Dr. Tasawar Hayat**
Designation: Professor
Office Address: Department of Mathematics, QAU Islamabad.

Supervisor Name: Signature:__________
Prof. Dr. Tasawar Hayat

Name of Dean/HOD: Signature:__________
Prof. Dr. Sohail Nadeem

DEDICATED TO

MY BELOVED PARENTS

ELDEST BROTHER

AND

MY SUPERVISOR

ACKNOWLEDGEMENT

All praise for "Almighty Allah", the most Beneficent, the most merciful, the Lord of the whole world who has given me the courage and ability to complete this thesis. I am nothing without my Allah, but I can manage everything with His assistance. Also, I cannot forget the idea personality of the world for whom Allah has created the whole universe, who is forever a torch bearer of guidance for humanity, Hazrat Muhammad **(PBUH).**

I would like to express my gratitude to my worthy supervisor **Prof. Dr. Tasawar Hayat (National Distinguished Professor)** for his valuable suggestions and comments that helped me to accomplish this highly important research. His knowledge, accessibility and availability have been a critical impetus in driving this research. It would never have been possible for me to take this work to completion without his incredible support and encouragement. I am ever indebted and obliged to him.

I would like to convey my heartiest gratitude to my respectable senior and co-advisor **Dr. Muhammad Ijaz Khan** for his kind support and guidance that helped me to complete this important work. This discussions with him helped me to sort out the technical details of my work. I am thankful to them for being so cooperative, kind, and helpful.

My highest and special thanks go to my honorable teachers **Prof. Dr. Muhammad Ayub, Prof. Dr. Malik Yousaf, Prof. Dr. Masood Khan, Prof. Dr. Sohail Nadeem, Dr. Tayyab Kamran, Dr. Khalid Saifullah, Dr. Umer Hayyat and Dr. Amjad Hussain** for their valuable and constructive suggestions in all aspects.

I have been lucky enough to have good friends in my academic and social life and cannot forget their role in my education and university life. It is a matter of great delight and pleasure for me to mention my truly wonderful friends and colleagues **Especially Aqeela Qaiser, Dr. Muhammad Ijaz Khan, Dr. Waleed Ahmed Khan, Dr. Arsalan Aziz, Mr. Salman Ahmed (Hong Kong), Dr. Shahid Farooq, Dr. Mair Khan, Dr. Imad Khan, Dr. Naeem Ullah, Dr. Bilal Ahmed, Dr. Khursheed Muhammad, Dr. Zakir Hussain, Mr. Sohail Ahmed, Dr. Muhammad Waqas, Mr. Habibullah, Mr. Waqar Ahmed, Dr. Sajid Qayyum, Dr. Waqar Azeem Khan, Dr. Irfan, Dr. Amir Hameed, Dr. Nadeem Abbas, Dr. Zubair Mughal, Dr. Usman Ali, Dr. Sumaira Qayyum and Dr. Rehana Rahim.**

Finally, I would like to especial thanks to my best friend **Syed Waqar Hussain Shah.**

I want to convey my deepest thanks and compliment to my beloved grandfather **Farooq Shah (Late)**, my loving and caring mother **Naseem Akhtar (Late)**, my toughest from outside but coolest from inside father **Ghulam Shah (Late)**, my brothers **Qabal Shah, Asmat Shah, Maqsad Shah**, my sisters **Samina Bibi**, **Safina Bibi** and **Khadija Bibi** for their endless love, prayers, encouragement, cordial cooperation and continuous support. They selflessly encouraged me to explore new directions in my life and seek my own destiny. This journey would have not been possible without my above-mentioned family members, and I dedicated this milestone to them.

Faisal Shah

Preface

Various base liquids such as ethylene, oil, water, and glycols etc. have low thermal conductivity. Thus, an improvement in the thermal efficiency of these liquids seems necessary in achieving the engineers and scientists' expectations. Nanofluid consists of base liquid and nanoscale material (1-100 nm). In thermal engineering, heat exchangers, electronic chemical processes, cancer therapy and biomedicine, nanofluids are found very useful. Nanoparticles include namely $\gamma Al_2O_3, C_2H_6O_{2,}$oxides and carbides ceramics and semiconductors. Nanofluids are the new generation coolants which exhibit much better heat transfer performance than the ordinary liquid carrier. Especially two-phase flow problems used abundantly in petroleum, usage of waste water, combustion and smoke emission from automobiles process. Non-Newtonian fluids like second grade fluid model, third grade fluid model Jeffrey fluid model, Williamson and many others are regarded helpful in physiological phenomenon, pharmaceutical etc. Viscous fluid, second grade fluid model, third grade fluid model and Jeffrey fluid model, are incorporated in this thesis.

Mechanism of heat transfer has involvement in industries such as nuclear reactor, energy production and mobile device etc. For relatively higher temperature the surfaces heat transfer requires simultaneous study of various heat transporation process. Such process by which heat can be transmitted faster by the fluid are melting, absorption, combustion, conduction, convection and dispersal of radiation. Technologies and industries have widespread utilizations of melting phenomenon. Researchers paid particular attention to improving effective, safe, and energy depot technologies. These technologies are interrelated with the repossession of excess fuel, solar, electricity and food from plants. For example, three energy storage procedures have been introduced including latent, thermal energy and chemical energy. The economically sustainable heat energy storage is latent heat via material phase adjustment. Melting phenomenon has applications in many fields namely heat exchanger coils, based pump, the freeze treatment, solidification, welding processes and many others.

The boundary layer flows of viscous/non-Newtonian liquids over a stretched sheet have interest in various fields. Examples of these flows involve polymer sheet sectors, glass sheets, pharmacology, bioengineering, fusion technology, plastic wire making and emulsion of polymeric materials etc. Current product efficiency primarily depends on heat transfer rate and drag forces etc. Keeping all these dimensions in mind the main goal of this thesis is to study mathematical models with different aspect of heat transfer. The structure of this thesis is as follows.

Chapter 1 consist of some basic law of conservations. Mathematical model and boundary-layer expressions for Newtonian fluid, second grade, third grade and Jeffrey fluids are incorporated. Three different techniques are used to deal the flow problems. Basic concepts of these techniques namely HAM, OHAM and shooting technique is also provided.

Chapter 2 addresses the flow subject to effective Prandtl number and without effective Prandtl number via γAl_2O_3-H_2O and γAl_2O_3-$C_2H_6O_2$ nanoparticles. The resulting problem are solved through Optimal homotopy method (OHAM). Optimum values are determined for the auxiliary parameters. Impact of emerging parameters are graphically analyzed for (γAl_2O_3 -H_2O and γAl_2O_3 -$C_2H_6O_2$) nanoparticles. The contents of this chapter are published in Journal of **Molecular Liquids 266 (2016) 814-823.**

Chapter 3 deals the Mixed convective dissipative flow of effective Prandtl number subject to entropy optimization and melting heat. The governing flow expressions with boundary conditions are solved via built-in-Shooting technique. Computational solutions are identified and analyzed utilizing plots. The outcomes are reported in **International Communications in Heat and Mass Transfer 111(2020) 104454.**

Chapter 4 reports computational aspects for Entropy generation in MHD flow of viscous fluid subject to aluminum and ethylene glycol nanoparticles. Thermal radiation and Joule heating are examined. Electric field is absent. Uniform magnetic field is applied normal to the sheet. The relevant equation are solved via built-in- Shooting method. The various flow parameters are graphically discussed. The outcomes of this chapter are published in **Computer methods and programs in biomedicine 182(2019) 105057.**

Chapter 5 examines Thermal radiation and heat source/sink impacts in stagnation point flow of viscous nanomaterial. Radiative heat and convective conditions are also analyzed. Inclined magnetic field is taken. Homotopy analysis method is employed to find the serious solution. The contents of this chapter are available in **Indian Journal of Physics 94(2019) 657–664.**

Chapter 6 presents Computational analysis of 3D radiative Darcy-Forchheimer flow subject to suction/injection. Porous medium is characterized by Darcy-Forchheimer relation. Radiation, convective condition and slip effect are addressed. Stagnation point flow is examined. Non-linear ordinary differential system are solved through shooting method. Graphical results are portrayed and scrutinized with distinct values of dimensionless variables. The chapter key results can be found in **Computer Methods and Programs in Biomedicine 184(2020) 105104.**

Chapter 7 describes Utilization of entire modern aspect of Cattaneo-Christov model in mixed convective entropy optimized flow by Riga wall. Brownian motion and thermophoresis are adopted. Cattaneo-Christove model for heat and mass fluxes are used to examine the heat and mass transfer. Entropy generation is modeled. The numerical solutions are developed through ND solve technique. Graphical illustrations are given for the influence of sundry parameters. The outcomes of this chapter are submitted in **Numerical Method for Partial Differential Equations** for possible publication.

Chapter 8 discloses a novel perspective of Cattaneo-Christov model in MHD second grade nanofluid flow. Heat and mass transfer are based upon Cattaneo-Christov (CC) theory. Results are developed via OHAM. The outcomes of this chapter are published in **International Communications in Heat and Mass Transfer 119(2020) 104824.**

Chapter 9 describes Melting heat in Jeffrey fluid flow through permeable space. Energy equation is considered in the existence of melting heat and heat absorption/ generation. The results are constructed via OHAM. The outcomes of this chapter are published in **Thermal Science 23(2019) 3833-3842**.

Chapter 10 includes the Impact of entropy generation on third grade nanofluid flow over a stretchable Riga wall with Cattaneo-Christov double diffusions. Formulation also consists of heat generation and mixed convection. The key results of this chapter are submitted in **Numerical Method for Partial Differential Equations** for possible publication.

Contents

Chapter 1

Literature survey and methodologies

1.1 Introduction

Some literature surveys about stretching sheet, entropy generation, nanofluid, viscous fluid, non-Newtonian fluids, radiative heat flux, heat generation, viscous dissipation and magneto-hydrodynamic (MHD) boundary layer flow have been reviewed in this chapter. Viscous and non-Newtonian liquids (second grade, third grade, Jeffrey model) constitutive relations are included. Further, the basic concept of homotopy method, Optimal homotopy method and built-in-Shooting method are incorporated for the series solutions and numerical analysis respectively.

1.1.1 Nomeclature

u, v, w	Velocity Components along x, y, z directions respectively
$\mathbf{q}, \mathbf{J}$	Heat and Mass flux
T, C	Fluid(Temperature, Concentration)
T_w, C_w	Surface(Temperature, Concentration)
T_∞, C_∞	Ambient(Temperature, Concentration)
U_w, U_∞	Stretching and Ambient velocities
T_m, T_o	(Melting,Characteristic) Temperature
A	First Rivilin Erickson Tensor
a, b, c	Positive Constants
δ_E, δ_F	(Thermal, Solutal)Relaxation time
$k_j(j = p, f, nf)$	Thermal Conductivity
$(\nu, \mu)_j(j = f, nf)$	(Kinematic, Dynamic) Viscosity
$(J_o, \rho)_j(j = p, f, nf)$	(Current, Fluid) Density
g	Acceleration due to Gravity
ε	Drag Force Coefficient
β_t	Volumetric Coefficient
k^*	Porous Medium Permeability
C_p, c_s	Specific Heat, Heat Capacity
τ^*	Cauchy Stress Tensor
$Q(= M_o x)$	Permanent Variable Magnets Magnetization
a_1	Width for Electrodes and Magnets
D_B, D_T	(Brownian motion, Thermophoresis diffusion) Coefficient
$\alpha_j(j = f, nf)$	Thermal Diffusivity
$\beta_j(j = f, nf)$	Thermal Expansion Coefficient
ψ	Stream Function
η	Independent Variable
$(\rho C)_f$	Heat Capacity of Fluid
ϕ	Nanoparticles Volume Friction

$\tau\left(=\frac{(\rho C_p)_p}{(\rho C_f)_f}\right)$	Heat Capacity Ratio
x	Distance along the Plate
y	Distance Perpendicular to the Plate
h_f	Heat Transfer Coefficient
q_r	Thermal radiation
σ^*	Stefan-Boltzmann Constant
$\sigma_j(j=p,f,nf)$	Electric Conductivity
λ^*	Latent Heat of Fluid
β_1	Slip Constant
k_1^*	Absorption Constant
τ_{xy}	Wall Shear Stress along y direction
q_w	Heat Flux at Wall
q_m	Surface Mass Flux
$(f\ ', h'), t, J$	Dimensionless ((Velocities), Temperature, Concentration)
I, p	Identity Tensor, Pressure
S^*	Extra Stress Tensor
N_G	Entropy
Be	Bejan Number
C_f	Skin Friction Coefficient
Nu	Nusselt Number
Sh	Sherwood Number
Le	Lewis Number
M	Hartman Number
N_B	Brownian Motion Parameter
N_T	Thermophoresis Parameter
Pr	Prandtl Number
Da^{-1}	Inverse Darcy Number
λ	Mixed Convection Parameter
β	Local Inertia Coefficient Parameter

B	Non-Dimensional Parameter
Re_x	Local Reynold Number
γ_o	Chemical Reaction Parameter
γ_1	Thermal Relaxation Parameter
γ_2	Biot Number
γ_3	Solutal Concentration Parameter
γ_4	Concentration Difference Parameter
α	Thickness Parameter
n	Shape Parameter
ϵ	Stretching/Shrinking Parameter
δ	Heat Generation Parameter
Br	Brinkman Number
Ω	Dimensionless Temperature Difference
χ	Diffusion Parameter
V_o	Section/Injection Parameter
Ec	Eckert Number
Sc	Schmidt number
Gr	Grashof Number
R_d	Radiation Parameter
S	Ratio Parameter
$\alpha_1, \alpha_2, \alpha_3, \beta_1^* \beta_2^*, \beta_3^*$	Material Parameters
α^*	Second Grade Fluid Parameter
$\alpha_1^*, \alpha_2^*, \alpha_3^*$	Third Grade Fluid Parameters
β_2	Slip Parameter
K	Deborah Number
λ_1	Ratio of Relaxation and Retardation Times
λ_2	Retardation Time

tr	Trace
$SGNF$	Second Grade Nanofluid
$TGNF$	Third Grade Nanofluid
CC	Cattaneo Christov
MHD	Magnetohydrodynamic
HTR	Heat Transfer Rate
EGM	Entropy Generation Minimization
γAl_2O_3	Alumina
H_2O	Water
$C_2H_6O_2$	Ethylene Glycol

1.1.2 Subscript

w	Condition at Surface
∞	Ambient Condition
f	Base Fluid
p	Nano Solid Particles
nf	Nanofluid
m	Melting at Surface

1.2 Background

Mechanism of heat transfer has involvement in industries such as nuclear reactor, energy production and mobile device etc. For relatively higher temperature the surfaces heat transfer requires simultaneous study of various heat transporation process. Such process by which heat can be transmitted faster by the fluid are melting, absorption, combustion, conduction, convection and dispersal of radiation. Fourier [1] primarily introduced the concept of heat conduction. This leads to paradox of heat conduction. Thus Fourier's expression is formerly revised by Cattaneo [2]. He introduced the concept of thermal relaxation time. Christov [3] utilized the Oldroyed upper convective time derivative and thus relation is named as Cattaneo-Christov (CC) model [2]. Ciarletta and Straughan found unique solution for temperature via Cattaneo model [4]. Haddad [5] addressed the thermal volatility through porous medium via

Cattaneo-Christov (CC) model. Current attempts about Cattaneo -Christov (CC) model can be listed via refs. $[6-8]$. Effects of radiation are significant even in the sense of high temperature process and space technology. Ozisik [9], Sparrow [10] and Arpaci [11] specifically investigated the interaction between energy and convection through vertical sheet. Waleed et al. [12] examined the flow of nonlinear radiative nanomaterials and the minimization of entropy by a thin needle. Kumar et al. [13] investigated nanofluid stretched flow of nonlinear radiation. Babu and Sandeep [14] provided bio-convective flow by stretchable sheet. Recent researches about radiative heat flux can be seen via Refs. $[15-17]$. Technologies and industries have widespread utilizations of melting phenomenon. Researchers paid particular attention to improving effective, safe, and energy depot technologies. These technologies are interrelated with the repossession of excess fuel, solar, electricity and food from plants. For example three energy storage procedures have been introduced including latent, thermal energy and chemical energy. The economically sustainable heat energy storage is latent heat via material phase adjustment. Melting phenomenon has applications in many fields namely heat exchanger coils, based pump, the freeze treatment, solidification, welding processes and many others. Rahman et al. [18] addressed radiative MHD flow over an extended surface. Melting temperature of ice piece in the cascade of hot air is addressed by Robert [19]. Das [20] reported MHD flow with melting and radiation influences. Hayat et al. [21] examined the Cu-nanofluid flow in the presence of viscous dissipation and Joule heating.

Various base liquids such as ethylene, oil, water, and glycols etc have low thermal conductivity. Thus an improvement in the thermal efficiency of these liquids seems necessary in achieving the engineers and scientists expectations. Choi [22] initially used the term nanofluid to improve continuous-phase liquid thermal efficiency. Usman et al. [23] explored the Casson nanoliquid due to stretchable cylinder. Sheikholeslami et al. [24] explored nanofluid flow over a stretched surface in the presence of MHD. Gireesha et al. [25] analyzed nanofluid flow by materializing (KVL) model. Hayat et al. [26] investigated second grade flow in the existence of MHD. Mixed convective nano-liquid flow with heat source is discussed by Khan et al. [27]. Haiao [28] examined the dissipative flow of micropolar liquid over stretchable surface.

The boundary layer flows of viscous/non-Newtonian liquids over a stretched sheet have interest in various fields. Examples of these flows involve polymer sheet sectors, glass sheets, pharmacology, bioengineering, fusion technology, plastic wire making and emulsion of polymeric materials etc. Current product efficiency primarily depends on heat transfer rate and drag forces etc. These processes depend entirely on the phenomenon of the boundary layer along extended sheer and mass transfer rate. Rajagopal et al. [29] explored viscoelastic fluid flow by an extended surface. Riley [30] examined MHD flow by vertical plate. Impact of uniform fluid flow over an extended sheet with chemical reaction was analyzed by Fairbanks and Wike [31]. Andersson et al. [32] studied flow with chemical reactive influence. Magyari and Keller [33, 34] investigated boundary layer flow flows caused by stretching walls. Recent researches about stretching surface may be consulted via Refs. [35 − 38].

Investigation of non-Newtonian liquids is an active research area for the pervious few years. Numerous industrial materials are characterized as non-Newtonian fluids. Few examples include oils, moisturizers, paints, polymers, polymeric fluids, and suspension fluids. The characteristics of non-Newtonian liquids are distinct. Therefore many models in this direction are suggested. It is noticed from existing literature that second and third grade fluids are studied much in view of shear thinning/shear thickening and normal stress factors. Some developments about these liquids may be examined by the studies [39 − 43]. Recently Abbas et al.[44] explored the Maxwell fluid model in the presence of permeable channel. Thermodynamic constraints for third grade fluid are pointed out by Fosdick and Rajagopal [45]. Mastroberardino and Mahabaleswar [46] constructed viscoelastic mixed convective by stretching surface. Adesanya and Makinde [47] explored thermodynamics properties for third-grade liquid with internal heat generation. Various studies about third grade fluid are examined via Refs [48 − 52]. Jeffrey material is one of the non-Newtonian liquids which can predict the retardation and relaxation times effects. Non-Newtonian fluid model due to their applications in bio-engineering, geophysics, oil reservoir process and chemical and nuclear technologies have remarkable importance [53 − 56].

The fluid movement through permeable space is significant for thermal insulation, industrial production of oil, power generation and others. The flows in porous channel are common in groundwater discharge, oil revenue and many others. Darcy model is utilized for low velocity flow rate whereas for high velocity flow rate this model is extended to Darcy-Forchheimer relation with additional term in momentum equation [57]. Saddeek [58] inspected the dissipated flow over a permeable extended sheet. Some recently investigations about Darcy-Forchheimer medium can be found in Refs. [59 − 62].

To minimize the irreversibility one can utilize the concept of thermodynamics second (2nd) law. Entropy optimization (increase or decrease) is a principle of annihilation of current framework. Analysis of entropy is accomplished to improve efficiency of system. Joule heating, dissipation and mass and heat transfers etc., can be exploited as fundamentals of entropy generation (EG). Design variable subject to thermal structures negotiate not only with heat transportation improvement as well as with the quantity of intensity input in structures. Therefore determining of optimal obstinacy between the heat transportation rate (HTR) and need of intensity input turn out to be premier intention about design approximations of a thermal structure. Assessment of the dynamical productivity of real structures is developed by an energy assessment which can be used (energy) or correspondingly irreversible rate of entropy. Optimization and comparison of working heat exchanger are measured by thermodynamic parameters [63 − 67] and by specific economic parameters [68 − 72]. Technique enables the entropy production to be modified through various mechanisms and design features in order to find optimum geometric heat exchanger patterns [73]. Bejan [74] defined models of power plants functioning at absolute capacity while providing the lowest entropy generation rate. Salamon et al. [75] explained that in some structure conditions optimum power efficiency and minimum entropy generation rate may become equal. Haseli [76] discussed the process of Brayton processes in different configurations at a minimum EGM condition. Several investigators use energy storage and entropy production minimization to induce optimum simulations for the thermal system [77]. Torabi et al. [78] numerically calculated total entropy optimization rate in micro porous channels subject to temperature jump and velocity slip. Das and Basak [79] studied discrete solar heating methodologies subject to entropy optimization. They also examined heat transfer through natural convection process in discretely heated square cavity. Entropy optimization analysis for flow boiling condition in a helically coiled tube subject to constant heat flux is analyzed by Abdous et al. [80].

1.3 Viscous fluid

A fluid that follow Newton's viscosity law is called viscous fluids. For viscous incompressible fluid the Cauchy stress tensor ($\boldsymbol{\tau}^*$) is

$$\boldsymbol{\tau}^* = -p\mathbf{I} + \mu\mathbf{A}_1, \tag{1.1}$$

in which p denotes the pressure, $\mathbf{I}$ the identity tensor and $\mathbf{A}_1$ the first Rivlin-Ericksen tensor.

1.4 Non-Newtonian liquids

A fluid that does not follow Newton's viscosity law is known as non-Newtonian liquids. Examples include ketchup, honey, custard, paint, toothpaste, shampoo and blood at low shear rate etc.

1.4.1 Second grade fluid

The continuity, motion and second grade fluid relations are

$$\boldsymbol{\nabla}.\mathbf{V} = 0, \tag{1.2}$$

$$\rho\frac{d\mathbf{V}}{dt} = \operatorname{div}\boldsymbol{\tau}^*, \tag{1.3}$$

$$\boldsymbol{\tau}^* = -p\mathbf{I} + \mathbf{S}^*, \tag{1.4}$$

where an extra stress tensor $\mathbf{S}^*$ satisfies

$$\mathbf{S}^* = \mu\mathbf{A}_1 + \alpha_1\mathbf{A}_1 + \alpha_1\mathbf{A}_2 + \alpha_2\mathbf{A}_1^2, \tag{1.5}$$

$$\mathbf{A}_n = \frac{d}{dt}\mathbf{A}_{n-1} + \mathbf{A}_{n-1}(\nabla\mathbf{V}) + \mathbf{A}_{n-1}(\nabla\mathbf{V})^T,\ n \geq 1. \tag{1.6}$$

$$\mathbf{A}_1 = (\nabla\mathbf{V}) + (\nabla\mathbf{V})^T, \tag{1.7}$$

$$
(\nabla \mathbf{V}) = \begin{bmatrix} \frac{\partial u}{\partial x} & \frac{\partial u}{\partial y} & \frac{\partial u}{\partial z} \\ \frac{\partial v}{\partial x} & \frac{\partial v}{\partial y} & \frac{\partial v}{\partial z} \\ \frac{\partial w}{\partial x} & \frac{\partial w}{\partial y} & \frac{\partial w}{\partial z} \end{bmatrix}. \tag{1.8}
$$

1.4.2 Third grade fluid

An extra stress tensor $\mathbf{S}^*$ have obeys

$$
\mathbf{S}^* = \mu \mathbf{A}_1 + \alpha_1 \mathbf{A}_1 + \alpha_1 \mathbf{A}_2 + \alpha_2 \mathbf{A}_1^2 + \beta_1^* \mathbf{A}_3 + \beta_2^* \mathbf{A}_1 \mathbf{A}_2 + \beta_2^* \mathbf{A}_2 \mathbf{A}_1 + \beta_3^* (tr \mathbf{A}_1^2) \}, \tag{1.9}
$$

where μ denotes dynamic viscosity and $\alpha_i (i = 1, 2)$ and $\beta_j (j = 1 - 3)$ are the material constants of fluid.

1.4.3 Jeffrey fluid model

Constitutive relation for an extra stress tensor $\mathbf{S}^*$ satisfies

$$
\mathbf{S}^* = \frac{\mu}{1 + \lambda_1} \left[A + \lambda_2 \left(\frac{d}{dt} + (\mathbf{V} \cdot \boldsymbol{\nabla}) \mathbf{A} \right) \right] \Bigg\}, \tag{1.10}
$$

where λ_1 is the ratio of relaxation to retardation times and λ_2 the retardation time.

1.5 Methodologies

1.5.1 Homotopy analysis method (HAM)

In 1992, the homotopy method was first time given by Liao [92] for solutions of highly non-linear partial/ordinary systems. This method uses the concept of homotopy to construct a series solution for highly nonlinear systems. For nonlinear equation, we have

$$
\mathcal{N} [u(\eta)] = 0, \tag{1.11}
$$

$$
(1 - q^{**}) \mathcal{L} [u(\eta; q^{**}) - u_0(\eta)] = q^{**} \hbar \mathcal{N} [u(\eta; q^{**})], \tag{1.12}
$$

where $\hbar \neq 0$, $0 \leq q^{**} \leq 1$, $\mathcal{L}$ and $u_0(\eta)$ satisfying the boundary constrains. Put $q^{**} = 0$ and $q^{**} = 1$, one has

$$u(\eta;0) - u_0(\eta) = 0, \text{ and } u(\eta;1) - u(\eta) = 0, \tag{1.13}$$

Applying the concept of Taylor series, we get

$$u(\eta;q^{**}) = u_0(\eta) + \sum_{m^*=1}^{\infty} u_{m^*}(\eta) \left(q^{**}\right)^{m^*}, \quad u_{m^*}(\eta) = \frac{1}{m^*!} \frac{\partial^{m^*} u(\eta;q^{**})}{\partial \left(q^{**}\right)^{m^*}}\bigg|_{q^{**}=0}. \tag{1.14}$$

The m^{th} order expression is defined as

$$L\left[u_{m^*}(\eta) - \chi_{m^*} u_{m^*-1}(\eta)\right] = \hbar \mathcal{R}_{m^*}\left(u_{m^*-1}\right), \tag{1.15}$$

with

$$R_{m^*}\left(u_{m^*-1}\right) = \frac{1}{(m^*-1)!} \frac{\partial^{m^*-1} u(\eta;q^{**})}{\partial \left(q^{**}\right)^{m^*-1}}\bigg|_{q^{**}=0}, \tag{1.16}$$

$$\chi_{m^*} = \begin{cases} 0, & m^* \leq 1, \\ 1, & m^* > 1. \end{cases} \tag{1.17}$$

The final solution converges to $q^{**} = 1$ is obtained with the help of MATHEMATICA i.e.,

$$u(x) = u_0(\eta) + \sum_{m^*=1}^{\infty} u_{m^*}(\eta). \tag{1.18}$$

1.5.2 Bulit-in-Shooting technique

We have implemented built-in-Shooting technique [92] in chapters 2, 3,4 and 7 to construct the numerical solutions of differential equations in MATHEMATICA. This method directly solved the differential systems.

Chapter 2

Flow subject to effective Prandtl number and without effective Prandtl number via $\gamma Al_2O_3 - H_2O$ and $\gamma Al_2O_3 - C_2H_6O_2$ nanoparticles

Entropy generation and viscous dissipation in mixed convective radiative flow through a stretched sheet are examined. Modeling is based upon second law of thermodynamics. Effective Prandtl number (EPN) model is employed to analyze the features of entropy-generated flow. Nanomaterial subject to nanoparticles (γAl_2O_3 $-H_2O$ and γAl_2O_3 $-C_2H_6O_2$) are considered. The resulting problem are solved through Optimal homotopy method (OHAM). Optimum values are determined for the auxiliary parameters. Impact of emerging parameters are graphically analyzed for (γAl_2O_3 $-H_2O$ and γAl_2O_3 $-C_2H_6O_2$) nanoparticles. Major points are provided in concluding remarks.

2.1 Modeling

Mixed convective flow of viscous nanomaterial caused by stretching sheet is discussed. The stretching surface is taken at $y = 0$ ($Fig.$2.1). Fluid occupies the space $y > 0$. Radiation, dissipation and heat generation are present. Mathematical expressions for problem under consideration satisfy [81]:

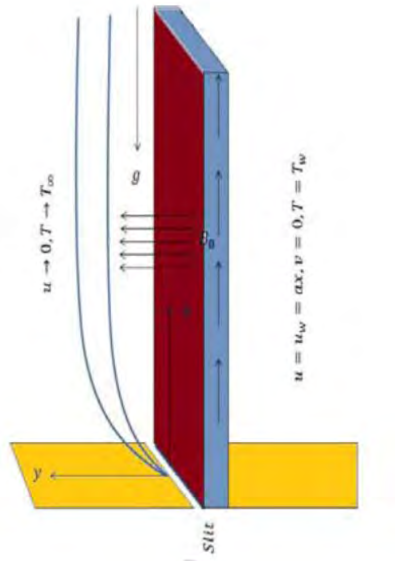

Fig. 2.1: Flow diagram.

$$\frac{\partial u}{\partial x} + \frac{\partial v}{\partial y} = 0, \tag{2.1}$$

$$u\frac{\partial u}{\partial x} + v\frac{\partial u}{\partial y} - \frac{\mu_{nf}}{\rho_{nf}}\frac{\partial^2 u}{\partial y^2} - g\frac{(\rho\beta)_{nf}}{\rho_{nf}}(T - T_\infty) = 0, \tag{2.2}$$

$$\left(u\frac{\partial T}{\partial x} + v\frac{\partial T}{\partial y}\right) = \frac{k_{nf}}{(\rho c_p)_{nf}}\frac{\partial^2 T}{\partial y^2} + \frac{1}{(\rho c_p)_{nf}}\left(\frac{\partial q_r}{\partial y}\right) + \frac{\mu_{nf}}{(\rho c_p)_{nf}}\left(\frac{\partial u}{\partial y}\right)^2 + \frac{Q_0}{(\rho c_p)_{nf}}(T - T_\infty), \tag{2.3}$$

with

$$\left.\begin{array}{c} u = U_w = ax, \quad v = 0, \quad T = T_w \text{ at } y = 0, \\ u \to 0, \quad T \to T_\infty \quad \text{when } y \to \infty. \end{array}\right\} \tag{2.4}$$

2.2 Thermophysical characteristics of $Al_2O_3 - H_2O$ and $Al_2O_3 - C_2H_6O_2$ nanoparticles [82-86].

Here one has

$$\frac{\rho_{nf}}{\rho_f} = (1-\phi) + \rho\frac{\rho_s}{\rho_f}, \tag{2.5}$$

$$\frac{(\rho c_p)_{nf}}{(\rho c_p)_f} = (1-\phi) + \phi\frac{(\rho c_p)_s}{(\rho c_p)_f}, \tag{2.6}$$

$$\frac{(\rho\beta)_{nf}}{(\rho\beta)_f} = (1-\phi) + \phi\frac{(\rho\beta)_s}{(\rho\beta)_f}, \tag{2.7}$$

$$\frac{\mu_{nf}}{\mu_f} = 123\phi^2 + 7.3\phi + 1, \text{ for } \gamma Al_2O_3 - H_2O, \tag{2.8}$$

$$\frac{\mu_{nf}}{\mu_f} = 306\phi^2 - 0.19\phi + 1 \text{ for } \gamma Al_2O_3 - C_2H_6O_2, \tag{2.9}$$

$$\frac{k_{nf}}{k_f} = 4.97\phi^2 + 2.72\phi + 1 \text{ for } \gamma Al_2O_3 - H_2O, \tag{2.10}$$

$$\frac{k_{nf}}{k_f} = 28.905\phi^2 + 2.8273\phi + 1 \text{ for } \gamma Al_2O_3 - C_2H_6O_2, \tag{2.11}$$

$$\frac{\mathrm{Pr}_{nf}}{\mathrm{Pr}_f} = 82.1\phi^2 + 3.9\phi + 1 \text{ for } \gamma Al_2O_3 - H_2O, \tag{2.12}$$

$$\frac{\mathrm{Pr}_{nf}}{\mathrm{Pr}_f} = 254.3\phi^2 + 3\phi + 1 \text{ for } \gamma Al_2O_3 - C_2H_6O_2, \tag{2.13}$$

Table 1: Thermophysical features of ethylene glycol ($C_2H_6O_2$), water (H_2O) and alumina (Al_2O_3).

	$C_p(Jk^{-1}g^{-1}K^{-1})$	$\rho(kgm^{-3})$	$\beta \times 10^{-5}\left(K^{-1}\right)$	$k(Wm^{-1}K^{-1})$
Alumina (Al_2O_3)	765	3970	0.85	40
Water (H_2O)	4182	998.3	20.06	0.60
Ethylene glycol ($C_2H_6O_2$)	2382	1116.6	65	0.249

We consider the transformations

$$\eta=\sqrt{\frac{a}{\upsilon_f}}y,\ u=axf\ '(\eta),\ v=-\sqrt{a\upsilon_f}f(\eta),\ t(\eta)=\frac{T-T_\infty}{(T_w-T_\infty)}. \tag{2.14}$$

2.3 Flow equations

Momentum and energy equations for both ($\gamma Al_2O_3-H_2O$ and $\gamma Al_2O_3-C_2H_6O_2$) nanofluids give

$$\left.\begin{array}{c}(123\phi^2+7.3\phi+1)f\ '''+\left(1-\phi+\phi\frac{\rho_s}{\rho_f}\right)(ff\ ''+f\ '^2)\\ +\left(1-\phi+\phi\frac{\rho_s}{\rho_f}\frac{\beta_s}{\beta_f}\right)\lambda t(\eta)=0,\ \text{for }\gamma Al_2O_3-H_2O\end{array}\right\} \tag{2.15}$$

$$\left.\begin{array}{c}(306\phi^2-0.19\phi+1)f\ '''+\left(1-\phi+\phi\frac{\rho_s}{\rho_f}\right)(ff\ ''+f\ '^2)\\ +\left(1-\phi+\phi\frac{\rho_s}{\rho_f}\frac{\beta_s}{\beta_f}\right)\lambda t(\eta)=0,\ \text{for }\gamma Al_2O_3-C_2H_6O_2\end{array}\right\} \tag{2.16}$$

$$f(0)=0,\ f'(0)=1,\ f'(\infty)=0, \tag{2.17}$$

$$\left.\begin{array}{c}\frac{d}{d\eta}\left[(4.97\phi^2+2.72\phi+1)+R_d(1+(\theta_w-1)t)^3t'(\eta)\right]\\ +\Psi\left[\begin{array}{c}f(\eta)t'(\eta)-f\ '(\eta)t(\eta)+\frac{Ec}{\left(1-\phi+\phi\frac{(\rho c_p)_s}{(\rho c_p)_f}\right)}(f\ ''(\eta))^2\\ +\frac{\delta}{\left(1-\phi+\phi\frac{(\rho c_p)_s}{(\rho c_p)_f}\right)}t(\eta)\end{array}\right]=0,\text{for }\gamma Al_2O_3-H_2O\end{array}\right\} \tag{2.18}$$

$$\left.\begin{array}{c}\frac{d}{d\eta}\left[(28.905\phi^2+2.8273\phi+1)+R_d(1+(\theta_w-1)t)^3t'(\eta)\right]\\ +\Psi\left[\begin{array}{c}f(\eta)t'(\eta)-f\ '(\eta)t(\eta)+\frac{Ec}{\left(1-\phi+\phi\frac{(\rho c_p)_s}{(\rho c_p)_f}\right)}(f\ ''(\eta))^2\\ +\frac{\delta}{\left(1-\phi+\phi\frac{(\rho c_p)_s}{(\rho c_p)_f}\right)}t(\eta)\end{array}\right]=0,\text{for }\gamma Al_2O_3-C_2H_6O_2\end{array}\right\} \tag{2.19}$$

$$t(0)=1\quad t(\infty)=0, \tag{2.20}$$

where Ψ for effective Prandtl number via $\gamma Al_2O_3-H_2O$ and $\gamma Al_2O_3-C_2H_6O_2$ nanofluids satisfies

$$\Psi = \frac{(\mathrm{Pr})_f \left(1-\phi+\phi\frac{\rho_s}{\rho_f}\right)(82.1\phi^2+3.9\phi+1)}{123\phi^2+7.3\phi+1}, \tag{2.21}$$

$$\Psi = \frac{(\mathrm{Pr})_f \left(1-\phi+\phi\frac{\rho_s}{\rho_f}\right)(254.3\phi^2-3\phi+1)}{306\phi^2-0.19\phi+1}. \tag{2.22}$$

In absence of effective Prandtl number via $\gamma Al_2O_3 - H_2O$ and $\gamma Al_2O_3 - C_2H_6O_2$ one has

$$\Psi = \frac{(\mathrm{Pr})_f \left(1-\phi+\phi\frac{\rho_s}{\rho_f}\right)}{4.97\phi^2-2.72\phi+1}, \tag{2.23}$$

$$\Psi = \frac{(\mathrm{Pr})_f \left(1-\phi+\phi\frac{\rho_s}{\rho_f}\right)}{28.905\phi^2+2.8273\phi+1}. \tag{2.24}$$

2.4 Physically quantities

2.4.1 Drag force coefficient ($\mathbf{C}_f$)

Skin friction in dimensional form is expressed as

$$C_f = \frac{\tau_w}{\rho_f u_w^2}, \tag{2.25}$$

where τ_w is defined as

$$\tau_w = -2\mu_{nf}\big|_{y=0} \left.\frac{\partial u}{\partial y}\right|_{y=0}, \tag{2.26}$$

Putting Eq. (2.26) in Eq. (2.25), one has

$$\left.\begin{array}{r} \frac{1}{2}\sqrt{\mathrm{Re}_x}C_f = -\left(123\varphi^2+7.3\phi+1\right) f''(0) \text{ for } \gamma Al_2O_3 - H_2O, \\ \frac{1}{2}\sqrt{\mathrm{Re}_x}C_f = -\left(306\varphi^2-0.19\phi+1\right) f''(0) \text{ for } \gamma Al_2O_3 - C_2H_6O_2. \end{array}\right\} \tag{2.27}$$

2.4.2 Nusselt number (Nu)

Mathematically we have

$$Nu = \frac{x q_w}{k_f\left(T_w - T_\infty\right)}, \tag{2.28}$$

where q_w is expressed as

$$q_w = -k_{nf}\left[\left(1+\frac{16\sigma T^3}{3kk_f}\right)\left(\frac{\partial T}{\partial y}\right)\right]_{y=0}. \tag{2.29}$$

Using Eq. (2.29) in Eq. (2.28) we have

$$\left.\begin{array}{l} (\mathrm{Re}_x)^{-1/2} Nu_x = \left[\begin{array}{c} (4.97\phi^2+2.72\phi+1) \\ +R_d(1+(\theta_w-1)t(0))^3 t'(0) \end{array}\right] \text{ for } \gamma Al_2O_3 - H_2O, \\ (\mathrm{Re}_x)^{-1/2} Nu_x = \left[\begin{array}{c} (28.905\phi^2+2.8273\phi+1) \\ +R_d(1+(\theta_w-1)t(0))^3 t'(0) \end{array}\right] \text{ for } \gamma Al_2O_3 - C_2H_6O_2 \end{array}\right\}. \tag{2.30}$$

2.5 Entropy generation modelling

Current flow model volumetric entropy (S_g) and characteristic entropy $(S_g)_0$ can be written as

$$S_g = \frac{k_f}{T_\infty^2}\left[\frac{k_{nf}}{k_f}\left(\frac{\partial T}{\partial y}\right)^2 + \frac{16\sigma^* T_\infty^3}{3kk_f}\left(\frac{\partial T}{\partial y}\right)^2\right] + \frac{\mu_{nf}}{T_\infty}\left(\frac{\partial u}{\partial y}\right)^2, \tag{2.31}$$

$$(S_g)_0 = \frac{k_{nf}}{T_\infty^2}\frac{(\Delta T)^2}{x^2}. \tag{2.32}$$

Mathematically total entropy generation is described as

$$N_G = \frac{S_g}{(S_g)_0}. \tag{2.33}$$

Dimensionless form of above equation for both ($\gamma Al_2O_3 - H_2O$ and $\gamma Al_2O_3 - C_2H_6O_2$) nanofluids are expressed as

$$\left.\begin{array}{l} N_G = t^2(\eta) + \mathrm{Re}\left[\begin{array}{c} (4.97\phi^2+2.72\phi+1)+ \\ R_d(1+(\theta_w-1)t(0))^3 t'^2(0) \end{array}\right] \\ +\left[\frac{123\phi^2+7.3\phi+1}{4.97\phi^2+2.72\phi+1}\right]\frac{Br}{\Omega}\,\mathrm{Re}\, f''^2 \text{ for } \gamma Al_2O_3 - H_2O \end{array}\right\}, \tag{2.34}$$

$$\left.\begin{array}{c} N_G = t^2(\eta) + \mathrm{Re}\begin{bmatrix} (28.905\phi^2 + 2.8273\phi + 1) + \\ R_d(1 + (\theta_w - 1)t(0))^3 t'^2(0) \end{bmatrix} \\ + \left[\frac{306\phi^2 - 0.19\phi + 1}{28.905\phi^2 + 2.8273\phi + 1}\right] \frac{Br}{\Omega} \mathrm{Re}\, f''^2 \text{for } \gamma Al_2O_3 - C_2H_6O_2 \end{array}\right\}. \tag{2.35}$$

Bejan number (Be) in non-Dimensional form is defined by

$$\left.\begin{array}{c} Be = \dfrac{\mathrm{Re}\left[(4.97\phi^2 + 2.72\phi + 1) + R_d(1 + (\theta_w - 1)t(0))^3 t'^2(0)\right]}{t^2(\eta) + \mathrm{Re}\begin{bmatrix} (4.97\phi^2 + 2.72\phi + 1) \\ + R_d(1 + (\theta_w - 1)t(0))^3 t'^2(0) \end{bmatrix} + \left[\frac{123\phi^2 + 7.3\phi + 1}{4.97\phi^2 + 2.72\phi + 1}\right] \frac{Br}{\Omega} \mathrm{Re}\, f''^2} \\ \text{for } \gamma Al_2O_3 - H_2O \end{array}\right\}, \tag{2.36}$$

$$\left.\begin{array}{c} Be = \dfrac{\mathrm{Re}\left[(28.905\phi^2 + 2.8273\phi + 1) + R_d(1 + (\theta_w - 1)t(0))^3 t'^2(0)\right]}{t^2(\eta) + \mathrm{Re}\begin{bmatrix} (28.905\phi^2 + 2.8273\phi + 1) \\ + R_d(1 + (\theta_w - 1)t(0))^3 t'^2(0) \end{bmatrix} + \left[\frac{306\phi^2 - 0.19\phi + 1}{28.905\phi^2 + 2.8273\phi + 1}\right] \frac{Br}{\Omega} \mathrm{Re}\, f''^2} \\ \text{for } \gamma Al_2O_3 - C_2H_6O_2 \end{array}\right\}. \tag{2.37}$$

2.6 Dimensionless parameters

$$\left.\begin{array}{c} R_d\left(= \frac{16\sigma^* T_\infty^3}{3kk_f}\right),\ Ec\left(= \frac{u_w^2}{ac_p}\right),\ \delta\left(= \frac{Q_o}{\rho c_p}\right),\ Br\left(= \frac{\mu_f}{k_f \Delta T}\right), \\ \Omega\left(= \frac{\Delta T}{T_\infty}\right),\ \lambda\left(= \frac{g\beta_f b}{a^2}\right),\ \mathrm{Re}_x\left(= \frac{xu_w}{\nu_f}\right) \end{array}\right\}. \tag{2.38}$$

2.7 Methodology

Initial approximations $(f_0(\eta),\ t_0(\eta))$ and linear operators $(\mathcal{L}_f(f), \mathcal{L}_t(t))$ are

$$\left.\begin{array}{c} f_0(\eta) = 1 - e^{(-\eta)},\ t_0(\eta) = e^{(-\eta)}, \\ \mathcal{L}_f(f) = \frac{d^3 f}{d\eta^3} - \frac{df}{d\eta},\ \mathcal{L}_t(t) = \frac{d^2 t}{d\eta^2} - t. \end{array}\right\} \tag{2.39}$$

Average residual errors for flow equations at k^{th} order are expressed as

$$\varepsilon_m^f(h_f) = \frac{1}{N+1} \sum_{j=0}^{N} \times \left[\sum_{i=0}^{m} (f_i)_{\eta = j\Pi\eta}\right]^2, \tag{2.40}$$

$$\varepsilon_m^t(h_f, h_t) = \frac{1}{N+1}\sum_{j=0}^{N} \times \left[\sum_{i=0}^{m}(f_i)_{\xi=j\Pi\eta}, \sum_{i=0}^{m}(t_i)_{\eta=j\Pi\eta}\right]^2, \tag{2.41}$$

where (ε_m^k) is defined by

$$\varepsilon_m^k = \varepsilon_m^f + \varepsilon_m^t. \tag{2.42}$$

Optimal estimations of convergence control variables are $(h_f = -0.85698)$ and $(h_t = -0.312346)$. Numerical estimation of total residual error (ε_m^k) is $\left(9.20133 \times 10^{-6}\right)$.

Table 2.1: Residual errors for various variables when $R_d = 0.4$, $\theta_w = 1.1$, $Br = 0.4$, $\delta = 0.1$, $\mathrm{Re} = 0.3$, $\lambda = 0.2$, $\mathrm{Pr} = 1.0$ and $Ec = 0.1$.

m	ε_m^f	ε_m^t
2	8.94180×10^{-8}	6.84831×10^{-6}
6	5.20171×10^{-12}	6.1285×10^{-8}
8	3.21087×10^{13}	5.15682×10^{-8}
10	3.58381×10^{-15}	508389×10^{-10}
16	1.2359×10^{-21}	2.58971×10^{-11}
22	2.5872×10^{-24}	3.80485×10^{-12}
24	1.58101×10^{-27}	5.9729×10^{-14}

2.8 Analysis

2.8.1 Velocity

Effect of nanoparticles volume fraction $(\phi = 0.0, 0.2, 0.4, 0.8)$ on velocity field is depicted in Figs. 2.2(a, b). From Figs. 2.2(a, b) we noticed that (ϕ) remarkably enhances the velocity $f'(\eta)$ for both $\gamma Al_2O_3 - H_2O$ and $\gamma Al_2O_3 - C_2H_6O_2$ nanofluids.

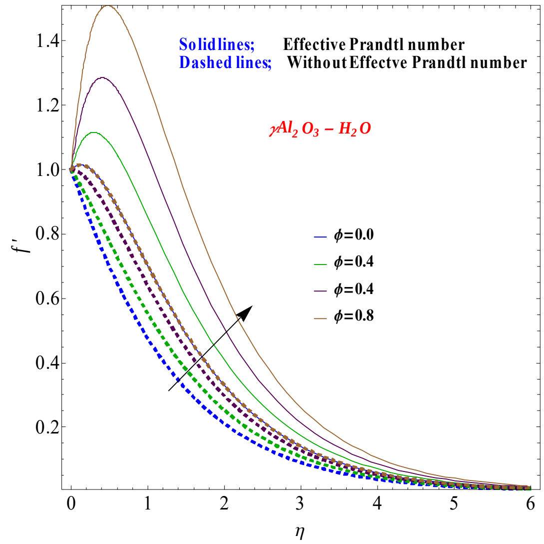

Fig. 2.2(a) : f' versus ϕ.

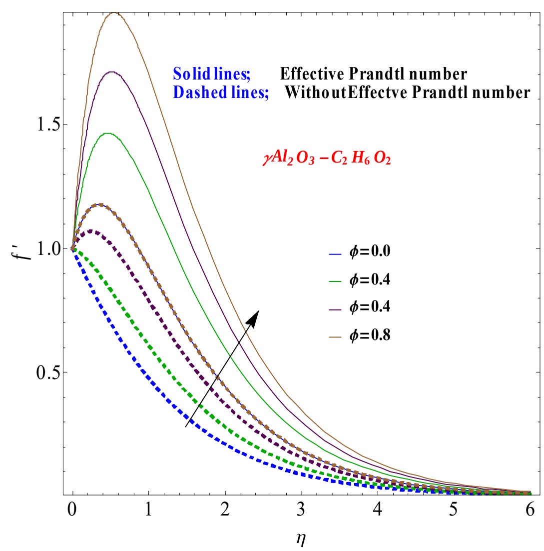

Fig. 2.2(b) : f' versus ϕ.

2.8.2 Temperature distribution

Influence of (ϕ) on $(t(\eta))$ is demonstrated in Figs. 2.3(a, b). In Fig. 2.3(a) it is scrutinized that $(t(\eta))$ shows contrast behavior for effective Prandtl number (EPN) and without effective Prandtl number for $(\gamma Al_2O_3 - H_2O)$ nanofluid. For higher $(\phi = 0.00, 0.01, 0.02, 0.03, 0.04)$ the temperature $t(\eta)$ decreases against effective Prandtl number (EPN) while an improvement is evaluated through $(\phi = 0.00, 0.01, 0.02, 0.03, 0.04)$ for without effective Prandtl number. Comparable outcomes is seen through ($\phi = 0.00, 0.01, 0.02, 0.03, 0.04$) for effective and without effective Prandtl numbers via $\gamma Al_2O_3 - C_2H_6O_2$ nanofluids (see Fig. 2.3(b)). Figs. 2.4(a) and 2.4(b) reveal the behavior of $t(\eta)$ via ($Ec = 1.0, 2.0, 3.0, 4.0$). From Fig. 2.4(a) an enhancement in ($t(\eta)$) for $\gamma Al_2O_3 - H_2O$ is noticed through higher (Ec). Physically higher values of (Ec) give rise to a significant variation in thermal field due to frictional heating for both scenarios $\gamma Al_2O_3 - H_2O$ and $\gamma Al_2O_3 - C_2H_6O_2$ (see Figs. 2.4(a, b). Eckert number (Ec) also describes the quantitative relation of kinetic energy and enthalpy. Higher (Ec) employ that dissipated heat is contained in material which reduces temperature ($t(\eta)$). Figs. 2.5(a, b) demonstrate the consequence of (R_d) on ($t(\eta)$). Temperature field is enhanced for larger (R_d). Physically radiative variable enhances the heat flux at surface which is responsible for an enhancement in thermal field for both cases of $\gamma Al_2O_3 - H_2O$ and $\gamma Al_2O_3 - C_2H_6O_2$ nanofluids.

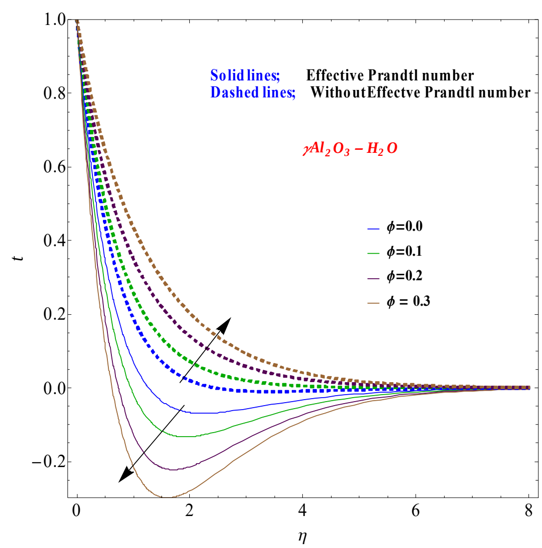

Fig. 2.3(a) : t versus ϕ.

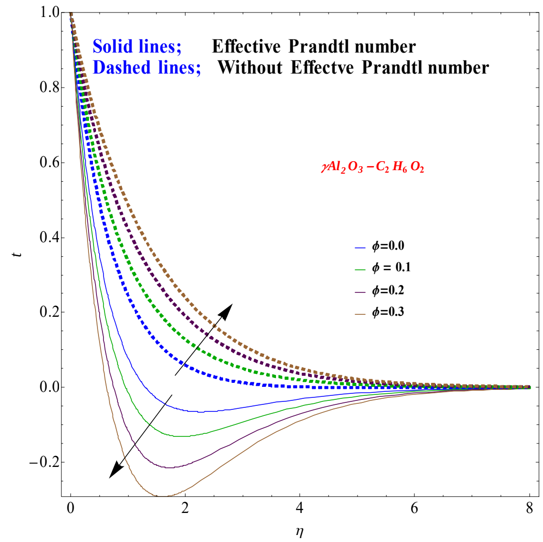

Fig. 2.3(b) : t versus ϕ.

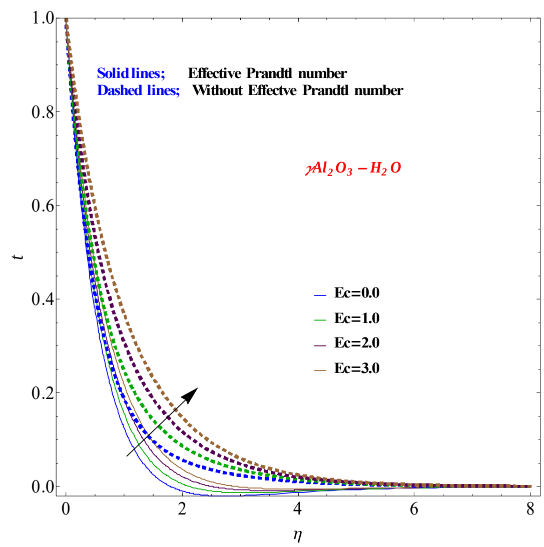

Fig. 2.4(a) : t versus Ec.

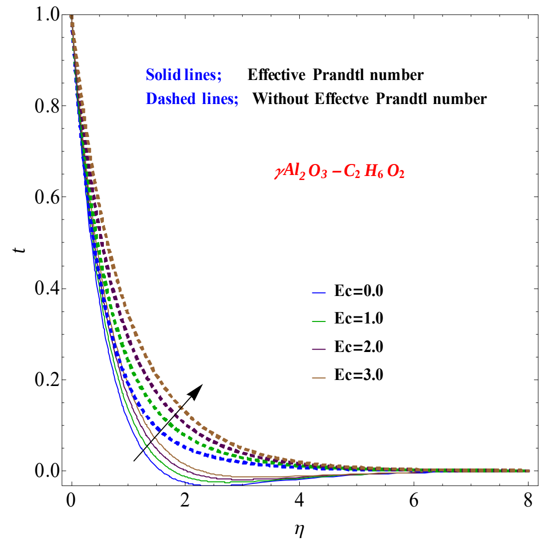

Fig. 2.4(b) : t versus Ec.

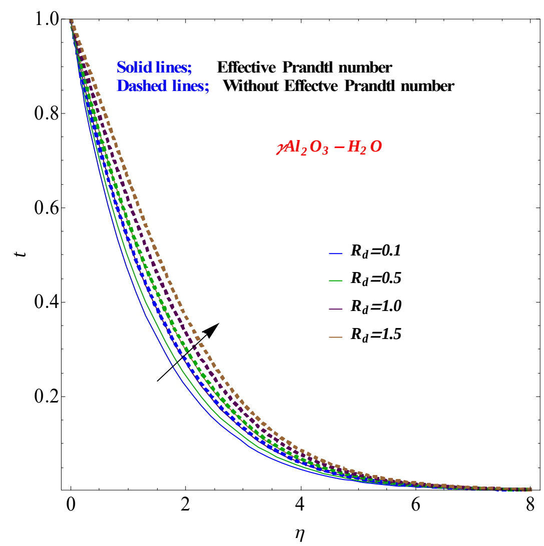

Fig. 2.5(a) : t versus R_d.

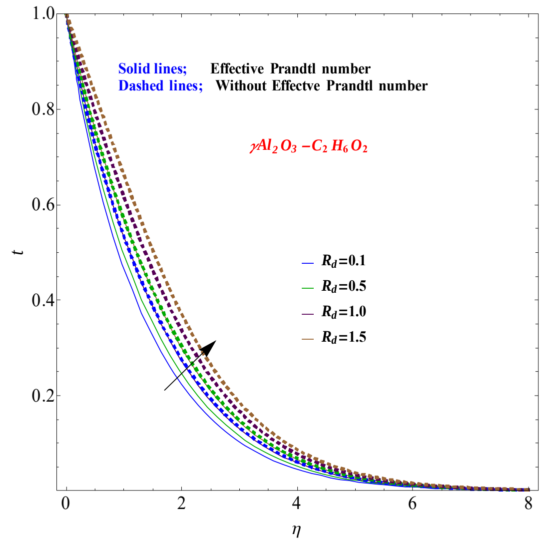

Fig. 2.5(b) : t versus R_d.

2.8.3 Entropy generation rate

Change in Brinkman number on $(N_G(\eta))$ is depicted in Figs. 2.6(a, b). Clearly $(N_G(\eta))$ is an increasing function of (Br) for both $\gamma Al_2O_3 - H_2O$ and $\gamma Al_2O_3 - C_2H_6O_2$ nanofluids. Infact significant quantity of heat releases within layer of liquid particles and as a result an improvement in entropy is noticed. Figs. 2.6(a, b) illustrate impact of (R_d) on $(N_G(\eta))$ for both $\gamma Al_2O_3 - H_2O$ and $\gamma Al_2O_3 - C_2H_6O_2$ nanofluids. Figs. 2.7(a, b) illustrated that an enhancement in (R_d) leads to increase of $(N_G(\eta))$. It is perceived that $(N_G(\eta))$ dominates in case of $\gamma Al_2O_3 - H_2O$ and $\gamma Al_2O_3 - C_2H_6O_2$ nanofluids. Significance of (θ_w) on $(N_G(\eta))$ is shown in Figs. 2.8(a, b). Here $(N_G(\eta))$ is an increasing function of (θ_w) for both $\gamma Al_2O_3 - H_2O$ and $\gamma Al_2O_3 - C_2H_6O_2$ nanofluids. For larger (θ_w) the irreversibility rate of the system enhances. As a result $(N_G(\eta))$ is increased. Furthermore $(N_G(\eta))$ dominants is case of effective Prandtl number (EPN) when compared with without effective Prandtl number in the presence of $\gamma Al_2O_3 - H_2O$ and $\gamma Al_2O_3 - C_2H_6O_2$ nanofluids.

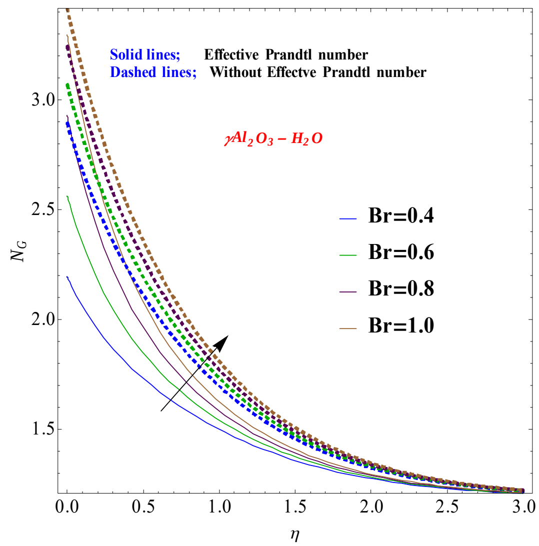

Fig. 2.6(a) : N_G versus Br.

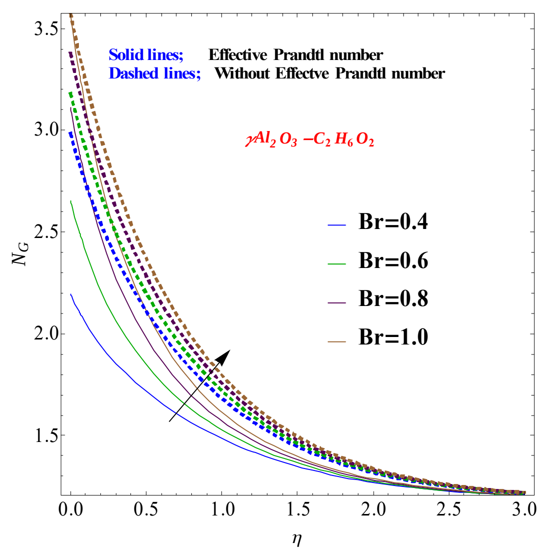

Fig. 2.6(b) : N_G versus Br.

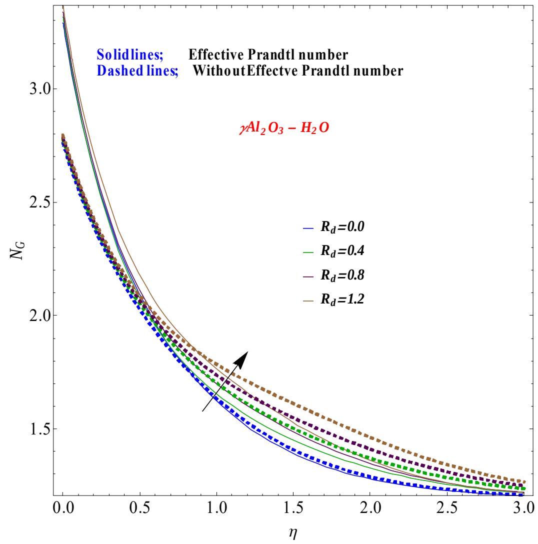

Fig. 2.7(a) : N_G versus R_d.

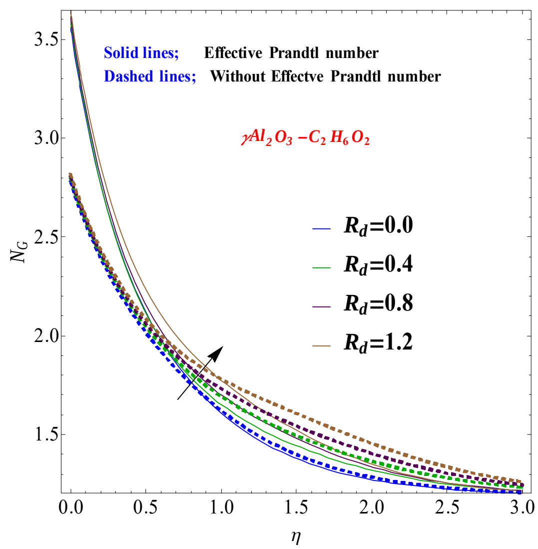

Fig. 2.7(b) : N_G versus R_d.

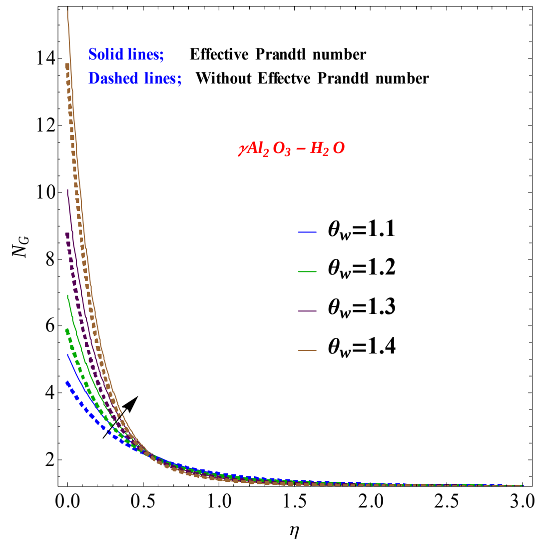

Fig. 2.8(a) : N_G versus θ_w.

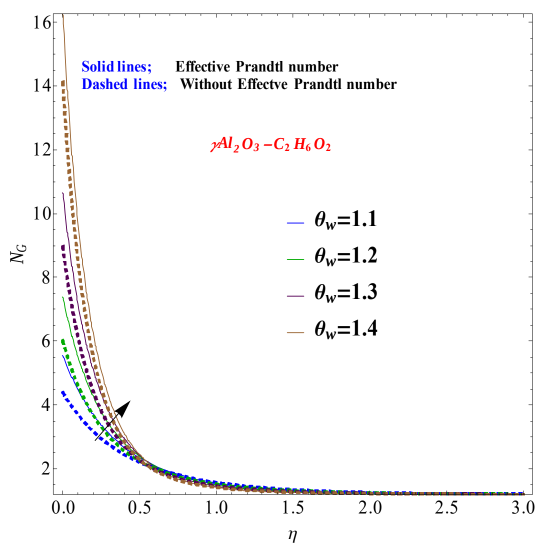

Fig. 2.8(b) : N_G versus θ_w.

2.8.4 Bejan Number

Attribute of (Br) on (Be) is exhibited in Figs. 2.9(a,b). Clearly (Be) is decreasing function of (Br) for both $\gamma Al_2O_3 - H_2O$ and $\gamma Al_2O_3 - C_2H_6O_2$ nanofluids. It is due to the fact that viscosity dominants against larger (Br). That is why Bejan number reduces. Radiation variable (R_d) on (Be) is explored in Figs. 2.10(a,b). Here (Be) enhances through higher (R_d) for both $\gamma Al_2O_3 - H_2O$ and $\gamma Al_2O_3 - C_2H_6O_2$ nanofluids. Internal energy of system improves and consequently an augmentation is observed in Bejan number.

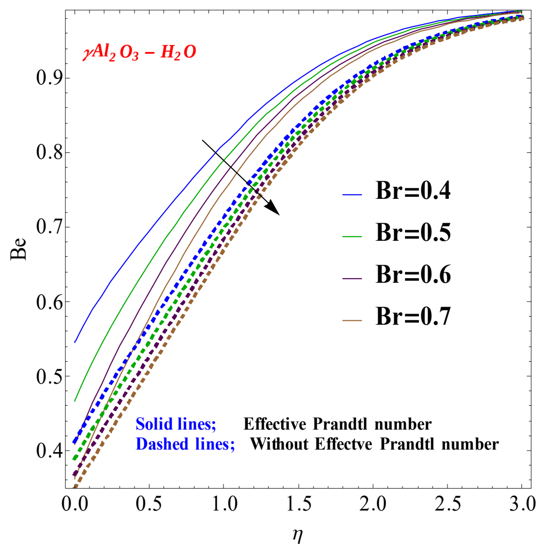

Fig. 2.9(a) : Be versus Br.

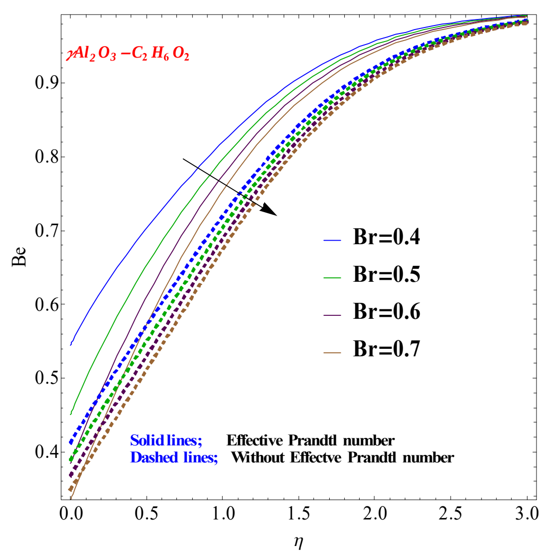

Fig. 2.9(b) : Be versus Br.

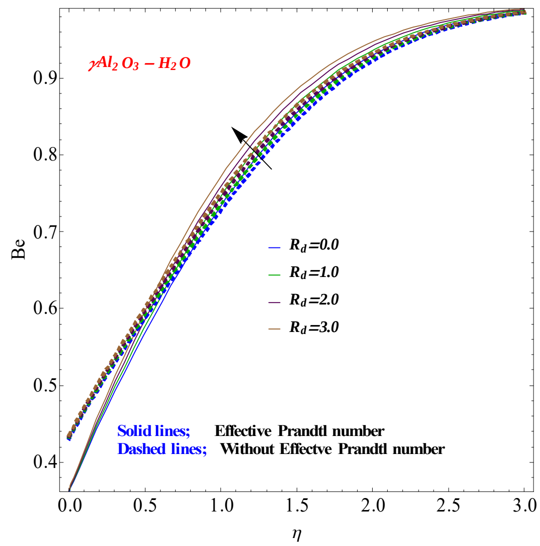

Fig. 2.10(a) : Be versus R_d.

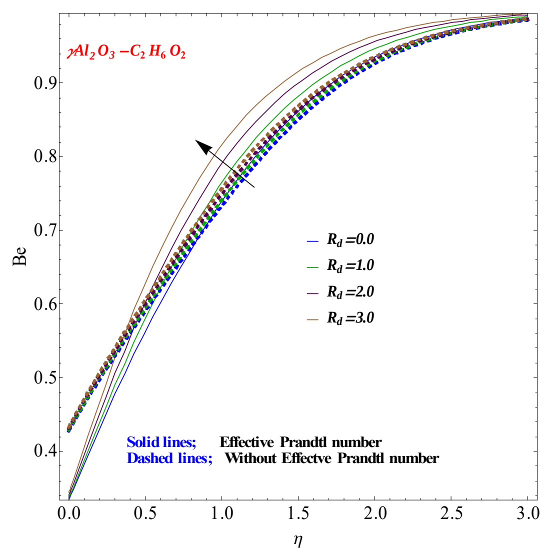

Fig. 2.10(b) : Be versus R_d.

2.9 Engineering quantities

2.9.1 Drag force (C_f) and heat transfer rate (Nu)

Figs. $2.11(a, b)$ illuminate the impacts of (C_f) through (λ) and (ϕ). Skin friction (C_f) increases via an enhancement in $(\lambda = 0.0, 0.1, 0.2, 0.3)$ and (ϕ) for both $\gamma Al_2O_3 - H_2O$ and $\gamma Al_2O_3 - C_2H_6O_2$ nanofluids (see Figs. $2.11(a, b)$). Nusselt number (Nu) through $(Ec = 0.2, 0.3, 0.4, 0.5)$

and (ϕ) for both $\gamma Al_2O_3 - H_2O$ and $\gamma Al_2O_3 - C_2H_6O_2$ nanofluids are sketched in Figs. $2.12(a,b)$. Here (Nu) boosts in presence of (ϕ) and (Ec).

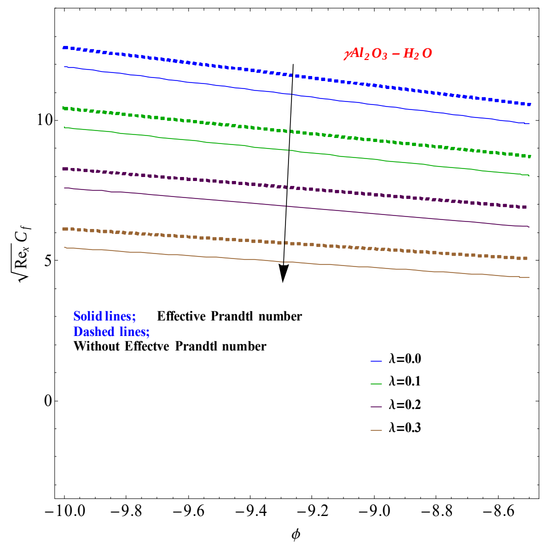

Fig. $2.11(a)$: C_f versus ϕ and λ.

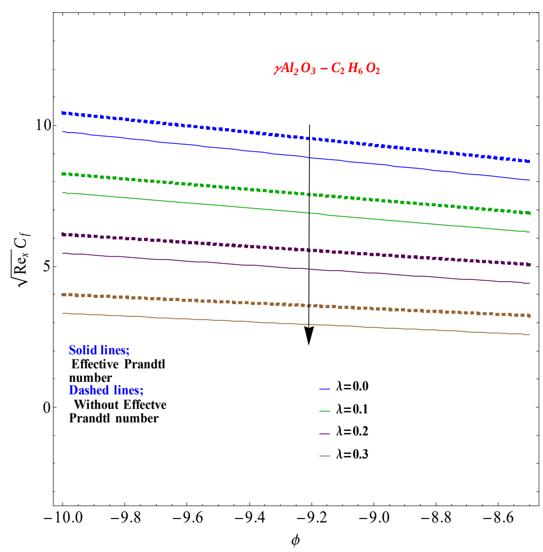

Fig. $2.11(b)$: C_f versus ϕ and λ.

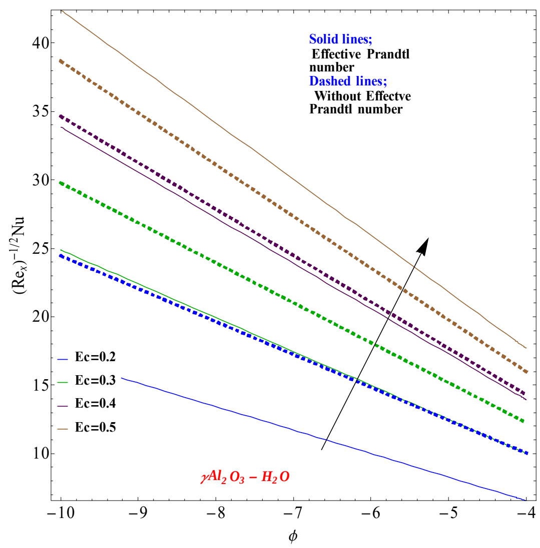

Fig. 2.12(a) : Nu versus ϕ and Ec.

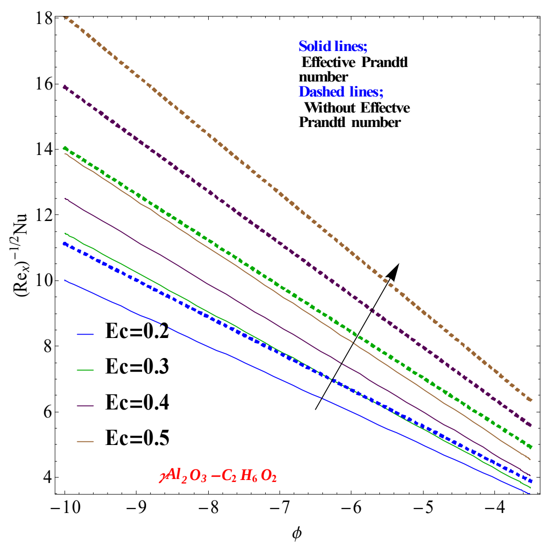

Fig. 2.12(b) : Nu versus ϕ and Ec.

2.10 Conclusions

Main findings are concluded as follows

- $f'(\eta)$ is increased for larger ϕ.
- $t(\eta)$ shows different impact for effective and non-effective Prandtl numbers.
- For higher Br, R_d and θ_w the $(N_G(\eta))$ is increased.

- Influences of (Br) and (R_d) on (Be) are absolutely inverse.
- (λ) leads to an increment in (C_f) and (Nu).

Chapter 3

Mixed convective dissipative flow of effective Prandtl number subject to entropy optimization and melting heat

This chapter investigates the outcomes of melting heat in mixed convective flow over a stretchable sheet. Heat generation and Joule heating effects are also taken in energy equation. Here ($\gamma Al_2O_3{-}H_2O$ and $\gamma Al_2O_3{-}C_2H_6O_2$) nanofluids are considered. With and without effective Prandtl models are analyzed for boundary layer flows. Entropy analysis is utilized from Second thermodynamics law. Various parameters are discussed graphically. Additionally the skin friction and heat transport rate have been discussed through tabulated values.

3.1 Mathematical formulation

Consider flows of ($\gamma Al_2O_3 - H_2O$ and $\gamma Al_2O_3 - C_2H_6O_2$) nanofluids. The assumption in mathematical equations are as follows.

(1) We made that ($u_w = ax$) is the velocity of stretching sheet.

(2) Neglects the induced magnetic field for very small Reynold number.

(3) Melting temperature (T_m) at surface is less than ambient temperature (T_∞).

(4) Entropy generation is accounted.

(5) Thermal equilibrium between ($\gamma Al_2O_3 - H_2O$ and $\gamma Al_2O_3 - C_2H_6O_2$) nanoparticles and base fluid is assumed. The governing equations are

$$\frac{\partial u}{\partial x} = -\frac{\partial v}{\partial y}, \tag{3.1}$$

$$\left. u\frac{\partial u}{\partial x} = \frac{\sigma_{nf}}{\sigma_f}B_0^2 u - v\frac{\partial u}{\partial y} + g\frac{(\rho\beta)_{nf}}{\rho_{nf}}(T - T_\infty) + \frac{\mu_{nf}}{\rho_{nf}}\frac{\partial^2 u}{\partial y^2}, \right\} \tag{3.2}$$

$$\left(u\frac{\partial T}{\partial x} + v\frac{\partial T}{\partial y}\right) = \frac{k_{nf}}{(\rho c_p)_{nf}}\frac{\partial^2 T}{\partial y^2} + \frac{\sigma_{nf}}{(\rho c_p)_{nf}}B_0^2 u^2 + \frac{Q_0}{(\rho c_p)_{nf}}(T - T_\infty) + \frac{\mu_{nf}}{(\rho c_p)_{nf}}\left(\frac{\partial u}{\partial y}\right)^2, \tag{3.3}$$

with

$$\left.\begin{array}{c} u = u_w = ax, \quad v = 0, \quad T = T_w \text{ at } y = 0, \\ u = 0, \quad T \to T_\infty \text{ when } y \to \infty. \end{array}\right\} \tag{3.4}$$

$$k_{nf}\left(\frac{\partial T}{\partial y}\right)_{y=0} - \rho_{nf}\left[\lambda^* + c_s\left(T_m - T_o\right)\right]v(x,0) = 0. \tag{3.5}$$

3.2 Thermophysical properties of nanoparticles $[82 - 86]$

$$\frac{\rho_{nf}}{\rho_f} = (1-\phi) + \phi\frac{\rho_s}{\rho_f}, \tag{3.6}$$

$$\frac{(\rho c_p)_{nf}}{(\rho c_p)_f} = (1-\phi) + \phi\frac{(\rho c_p)_s}{(\rho c_p)_f}, \tag{3.7}$$

$$\frac{(\rho\beta)_{nf}}{(\rho\beta)_f} = (1-\phi) + \phi\frac{(\rho\beta)_s}{(\rho\beta)_f}, \tag{3.8}$$

$$\frac{\sigma_{nf}}{\sigma_f} = \left[1 + \frac{3\left(\frac{\sigma_s}{\sigma_f} - 1\right)\phi}{\left(\frac{\sigma_s}{\sigma_f} + 2\right) - \left(\frac{\sigma_s}{\sigma_f} - 1\right)\phi}\right], \tag{3.9}$$

$$\frac{\mu_{nf}}{\mu_f} = 123\phi^2 + 7.3\phi + 1, \text{ for } Al_2O_3 - H_2O, \tag{3.10}$$

$$\frac{\mu_{nf}}{\mu_f} = 306\phi^2 - 0.19\phi + 1 \text{ for } Al_2O_3 - C_2H_6O_2, \tag{3.11}$$

$$\frac{\Pr_{nf}}{\Pr_f} = 82.1\phi^2 + 3.9\phi + 1 \text{ for } \gamma Al_2O_3 - H_2O, \tag{3.12}$$

$$\frac{\Pr_{nf}}{\Pr_f} = 254.3\phi^2 + 3\phi + 1 \text{ for } Al_2O_3 - C_2H_6O_2, \tag{3.13}$$

$$\frac{k_{nf}}{k_f} = 4.97\phi^2 + 2.72\phi + 1 \text{ for } Al_2O_3 - H_2O, \tag{3.14}$$

$$\frac{k_{nf}}{k_f} = 28.905\phi^2 + 2.8273\phi + 1 \text{ for } Al_2O_3 - C_2H_6O_2, \tag{3.15}$$

Table 3.1: Numerical values of nanofluids.

	$C_p(Jk^{-1}g^{-1}K^{-1})$	$\rho(kgm^{-3})$	$\beta \times 10^{-5}\left(K^{-1}\right)$	$k(Wm^{-1}K^{-1})$	$\sigma(\Omega^{-1}m^{-1})$
(Al_2O_3)	765	3970	0.85	40	10^{-12}
(H_2O)	4182	998.3	20.06	0.06	0.05
$(C_2H_6O_2)$	2382	1116.6	65	0.249	1.07×10^{-7}

Table 3.2: Comparative findings of current study with Rashidi ant Ishak et al [87, 88]

λ	Pr	Ishak et al. [87]	Rashidi et al. [88]	Present
	0.72	0.8086	0.80883	0.80886
	1.0	1.000	1.0001	1.0001
	3.0	1.9273	1.92368	1.92221
	7.0	3.0723	3.07225	3.07215
	10	3.7207	3.72067	3.72167
	100	12.2941	12.29408	12.29511
1	1	1.0873	1.08728	1.08721
2		1.1423	1.14234	1.14402
3		1.1853	1.18528	1.18512

3.3 Non-Dimensional expressions

Consider the transformations

$$\frac{\eta}{y} = \sqrt{\frac{a}{\upsilon_f}},\ \frac{u}{f\,'(\eta)} = ax,\ \frac{v}{f(\eta)} = -\sqrt{a\nu_f},\ t(\eta) = \frac{T - T_m}{(T_\infty - T_m)}. \tag{3.16}$$

The momentum and energy equations for both ($\gamma Al_2O_3 - H_2O$ and $\gamma Al_2O_3 - C_2H_6O_2$) nanofluids take the following forms

$$\left.\begin{array}{c} (123\phi^2 + 7.3\phi + 1)f\,''' + \left(1 - \phi + \phi\frac{\rho_s}{\rho_f}\right)(ff\,'' + f\,'f\,') + \\ + \left(1 - \phi + \phi\frac{\rho_s}{\rho_f}\frac{\beta_s}{\beta_f}\right)\lambda t(\eta) + \left[1 + \frac{3\left(\frac{\sigma_s}{\sigma_f} - 1\right)\phi}{\left(\frac{\sigma_s}{\sigma_f} + 2\right) - \left(\frac{\sigma_s}{\sigma_f} - 1\right)\phi}\right](M)f\,'f\,' = 0,\ \text{for } \gamma Al_2O_3 - H_2O \end{array}\right\} \tag{3.17}$$

$$\left.\begin{array}{c} (306\phi^2 - 0.19\phi + 1)f\,''' + \left(1 - \phi + \phi\frac{\rho_s}{\rho_f}\right)(ff\,'' + f\,'f\,') + \\ \left(1 - \phi + \phi\frac{\rho_s}{\rho_f}\frac{\beta_s}{\beta_f}\right)\lambda t(\eta) + \left[1 + \frac{3\left(\frac{\sigma_s}{\sigma_f} - 1\right)\phi}{\left(\frac{\sigma_s}{\sigma_f} + 2\right) - \left(\frac{\sigma_s}{\sigma_f} - 1\right)\phi}\right](M)f\,'f\,' = 0,\ \text{for } \gamma Al_2O_3 - C_2H_6O_2 \end{array}\right\} \tag{3.18}$$

$$\left.\begin{array}{c} (4.97\phi^2 + 2.72\phi + 1)t''(\eta) \\ +\Psi^\circ \left[\begin{array}{c} \left(1 - \phi + \phi\frac{(\rho c_p)_s}{(\rho c_p)_f}\right)t'(\eta) + \left[1 + \frac{3\left(\frac{\sigma_s}{\sigma_f} - 1\right)\phi}{\left(\frac{\sigma_s}{\sigma_f} + 2\right) - \left(\frac{\sigma_s}{\sigma_f} - 1\right)\phi}\right](M)(Ec)f\,'f\,' \\ + \left(123\phi^2 + 7.3\phi + 1\right)(Ec)(f\,''(\eta))^2 + \delta t(\eta) \end{array}\right] = 0 \\ \text{for } \gamma Al_2O_3 - H_2O \end{array}\right\}, \tag{3.19}$$

$$\left.\begin{array}{c} (28.905\phi^2 + 2.8273\phi + 1)t''(\eta) \\ +\Psi^\circ \left[\begin{array}{c} \left(1 - \phi + \phi\frac{(\rho c_p)_s}{(\rho c_p)_f}\right)t'(\eta) + \left[1 + \frac{3\left(\frac{\sigma_s}{\sigma_f} - 1\right)\phi}{\left(\frac{\sigma_s}{\sigma_f} + 2\right) - \left(\frac{\sigma_s}{\sigma_f} - 1\right)\phi}\right](M)(Ec)f\,'f\,' \\ + \left(306\phi^2 - 0.19\phi + 1\right)(Ec)(f\,''(\eta))^2 + \delta t(\eta) \end{array}\right] = 0 \\ \text{for } \gamma Al_2O_3 - C_2H_6O_2 \end{array}\right\}, \tag{3.20}$$

$$f(0) = 0,\ f\,'(0) - 1 = 0,\ f\,'(\infty) = 0, \tag{3.21}$$

$$t(0) = 0, \quad t(\infty) - 1 = 0, \tag{3.22}$$

$$\frac{(\mathrm{Pr})_f \left(1 - \phi + \phi \frac{\rho_s}{\rho_f}\right) (82.1\phi^2 + 3.9\phi + 1)}{\left(123\phi^2 + 7.3\phi + 1\right)} f(0) + \left(1 - \phi + \phi \frac{(c_p)_s}{(c_p)_f}\right) (Mn) t'(0) = 0, \tag{3.23}$$

$$\frac{(\mathrm{Pr})_f \left(1 - \phi + \phi \frac{\rho_s}{\rho_f}\right) (254.3\phi^2 - 3\phi + 1)}{\left(306\phi^2 - 0.19\phi + 1\right)} f(0) + \left(1 - \phi + \phi \frac{(c_p)_s}{(c_p)_f}\right) (Mn) t'(0) = 0, \tag{3.24}$$

$$(\mathrm{Pr})_f \left(1 - \phi + \phi \frac{\rho_s}{\rho_f}\right) f(0) + \left(4.97\phi^2 + 2.72\phi + 1\right) t'(0) = 0, \tag{3.25}$$

$$(\mathrm{Pr})_f \left(1 - \phi + \phi \frac{\rho_s}{\rho_f}\right) f(0) + \left(28.905\phi^2 + 2.8273\phi + 1\right) t'(0) = 0, \tag{3.26}$$

where Ψ° in absence of effective Prandtl number via $\gamma Al_2O_3 - H_2O$ and $\gamma Al_2O_3 - C_2H_6O_2$ nanofluids is given as

$$\Psi^{\circ} = \frac{(\mathrm{Pr})_f \left(1 - \phi + \phi \frac{\rho_s}{\rho_f}\right)}{4.97\phi^2 - 2.72\phi + 1}, \tag{3.27}$$

$$\Psi^{\circ} = \frac{(\mathrm{Pr})_f \left(1 - \phi + \phi \frac{\rho_s}{\rho_f}\right)}{28.905\phi^2 + 2.8273\phi + 1}, \tag{3.28}$$

$$\Psi^{\circ} = \frac{(\mathrm{Pr})_f \left(1 - \phi + \phi \frac{\rho_s}{\rho_f}\right) (82.1\phi^2 + 3.9\phi + 1)}{123\phi^2 + 7.3\phi + 1}, \tag{3.29}$$

$$\Psi^{\circ} = \frac{(\mathrm{Pr})_f \left(1 - \phi + \phi \frac{\rho_s}{\rho_f}\right) (254.3\phi^2 - 3\phi + 1)}{306\phi^2 - 0.19\phi + 1}, \tag{3.30}$$

Note that incompressibility condition is satisfied.

3.4 Engineering curiosity

3.4.1 Drag force ($\mathbf{C}_f$)

Mathematical description of skin friction is define by

$$C_f = \frac{\tau_w}{\rho_f u_w^2}, \tag{3.31}$$

$$\left. \tau_w = -2\mu_{nf}\big|_{y=0} \left.\frac{\partial u}{\partial y}\right|_{y=0} \right\}. \tag{3.32}$$

From above equations we get

$$\left. \begin{array}{r} \frac{1}{2}\sqrt{\mathrm{Re}_x}C_f = -\left(123\phi^2 + 7.3\phi + 1\right) f\,''(0) \text{ for } \gamma Al_2O_3 - H_2O, \\ \frac{1}{2}\sqrt{\mathrm{Re}_x}C_f = -\left(306\phi^2 - 0.19\phi + 1\right) f\,''(0) \text{ for } \gamma Al_2O_3 - C_2H_6O_2 \end{array} \right\}. \tag{3.33}$$

3.4.2 Heat transfer rate

Mathematically we have

$$Nu = \frac{xq_w}{k_f\left(T_w - T_\infty\right)}, \tag{3.34}$$

where q_w is expressed as

$$q_w = -k_{nf}\left(\frac{\partial T}{\partial y}\right)_{y=0}. \tag{3.35}$$

Through Eqs. (3.34) and Eq. (3.35) we have

$$\left. \begin{array}{r} (\mathrm{Re}_x)^{-1/2}Nu_x = \left[(4.97\phi^2 + 2.72\phi + 1)t'(0)\right] \text{ for } \gamma Al_2O_3 - H_2O, \\ (\mathrm{Re}_x)^{-1/2}Nu_x = \left[(28.905\phi^2 + 2.8273\phi + 1)t'(0)\right] \text{ for } \gamma Al_2O_3 - C_2H_6O_2, \end{array} \right\} \tag{3.36}$$

3.5 Entropy expression

Entropy rate (N_G) is the ratio of volumetric (E_g) to normal $(E_g)_0$ entropy rate i.e.,

$$N_G = \frac{E_g}{(E_g)_0}, \tag{3.37}$$

$$E_g = \frac{k_{nf}}{T_\infty^2}\left(\frac{\partial T}{\partial y}\right)^2 + \frac{\sigma_{nf} B_o^2}{T_m} u^2 + \frac{\mu_{nf}}{T_\infty}\left(\frac{\partial u}{\partial y}\right)^2 \Bigg\}, \tag{3.38}$$

$$(E_g)_0 = \frac{k_{nf}}{T_\infty^2}\frac{(\Delta T)}{x^2}, \tag{3.39}$$

Entropy generation in non-dimensional form for both ($\gamma Al_2O_3 - H_2O$ and $\gamma Al_2O_3 - C_2H_6O_2$) nanofluids are

$$\left.\begin{array}{c} N_G = \left[(4.97\phi^2 + 2.72\phi + 1)t'^2(0)\right] + \left[\frac{123\phi^2+7.3\phi+1}{4.97\phi^2+2.72\phi+1}\right]\frac{Br}{\Omega}\operatorname{Re} f\ ''^2 \\ + \left[1 + \frac{3\left(\frac{\sigma_s}{\sigma_f}-1\right)\phi}{\left(\frac{\sigma_s}{\sigma_f}+2\right)-\left(\frac{\sigma_s}{\sigma_f}-1\right)\phi}\right](M)\frac{Br}{\Omega}\operatorname{Re} f\ '^2 \\ \text{for } \gamma Al_2O_3 - H_2O \end{array}\right\}, \tag{3.40}$$

$$\left.\begin{array}{c} N_G = \left[(28.905\phi^2 + 2.8273\phi + 1)t'^2(0)\right] + \left[\frac{306\phi^2-0.19\phi+1}{28.905\phi^2+2.8273\phi+1}\right]\frac{Br}{\Omega}\operatorname{Re} f\ ''^2 \\ + \left[1 + \frac{3\left(\frac{\sigma_s}{\sigma_f}-1\right)\phi}{\left(\frac{\sigma_s}{\sigma_f}+2\right)-\left(\frac{\sigma_s}{\sigma_f}-1\right)\phi}\right](M)\frac{Br}{\Omega}\operatorname{Re} f\ '^2 \\ \text{for } \gamma Al_2O_3 - C_2H_6O_2 \end{array}\right\}, \tag{3.41}$$

In non-dimensional form, Bejan number is

$$\left.\begin{array}{c} Be = \dfrac{\left[(4.97\phi^2+2.72\phi+1)t'^2(0)\right]}{\begin{array}{c}\left[(4.97\phi^2 + 2.72\phi + 1)t'^2(0)\right] + \left[\frac{123\phi^2+7.3\phi+1}{4.97\phi^2+2.72\phi+1}\right]\frac{Br}{\Omega}\operatorname{Re} f\ ''^2 \\ + \left[1 + \frac{3\left(\frac{\sigma_s}{\sigma_f}-1\right)\phi}{\left(\frac{\sigma_s}{\sigma_f}+2\right)-\left(\frac{\sigma_s}{\sigma_f}-1\right)\phi}\right](M)\frac{Br}{\Omega}\operatorname{Re} f\ '^2\end{array}}, \\ \text{for } \gamma Al_2O_3 - H_2O \end{array}\right\} \tag{3.42}$$

$$
\left.\begin{aligned}
Be = \frac{\left[(28.905\phi^2 + 2.8273\phi + 1)t'^2(0)\right]}{\left[(28.905\phi^2 + 2.8273\phi + 1)t'^2(0)\right] + \left[\frac{306\phi^2 - 0.19\phi + 1}{28.905\phi^2 + 2.8273\phi + 1}\right]\frac{Br}{\Omega}\operatorname{Re} f''^2}, \ \gamma Al_2O_3 - C_2H_6O_2 \\
+ \left[1 + \frac{3\left(\frac{\sigma_s}{\sigma_f} - 1\right)\phi}{\left(\frac{\sigma_s}{\sigma_f} + 2\right) - \left(\frac{\sigma_s}{\sigma_f} - 1\right)\phi}\right](M)\frac{Br}{\Omega}\operatorname{Re} f'^2
\end{aligned}\right\} \tag{3.43}
$$

3.5.1 Dimensionless parameters

$$
\left.\begin{aligned}
\lambda\left(= \frac{Gr_x}{\operatorname{Re}_x^2}\right), \ (\Pr)_f\left(\frac{\nu_f}{\alpha}\right), \ Gr_x\left(= \frac{g\beta_f(T - T_m)}{\nu_f}\right), \\
\operatorname{Re}_x\left(= \frac{u_w x}{\nu_f}\right), \ M\left(= \frac{\sigma_f B_0^2}{\rho_f a}\right), \ Mn(= \frac{(c_p)_f[T_\infty - T_m]}{\lambda^* + c_s[T_m - T_0]}), \\
Ec(= \frac{a u_w^2}{(T_\infty - T_m)(c_p)_f}), \ \delta(= \frac{Q_o}{(\rho c_p)_f}), \ Br\left(= \frac{\mu_f}{k_f \Delta T}\right), \ \Omega\left(= \frac{\Delta T}{T_\infty}\right)
\end{aligned}\right\}. \tag{3.44}
$$

3.6 Solution methodology

The governing flow expressions $(3.17-3.20)$ with boundary conditions $(3.20-3.21)$ are solved via built-in-Shooting technique. Computational solutions are identified and analyzed utilizing plots.

3.7 Results and discussion

3.7.1 Velocity components

Figs. $[3.1(a), 3.1(b)]$ show the impact of (ϕ) on $(f'(\eta))$. Here we noted that for $(\phi = 0.01, 0.03, 0.05, 0.07, 0.09)$ the $(f'(\eta))$ enhances for both $\gamma Al_2O_3 - H_2O$ and $\gamma Al_2O_3 - C_2H_6O_2$. Infact for deferment of nano-sized particles in base fluid the cohesive forces between fluid particles become greater. Figs. $[3.2(a), 3.2(b)]$ describe the behavior of $(f'(\eta))$ for $(M = 0.0, 0.3, 0.6, 0.9, 1.2)$. Physically magnetic parameter (M) is associated with Lorentz (electromagnetic) force so larger (M) produce more resistance therefore velocity declines. Performance of $(f'(\eta))$ with respect to (Mn) is conscripted through Figs. $[3.3(a), 3.3(b)]$. Velocity rapidly enhances for higher values of (Mn)

for both $\gamma Al_2O_3 - H_2O$ and $\gamma Al_2O_3 - C_2H_6O_2$ nanofluids.

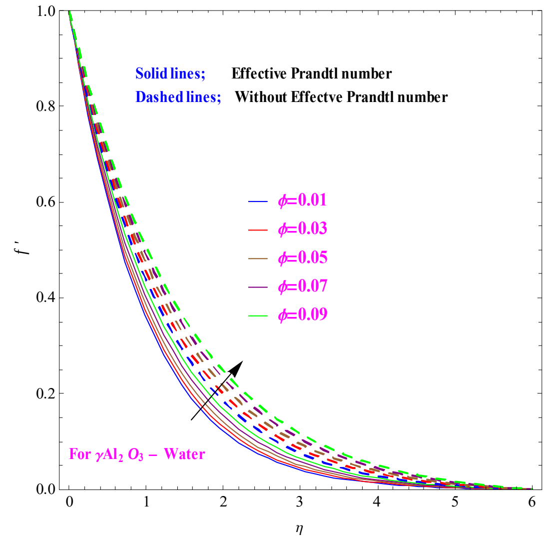

Fig. 3.1(a) : ϕ on f'.

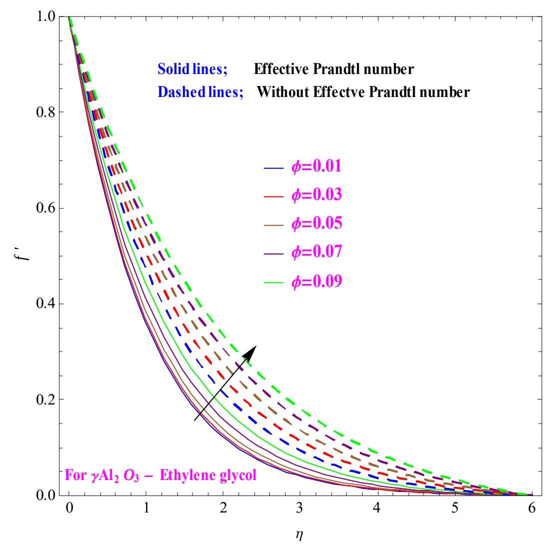

Fig. 3.1(b) : ϕ on f'.

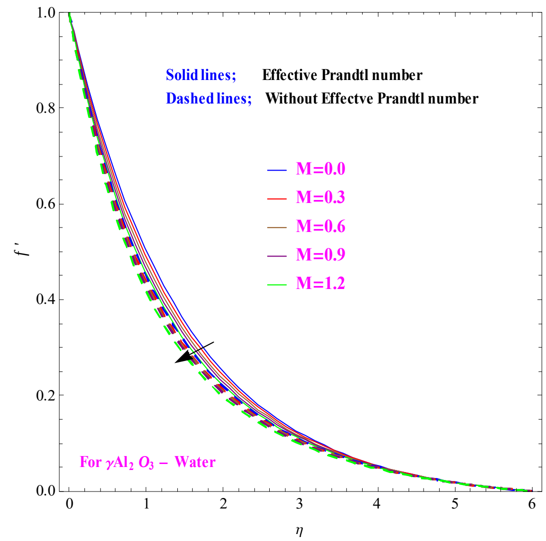

Fig. 3.2(a) : M on f'.

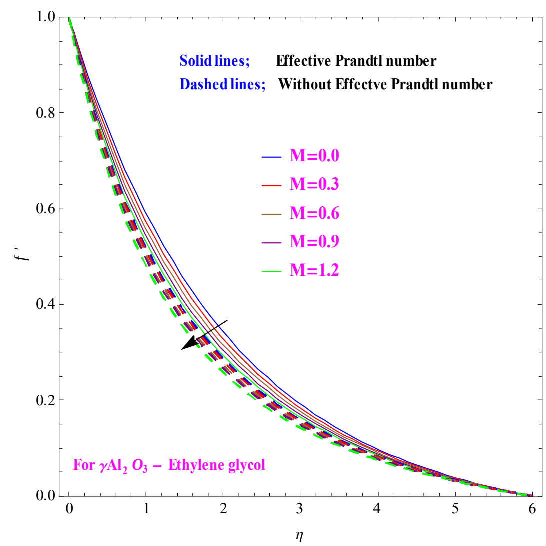

Fig. 3.2(b) : M on f'.

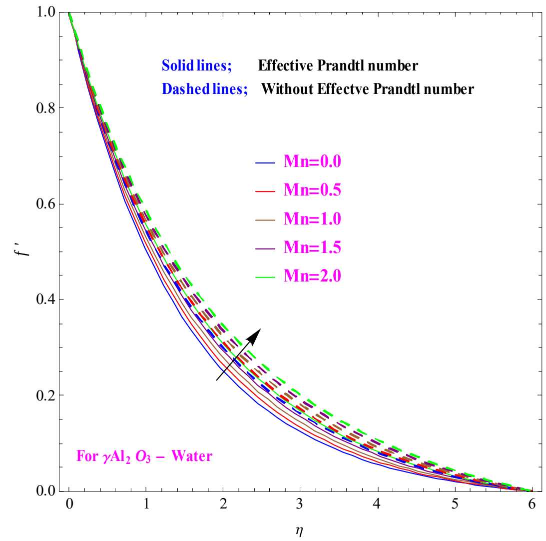

Fig. 3.3(a) : Mn on f'.

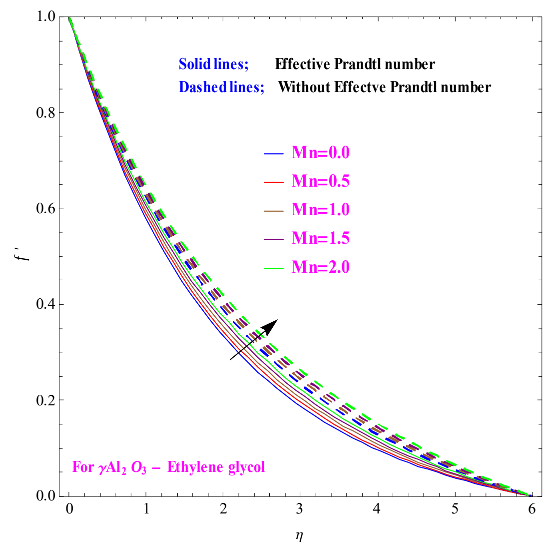

Fig. 3.3(b) : Mn on f'.

3.7.2 Temperature

Figs. $[3.4(a), 3.4(b)]$ demonstrate the impact of volume fraction (ϕ) on Temperature. Temperature enhances in case of effective Prandtl number (EPN) whereas opposite scenario is noticed in the absence of effective Prandtl number (EPN). Ethylene glycol thermal conductivity is less than water. Impact of (M) on $t(\eta)$ is examined in Figs. $[3.5(a), 3.5(b)]$. Physically electromagnetic force gives more resistance to motion of fluid. Therefore more heat is produced inside the system and thus temperature increases. Outcomes of (Mn) on $t(\eta)$ is presented in Figs. $[3.6(a), 3.6(b)]$. Since melting causes surface and fluid temperature reduce therefore the temperature $t(\eta)$ declines (see [Figs. $[3.6(a), 3.6(b)]$]).

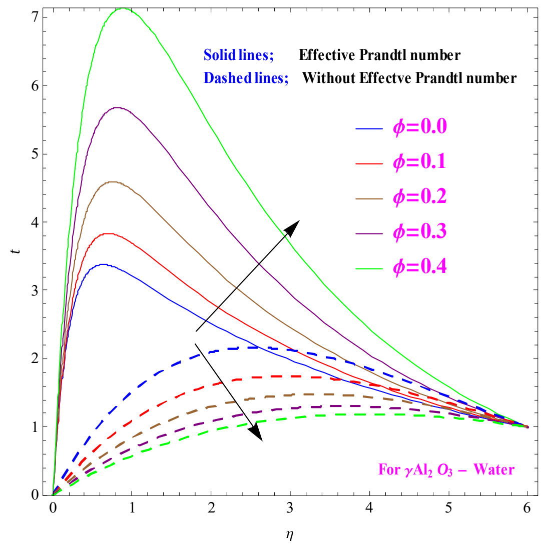

Fig. $3.4(a)$: ϕ on t.

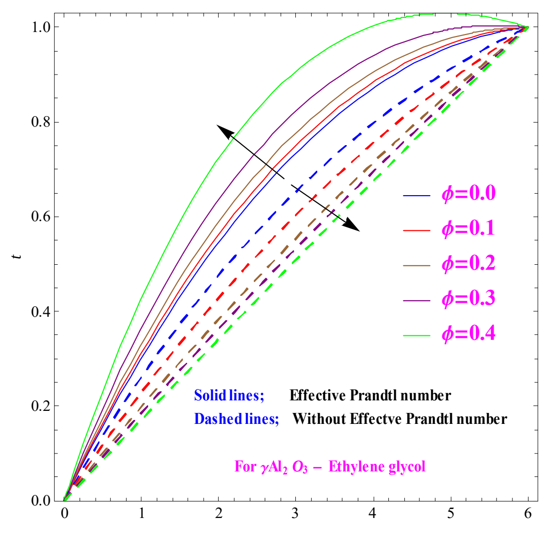

Fig. $3.4(b)$: ϕ on t.

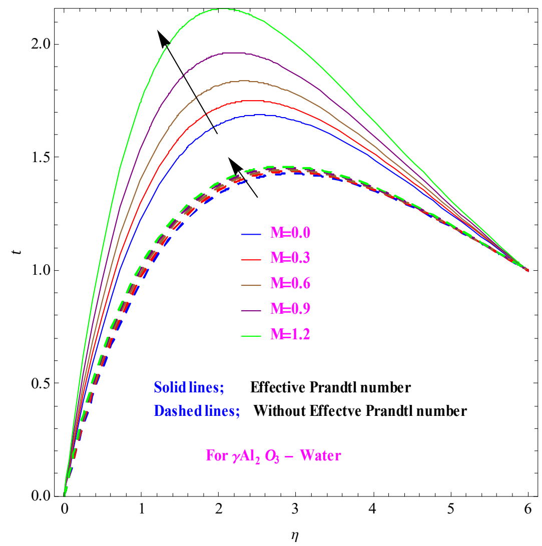

Fig. 3.5(a) : M on t.

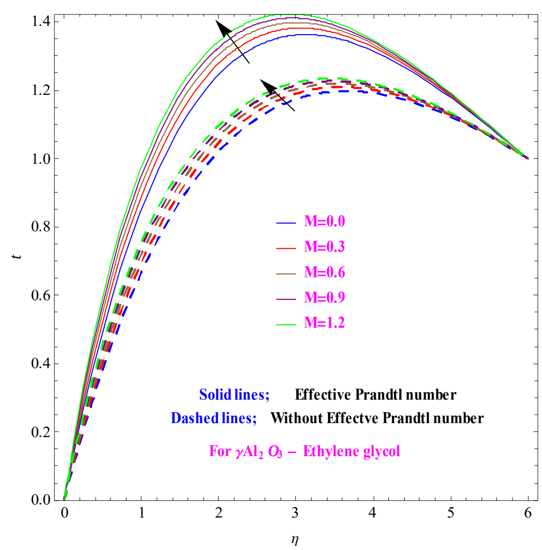

Fig. 3.5(b) : M on t.

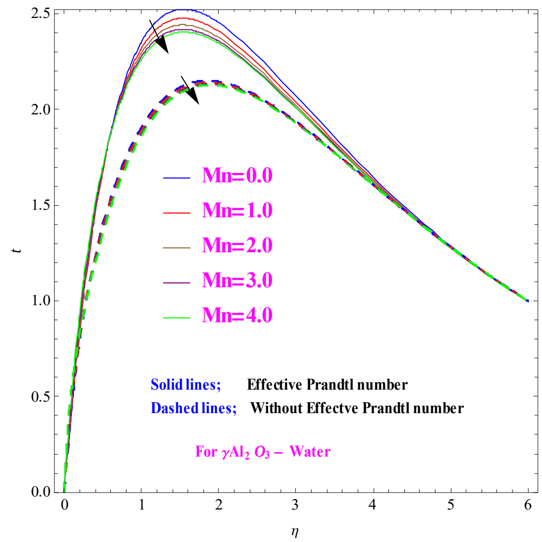

Fig. 3.6(a) : Mn on t.

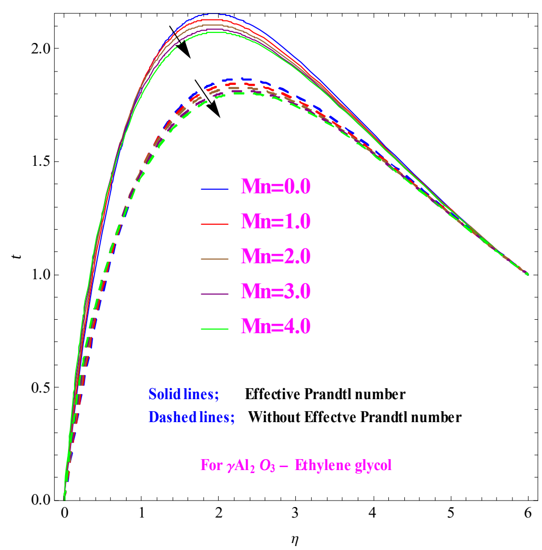

Fig. 3.6(b) : Mn on t.

3.7.3 Entropy and Bejan number

Figs. $[3.7(a), 3.7(b)]$ and $[3.8(a), 3.8(b)]$ are displayed for the behavior of (M) on $N_G(\eta)$ and Be respectively. For $(M = 0.0, 0.3, 0.6, 0.9, 1.2)$ $N_G(\eta)$ is increased. Clearly electromagnetic force produces extra disturbance in the system. Therefore $N_G(\eta)$ enhances for both $\gamma Al_2O_3 - H_2O$ and $\gamma Al_2O_3 - C_2H_6O_2$ nanofluids. Rate of heat transfer in both cases is less dominant than total irreversibilities. As a result (Be) is reduced (see Figs $[3.8(a), 3.8(b)]$).

Figs. $[3.9(a), 3.9(b)]$ and $[3.10(a), 3.10(b)]$ show behaviors of $(N_G(\eta))$ and (Be) for increasing values of (Br) for both $\gamma Al_2O_3 - H_2O$ and $\gamma Al_2O_3 - C_2H_6O_2$ nanofluids. Thermal energy of the elements as well as disorderliness inside the structure improves for larger (Br) which subsequently upsurges $(N_G(\eta))$. Figs. $[3.10(a), 3.10(b)]$ present that Be reduces for $(Br = 0.1, 0.2, 0.3, 0.4, 0.5)$. Figs. $[3.11(a), 3.11(b)]$ and $[3.12(a), 3.12(b)]$ show the increment of Re on $N_G(\eta)$ and Be. Entropy increases for $(\mathrm{Re} = 0.1, 0.2, 0.3, 0.4, 0.5)$ however Be decreases for $(\mathrm{Re} = 0.1, 0.2, 0.3, 0.4, 0.5)$. Physically for growing standards of $(\mathrm{Re} = 0.1, 0.2, 0.3, 0.4, 0.5)$ extra disturbance in the liquid elements is noted. Thus more heat transfer upsurges $(N_G(\eta))$. Total heat transfer outcome is conquered by total entropy. That is why (Be) is diminished.

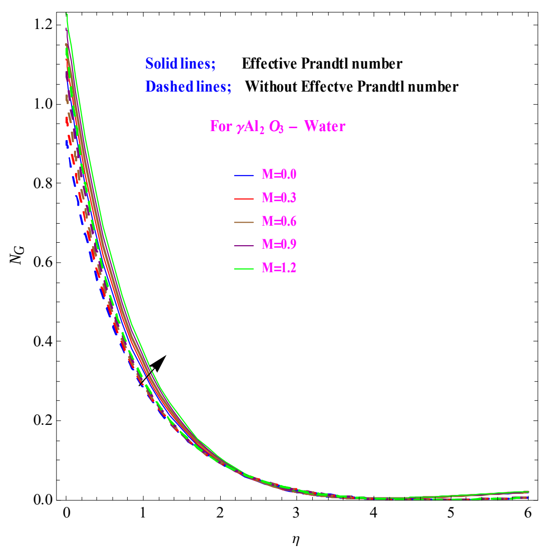

Fig. $3.7(a)$: M on N_G.

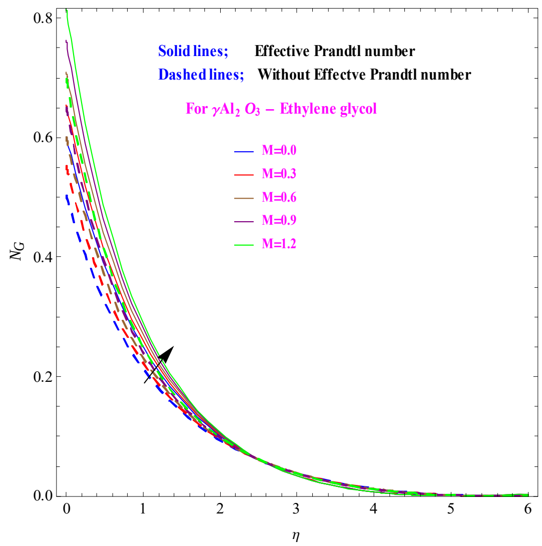

Fig. 3.7(b) : M on N_G.

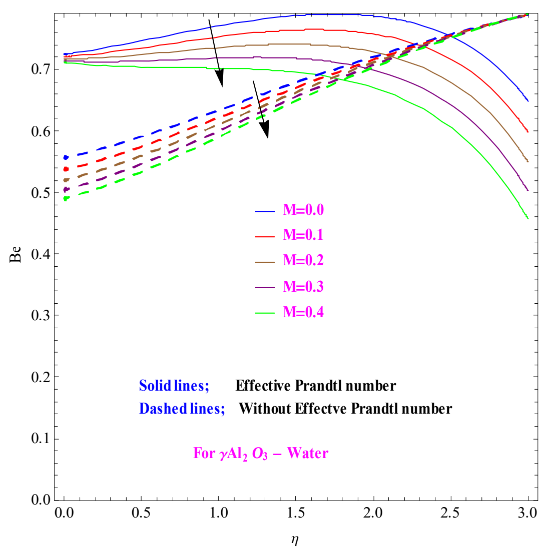

Fig. 3.8(a) : M on Be.

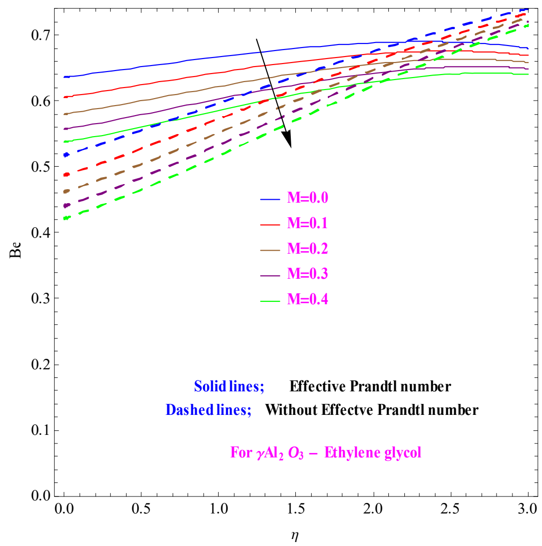

Fig. 3.8(b) : M on Be.

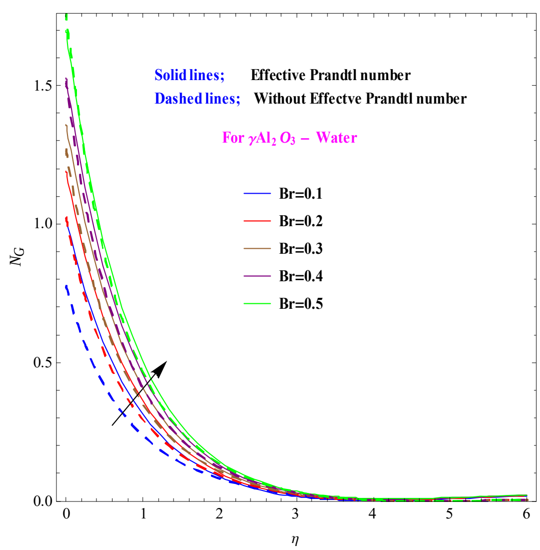

Fig. 3.9(a) : Br on N_G.

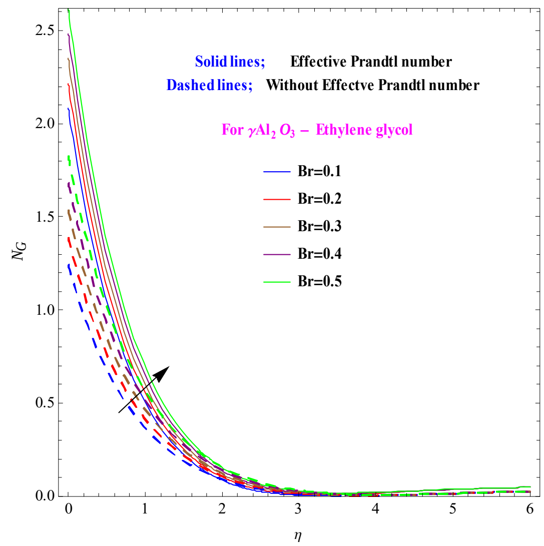

Fig. 3.9(b) : Br on N_G.

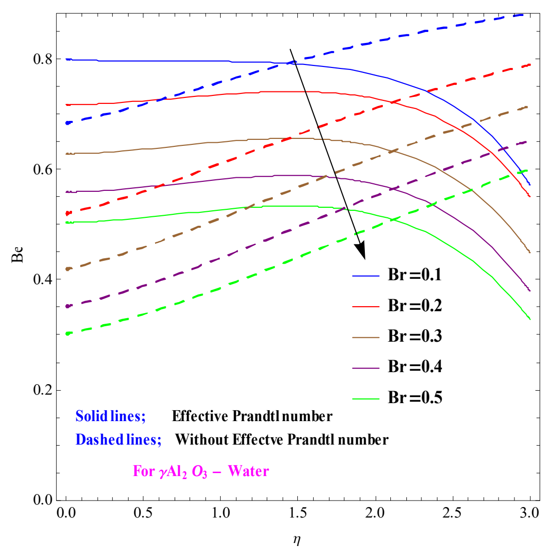

Fig. 3.10(a) : Br on Be.

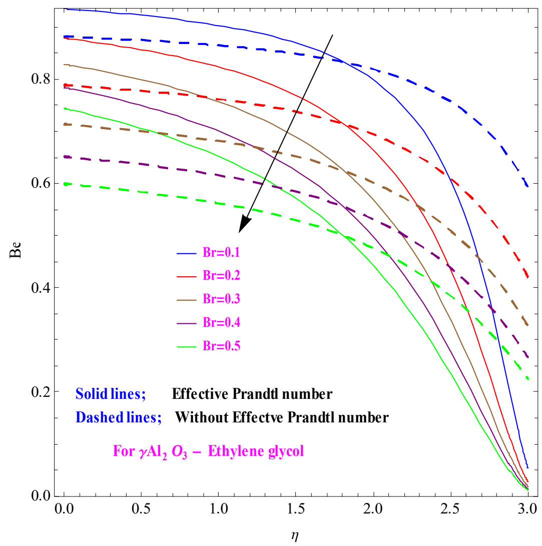

Fig. 3.10(b) : Br on Be.

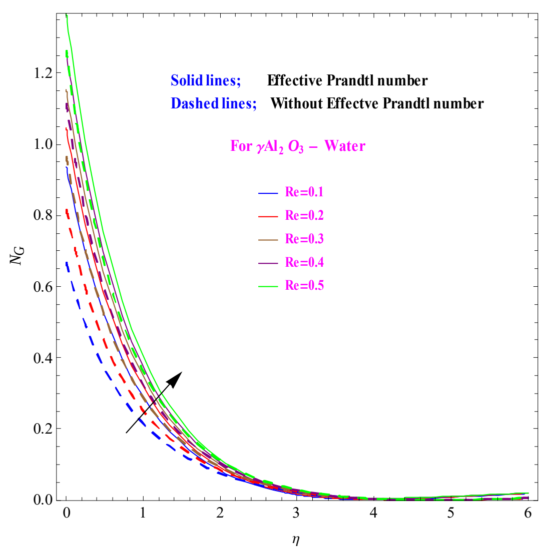

Fig. 3.11(a) : Re on N_G.

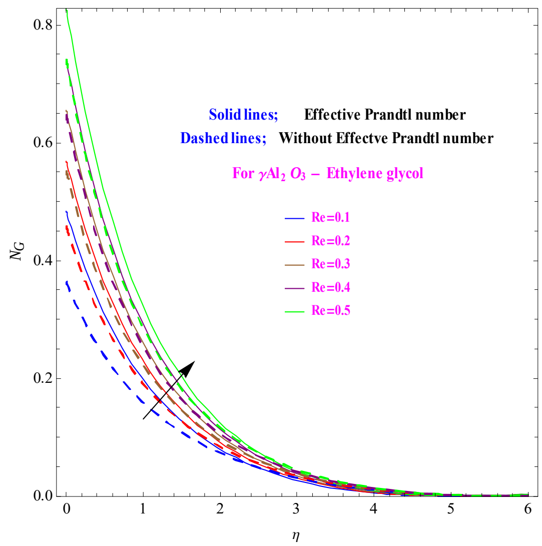

Fig. 3.11(b):Re on N_G.

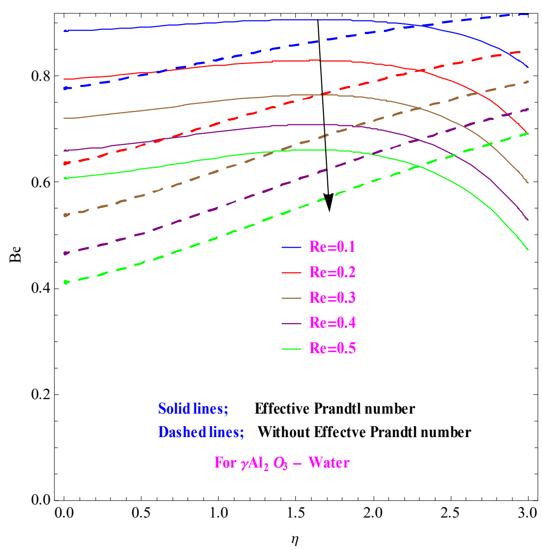

Fig. 3.12(a) : Re on Be.

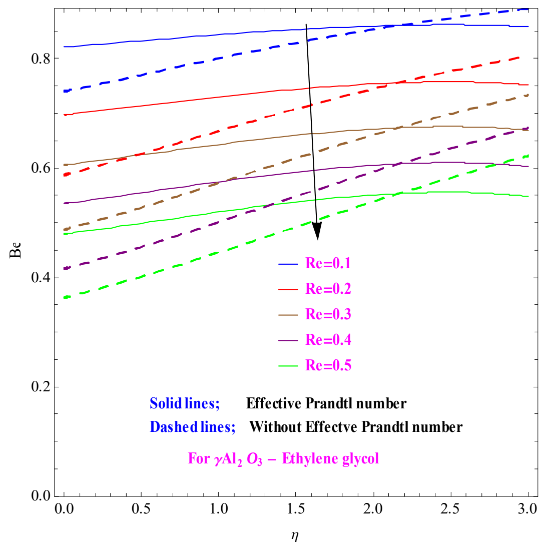

Fig. 3.12(b):Re on Be.

3.8 Engineering curiosity

Tables (3.3) and (3.4) show outcomes of (ϕ), (M) and (λ) on C_f for both $\gamma Al_2O_3 - H_2O$ and $\gamma Al_2O_3 - C_2H_6O_2$ nanofluids. Drag force enhances for larger (M) and (λ) whereas reverse performance is noted for ($\phi = 0.01, 0.02, 0.03$). Tables (3.5, 3.6) reveal that for ($M = 0.1, 0.2, 0.3$), ($Mn = 0.1, 0.2, 0.3$) and ($Ec = 0.1, 0.2, 0.3$) the heat transfer rate increases for both $\gamma Al_2O_3 - H_2O$ and $\gamma Al_2O_3 - C_2H_6O_2$ nanofluids respectively.

3.8.1 Table 3.3

ϕ	M	λ	C_f for $(\gamma Al_2O_3 - H_2O)$	
			With effective Prandtl number	Without effective Prandtl number
0.01			1.96568	5.94156
0.02			0.99038	1.13117
0.03			0.62106	0.78824
	0.1		1.84676	2.28791
	0.2		1.88411	2.33051
	0.3		1.89012	2.37241
		0.1	1.84676	2.28791
		0.2	1.66873	2.58856
		0.3	1.48412	2.78598

3.8.2 Table 3.4

ϕ	M	λ	Skin friction subject to $(\gamma Al_2O_3 - C_2H_6O_2)$	
			With effective Prandtl number	Without effective Prandtl number
0.01			1.58137	0.74676
0.02			0.63572	1.42721
0.03			0.25109	1.52724
	0.1		2.19881	2.32507
	0.2		2.25331	2.38128
	0.3		2.30667	2.43634
		0.1	2.19881	2.32507
		0.2	2.37271	2.48768
		0.3	2.57872	2.67905

3.8.3 Table 3.5

M	Mn	Ec	Transfer rate subject to $(\gamma Al_2O_3 - H_2O)$	
			With effective Prandtl number	Without effective Prandtl number
0.1			2.53315	1.86582
0.2			2.56957	1.88775
0.3			2.60705	1.90925
	0.1		2.53315	1.86582
	0.2		2.54897	1.88486
	0.3		2.56644	1.90522
		0.1	2.21374	1.52907
		0.2	2.32026	1.64006
		0.3	2.42674	1.75232

3.8.4 Table 3.6

M	Mn	Ec	Heat transfer rate subject to $(\gamma Al_2O_3 - C_2H_6O_2)$	
			With effective Prandtl number	Without effective Prandtl number
0.1			1.87578	1.40596
0.2			1.90829	1.43021
0.3			1.93996	1.45384
	0.1		1.87578	1.40596
	0.2		1.86725	1.41341
	0.3		1.85915	1.42124
		0.1	1.60562	1.19401
		0.2	1.69539	1.26424
		0.3	1.78551	1.33489

3.9 Final remarks

- Velocity enhances for larger (ϕ) and (Mn) for both $\gamma Al_2O_3 - H_2O$ and $\gamma Al_2O_3 - C_2H_6O_2$ nanofluids.
- In melting case fluid temperature reduces.
- (Be) reduces for ($\mathrm{Re} = 0.1, 0.2, 0.3, 0.4, 0.5$) but opposite response is seen for $N_G(\eta)$.
- (C_f) is increased for higher (M).
- Heat transfer rate upsurges for more (M) and (Mn).

Chapter 4

Entropy generation in MHD flow of viscous fluid subject to aluminum (γAl_2O_3) and ethylene glycol $(C_2H_6O_2)$ nanoparticles

This chapter analyzed the MHD (2D) flow of viscous fluid with alumina-water $(\gamma Al_2O_3 - H_2O)$ and ethylene-glycol $(\gamma Al_2O_3 - C_2H_6O_2)$ over a stretched surface. Thermal radiation and Joule heating are examined. Electric field is absent. Uniform magnetic field is applied normal to the sheet. Momentum slip is also taken into account for both $(\gamma Al_2O_3 - H_2O \ and \ \gamma Al_2O_3 - C_2H_6O_2)$ nanofluids. The relevant equation are solved via built-in- Shooting method. The various flow parameters are graphically discussed. Skin friction and Sherwood and Nusselt numbers are calculated numerically and analyzed through Tables.

4.1 Modelling

We scrutinize MHD two-dimensional (2D) flow of $(\gamma Al_2O_3 - H_2O$ and $\gamma Al_2O_3 - C_2H_6O_2)$ nanofluids over a stretched surface. Extra heating factors like thermal radiation, Joule heating and viscous dissipation is taken in energy equation. Slip effect is considered on boundary of sheet. Thermophysical properties of both nanoparticles are given in Table (4.1). Relevant expressions are as follow.

$$\frac{\partial u}{\partial x}+\frac{\partial v}{\partial y}=0, \tag{4.1}$$

$$\left. u\frac{\partial u}{\partial x}+v\frac{\partial u}{\partial y}=\frac{\mu_{nf}}{\rho_{nf}}\frac{\partial^2 u}{\partial y^2}+g\frac{(\rho\beta)_{nf}}{\rho_{nf}}(T-T_\infty)+\frac{\sigma_{nf}}{\sigma_f}B_0^2u-\epsilon\frac{\nu_{nf}}{k}u\right\}, \tag{4.2}$$

$$\left.\begin{array}{c} u\frac{\partial T}{\partial x}+v\frac{\partial T}{\partial y}=\frac{k_{nf}}{(\rho c_p)_{nf}}\frac{\partial^2 T}{\partial y^2}+\frac{\sigma_{nf}}{(\rho c_p)_{nf}}B_0^2u^2 \\ +\frac{\mu_{nf}}{(\rho c_p)_{nf}}\left(\frac{\partial u}{\partial y}\right)^2+\frac{1}{(\rho c_p)_{nf}}\left(\frac{\partial q_r}{\partial y}\right) \end{array}\right\}, \tag{4.3}$$

$$\left.\begin{array}{c} u=U_w=ax+\beta_1\frac{\partial u}{\partial y},\quad v=0,\quad T=T_w \text{ at } y=0, \\ u=0,\quad T\to T_\infty \text{ when } y\to\infty. \end{array}\right\} \tag{4.4}$$

$$k_{nf}\left(\frac{\partial T}{\partial y}\right)_{y=0}-\rho_{nf}\left[\lambda^*+c_s\left(T_m-T_o\right)\right]v(x,0)=0. \tag{4.5}$$

Table 4.1:

	$C_p(Jk^{-1}g^{-1}K^{-1})$	$\rho(kgm^{-3})$	$\beta\times10^{-5}\left(K^{-1}\right)$	$k(Wm^{-1}K^{-1})$	$\sigma(\Omega^{-1}m^{-1})$
(Al_2O_3)	765	3970	0.85	40	10^{-12}
(H_2O)	4182	998.3	20.06	0.06	0.05
$(C_2H_6O_2)$	2382	1116.6	65	0.249	1.07×10^{-7}

4.2 Thermophysical characteristics of $(Al_2O_3-H_2O$ and $Al_2O_3-C_2H_6O_2)$ nanofluids $[82-86]$.

$$\frac{\rho_{nf}}{\rho_f}=(1-\phi)+\phi\frac{\rho_s}{\rho_f}, \tag{4.6}$$

$$\frac{(\rho c_p)_{nf}}{(\rho c_p)_f}=(1-\phi)+\phi\frac{(\rho c_p)_s}{(\rho c_p)_f}, \tag{4.7}$$

$$\frac{(\rho\beta)_{nf}}{(\rho\beta)_f}=(1-\phi)+\phi\frac{(\rho\beta)_s}{(\rho\beta)_f}, \tag{4.8}$$

$$\frac{\sigma_{nf}}{\sigma_f}=\left[1+\frac{3\left(\frac{\sigma_s}{\sigma_f}-1\right)\phi}{\left(\frac{\sigma_s}{\sigma_f}+2\right)-\left(\frac{\sigma_s}{\sigma_f}-1\right)\phi}\right] \tag{4.9}$$

$$\frac{\mu_{nf}}{\mu_f} = 123\phi^2 + 7.3\phi + 1, \text{ for } Al_2O_3 - H_2O, \tag{4.10}$$

$$\frac{\mu_{nf}}{\mu_f} = 306\phi^2 - 0.19\phi + 1 \text{ for } Al_2O_3 - C_2H_6O_2, \tag{4.11}$$

$$\frac{\Pr_{nf}}{\Pr_f} = 82.1\phi^2 + 3.9\phi + 1 \text{ for } \gamma Al_2O_3 - H_2O, \tag{4.12}$$

$$\frac{\Pr_{nf}}{\Pr_f} = 254.3\phi^2 + 3\phi + 1 \text{ for } Al_2O_3 - C_2H_6O_2, \tag{4.13}$$

$$\frac{k_{nf}}{k_f} = 4.97\phi^2 + 2.72\phi + 1 \text{ for } Al_2O_3 - H_2O, \tag{4.14}$$

$$\frac{k_{nf}}{k_f} = 28.905\phi^2 + 2.8273\phi + 1 \text{ for } Al_2O_3 - C_2H_6O_2. \tag{4.15}$$

We consider the suitable transformations

$$\frac{\eta}{y} = \sqrt{\frac{a}{\upsilon_f}},\ \frac{u}{f\,'(\eta)} = ax,\ \frac{v}{f(\eta)} = -\sqrt{a\upsilon_f},\ t(\eta) = \frac{T - T_m}{(T_\infty - T_m)}. \tag{4.16}$$

4.3 Dimensionless forms of flow equations

Through momentum and energy equations for both ($\gamma Al_2O_3 - H_2O$ and $\gamma Al_2O_3 - C_2H_6O_2$) nanofluids, we have

$$\left.\begin{array}{c} (123\phi^2 + 7.3\phi + 1)f\,''' + \left(1 - \phi + \phi\frac{\rho_s}{\rho_f}\right)(ff\,'' + f\,'^2) + \\ + \left(1 - \phi + \phi\frac{\rho_s}{\rho_f}\frac{\beta_s}{\beta_f}\right)\lambda t(\eta) + \left[1 + \frac{3\left(\frac{\sigma_s}{\sigma_f} - 1\right)\phi}{\left(\frac{\sigma_s}{\sigma_f} + 2\right) - \left(\frac{\sigma_s}{\sigma_f} - 1\right)\phi}\right] Mf\,'^2 + \\ (123\phi^2 + 7.3\phi + 1)Da^{-1}f\,' = 0,\ \text{for } \gamma Al_2O_3 - H_2O \end{array}\right\} \tag{4.17}$$

$$\left.\begin{array}{c}(306\phi^2-0.19\phi+1)f\,'''+\left(1-\phi+\phi\frac{\rho_s}{\rho_f}\right)(ff\,''+f\,'^2)+\\ \left(1-\phi+\phi\frac{\rho_s}{\rho_f}\frac{\beta_s}{\beta_f}\right)\lambda t(\eta)+\left[1+\frac{3\left(\frac{\sigma_s}{\sigma_f}-1\right)\phi}{\left(\frac{\sigma_s}{\sigma_f}+2\right)-\left(\frac{\sigma_s}{\sigma_f}-1\right)\phi}\right]Mf\,'^2+\\ (306\phi^2-0.19\phi+1)Da^{-1}f\,'=0,\ \text{for }\gamma Al_2O_3-C_2H_6O_2\end{array}\right\} \tag{4.18}$$

$$\left.\begin{array}{c}(((4.97\phi^2+2.72\phi+1)+R_d)t''(\eta))\\ +\Psi^\circ\left[\begin{array}{c}\left(1-\phi+\phi\frac{(\rho c_p)_s}{(\rho c_p)_f}\right)t'(\eta)+\left[1+\frac{3\left(\frac{\sigma_s}{\sigma_f}-1\right)\phi}{\left(\frac{\sigma_s}{\sigma_f}+2\right)-\left(\frac{\sigma_s}{\sigma_f}-1\right)\phi}\right]MEcf\,'^2\\ +\left(123\phi^2+7.3\phi+1\right)Ec(f\,''(\eta))^2\end{array}\right]=0\\ \text{for }\gamma Al_2O_3-H_2O\end{array}\right\}, \tag{4.19}$$

$$\left.\begin{array}{c}((28.905\phi^2+2.8273\phi+1)+R_d)t''(\eta))\\ +\Psi^\circ\left[\begin{array}{c}\left(1-\phi+\phi\frac{(\rho c_p)_s}{(\rho c_p)_f}\right)t'(\eta)+\left[1+\frac{3\left(\frac{\sigma_s}{\sigma_f}-1\right)\phi}{\left(\frac{\sigma_s}{\sigma_f}+2\right)-\left(\frac{\sigma_s}{\sigma_f}-1\right)\phi}\right]MEcf\,'^2\\ +\left(306\phi^2-0.19\phi+1\right)Ec(f\,''(\eta))^2\end{array}\right]=0,\text{for }\gamma Al_2O_3-C_2H_6O_2\end{array}\right\} \tag{4.20}$$

$$f(0)=0,\ f\,'(0)-\beta_2 f\,''(0)-1=0,\ f\,'(\infty)=0, \tag{4.21}$$

$$t(0)=0,\quad t(\infty)-1=0, \tag{4.22}$$

$$\frac{(\Pr)_f\left(1-\phi+\phi\frac{\rho_s}{\rho_f}\right)(82.1\phi^2+3.9\phi+1)}{\left(123\phi^2+7.3\phi+1\right)}f(0)+\left(1-\phi+\phi\frac{(c_p)_s}{(c_p)_f}\right)(Mn)t'(0)=0 \tag{4.23}$$

$$\frac{(\Pr)_f\left(1-\phi+\phi\frac{\rho_s}{\rho_f}\right)(254.3\phi^2-3\phi+1)}{\left(306\phi^2-0.19\phi+1\right)}f(0)+\left(1-\phi+\phi\frac{(c_p)_s}{(c_p)_f}\right)(Mn)t'(0)=0 \tag{4.24}$$

$$(\Pr)_f\left(1-\phi+\phi\frac{\rho_s}{\rho_f}\right)f(0)+\left(4.97\phi^2+2.72\phi+1\right)t'(0)=0 \tag{4.25}$$

$$(\mathrm{Pr})_f\left(1-\phi+\phi\frac{\rho_s}{\rho_f}\right)f(0)+\left(28.905\phi^2+2.8273\phi+1\right)t'(0)=0 \tag{4.26}$$

where Ψ° in absence of effective Prandtl number via $\gamma Al_2O_3-H_2O$ and $\gamma Al_2O_3-C_2H_6O_2$ nanofluids is given below

$$\Psi^\circ=\frac{(\mathrm{Pr})_f\left(1-\phi+\phi\frac{\rho_s}{\rho_f}\right)}{4.97\phi^2-2.72\phi+1}, \tag{4.27}$$

$$\Psi^\circ=\frac{(\mathrm{Pr})_f\left(1-\phi+\phi\frac{\rho_s}{\rho_f}\right)}{28.905\phi^2+2.8273\phi+1}, \tag{4.28}$$

$$\Psi^\circ=\frac{(\mathrm{Pr})_f\left(1-\phi+\phi\frac{\rho_s}{\rho_f}\right)(82.1\phi^2+3.9\phi+1)}{123\phi^2+7.3\phi+1}, \tag{4.29}$$

$$\Psi^\circ=\frac{(\mathrm{Pr})_f\left(1-\phi+\phi\frac{\rho_s}{\rho_f}\right)(254.3\phi^2-3\phi+1)}{306\phi^2-0.19\phi+1}, \tag{4.30}$$

4.3.1 Skin friction

Mathematically skin friction is

$$C_f=\frac{\tau_w}{\rho_f u_w^2}, \tag{4.31}$$

where (τ_w) is defined by

$$\tau_w=-2\mu_{nf}\big|_{y=0}\left.\frac{\partial u}{\partial y}\right|_{y=0}. \tag{4.32}$$

Putting Eqs. (4.32) in Eq. (4.31), we have

$$\left.\begin{aligned}\tfrac{1}{2}\sqrt{\mathrm{Re}_x}C_f&=-\left(123\phi^2+7.3\phi+1\right)f''(0)\text{ for }\gamma Al_2O_3-H_2O,\\ \tfrac{1}{2}\sqrt{\mathrm{Re}_x}C_f&=-\left(306\phi^2-0.19\phi+1\right)f''(0)\text{ for }\gamma Al_2O_3-C_2H_6O_2.\end{aligned}\right\} \tag{4.33}$$

4.3.2 Heat transfer rate

Mathematically we have

$$Nu = \frac{xq_w}{k_f\left(T_w - T_\infty\right)}, \tag{4.34}$$

where q_w is expressed as

$$q_w = -k_{nf}\left(1 + \frac{16\sigma^* T^3}{3kk_f}\right)\left(\frac{\partial T}{\partial y}\right)_{y=0}. \tag{4.35}$$

Solving Eq. (4.35) and Eq. (4.34) we have

$$\left.\begin{array}{r}(\mathrm{Re}_x)^{-1/2} Nu_x = \left[((4.97\phi^2 + 2.72\phi + 1) + R_d)t'(0)\right] \text{ for } \gamma Al_2O_3 - H_2O, \\ (\mathrm{Re}_x)^{-1/2} Nu_x = \left[((28.905\phi^2 + 2.8273\phi + 1) + R_d)t'(0)\right] \text{ for } \gamma Al_2O_3 - C_2H_6O_2.\end{array}\right\} \tag{4.36}$$

4.4 Entropy modelling

Mathematically entropy of the system obeys

$$N_G = \frac{E_g}{(E_g)_0}, \tag{4.37}$$

where $((E_g), (E_g)_0)$ is volumetric and total entropy rates respectively.

$$E_g = \frac{k_f}{T_\infty^2}\left[\frac{k_{nf}}{k_f}\left(\frac{\partial T}{\partial y}\right)^2 + \frac{16\sigma^* T^3}{3kk_f}\left(\frac{\partial T}{\partial y}\right)^2\right] + \frac{\sigma_{nf} B_o^2}{T_m}u^2 + \frac{\mu_{nf}}{T_\infty}\left(\frac{\partial u}{\partial y}\right)^2\Bigg\}. \tag{4.38}$$

$$(E_g)_0 = \frac{k_{nf}}{T_\infty^2}\frac{(\Delta T)}{x^2}, \tag{4.39}$$

The non-dimensional forms of entropy (N_G) and Bejan number (Be) for both ($\gamma Al_2O_3 - H_2O$ and $\gamma Al_2O_3 - C_2H_6O_2$) nanofluids are expressed as follows:

$$\left.\begin{array}{l} N_G = \left[((4.97\phi^2 + 2.72\phi + 1) + R_d)t'^2(0)\right] + \left[\frac{123\phi^2 + 7.3\phi + 1}{4.97\phi^2 + 2.72\phi + 1}\right]\frac{Br}{\Omega}\mathrm{Re}\, f''^2 \\ \quad + \left[1 + \frac{3\left(\frac{\sigma_s}{\sigma_f} - 1\right)\phi}{\left(\frac{\sigma_s}{\sigma_f} + 2\right) - \left(\frac{\sigma_s}{\sigma_f} - 1\right)\phi}\right](M)\frac{Br}{\Omega}\mathrm{Re}\, f'^2, \text{ for } \gamma Al_2O_3 - H_2O, \end{array}\right\} \tag{4.40}$$

$$\left.\begin{array}{c} N_G=\left[((28.905\phi^2+2.8273\phi+1)+R_d)t'^2(0)\right]+\left[\frac{306\phi^2-0.19\phi+1}{28.905\phi^2+2.8273\phi+1}\right]\frac{Br}{\Omega}\operatorname{Re} f\ ''^2 \\ +\left[1+\frac{3\left(\frac{\sigma_s}{\sigma_f}-1\right)\phi}{\left(\frac{\sigma_s}{\sigma_f}+2\right)-\left(\frac{\sigma_s}{\sigma_f}-1\right)\phi}\right](Mn)\frac{Br}{\Omega}\operatorname{Re} f\ '^2,\ \text{for } \gamma Al_2O_3-C_2H_6O_2. \end{array}\right\} \quad (4.41)$$

$$\left.\begin{array}{c} Be=\dfrac{\left[((4.97\phi^2+2.72\phi+1)+R_d)t'^2(0)\right]}{\begin{array}{c}\left[((4.97\phi^2+2.72\phi+1)+R_d)t'^2(0)\right]+\left[\frac{123\phi^2+7.3\phi+1}{4.97\phi^2+2.72\phi+1}\right]\frac{Br}{\Omega}\operatorname{Re} f\ ''^2 \\ +\left[1+\frac{3\left(\frac{\sigma_s}{\sigma_f}-1\right)\phi}{\left(\frac{\sigma_s}{\sigma_f}+2\right)-\left(\frac{\sigma_s}{\sigma_f}-1\right)\phi}\right](M)\frac{Br}{\Omega}\operatorname{Re} f\ '^2\end{array}} \\ \text{for } \gamma Al_2O_3-H_2O \end{array}\right\}, \quad (4.42)$$

$$\left.\begin{array}{c} Be=\dfrac{\left[((28.905\phi^2+2.8273\phi+1)+R_d)t'^2(0)\right]}{\begin{array}{c}\left[((28.905\phi^2+2.8273\phi+1)+R_d)t'^2(0)\right]+\left[\frac{306\phi^2-0.19\phi+1}{28.905\phi^2+2.8273\phi+1}\right]\frac{Br}{\Omega}\operatorname{Re} f\ ''^2 \\ +\left[1+\frac{3\left(\frac{\sigma_s}{\sigma_f}-1\right)\phi}{\left(\frac{\sigma_s}{\sigma_f}+2\right)-\left(\frac{\sigma_s}{\sigma_f}-1\right)\phi}\right](M)\frac{Br}{\Omega}\operatorname{Re} f\ '^2\end{array}} \\ \text{for } \gamma Al_2O_3-C_2H_6O_2 \end{array}\right\}, \quad (4.43)$$

4.4.1 Dimensionless parameters

$$\left.\begin{array}{c} \lambda\left(=\frac{Gr_x}{\operatorname{Re}_x^2}\right),\ M\left(=\frac{\sigma_f B_0^2}{\rho_f a}\right),\ \operatorname{Re}_x\left(=\frac{u_w x}{\nu_f}\right),\ Gr_x\left(=\frac{g\beta_f(T-T_m)}{\nu_f}\right), \\ Ec\left(=\frac{a u_w^2}{(T_\infty-T_m)(c_p)_f}\right),\ Mn\left(=\frac{(c_p)_f[T_\infty-T_m]}{\lambda^*+c_s[T_m-T_0]}\right),\ Br\left(=\frac{\mu_f}{k_f\Delta T}\right), \\ R_d\left(=\frac{16\sigma^* T^3}{3kk_f}\right),\ Da^{-1}\left(=\frac{\epsilon\nu_f}{k_1}\right),\ \Omega\left(=\frac{\Delta T}{T_\infty}\right). \end{array}\right\} \quad (3.44)$$

4.5 Discussion

4.5.1 Velocity field

Figs. 4.1(a,b) is described to perceive the impact of (M) on $f\ '(\eta)$. Magnetic parameter decays the velocity due to resistance produced by Lorentz force. Figs. 4.2$(a.b)$ show the impact of $f\ '(\eta)$ with respect to $\left(Da^{-1}\right)$. Since this parameter is associated with permeability of the medium so increase in velocity is observed for both ($\gamma Al_2O_3-H_2O$ and $\gamma Al_2O_3-C_2H_6O_2$) nanofluids.

Comparable result is seen for developed values of slip parameter parameter as revealed in Figs. 4.3(a, b). Impact of (λ) on $f\ '(\eta)$ is shown in Figs. 4.4(a, b). It is noted that $f\ '(\eta)$ is increased for $(\lambda = 0.0, 0.1, 0.2, 0.3, 0.4)$ through both $(\gamma Al_2O_3 - H_2O$ and $\gamma Al_2O_3 - C_2H_6O_2)$ nanofluids.

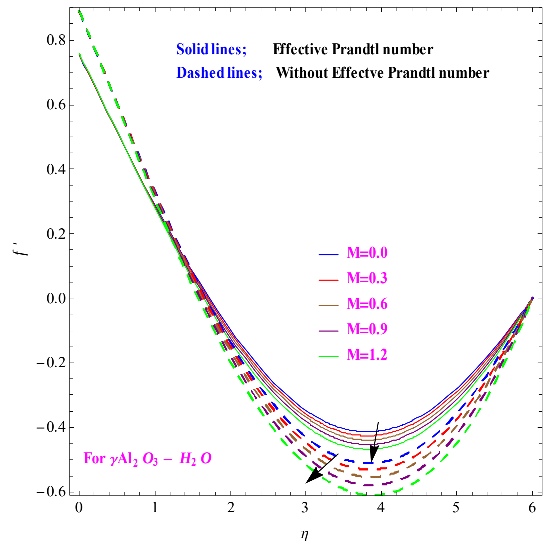

Fig. 4.1(a) : M on f'.

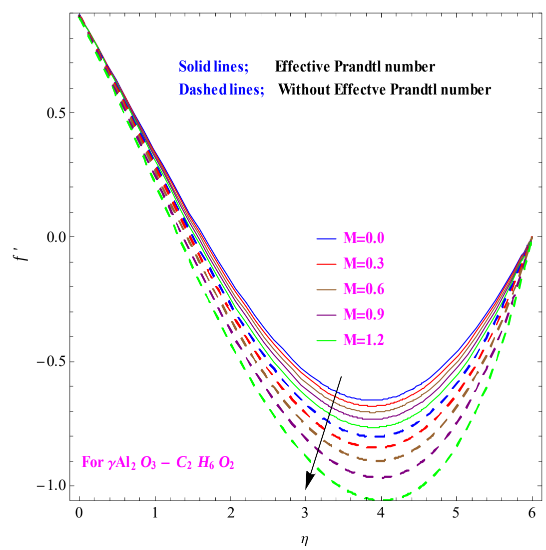

Fig. 4.1(b) : M on f'.

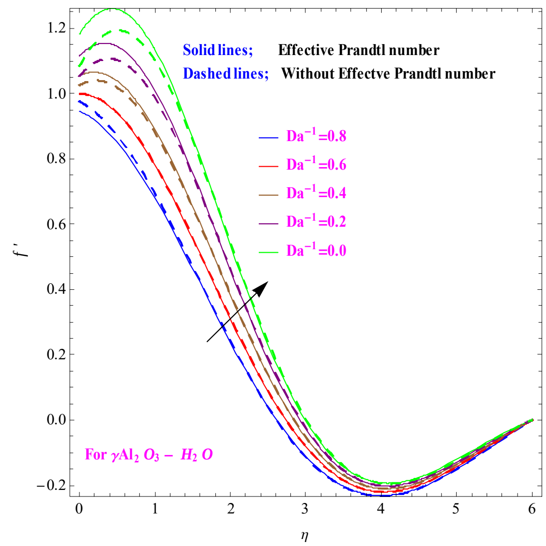

Fig. 4.2(a) : Da^{-1} on f'.

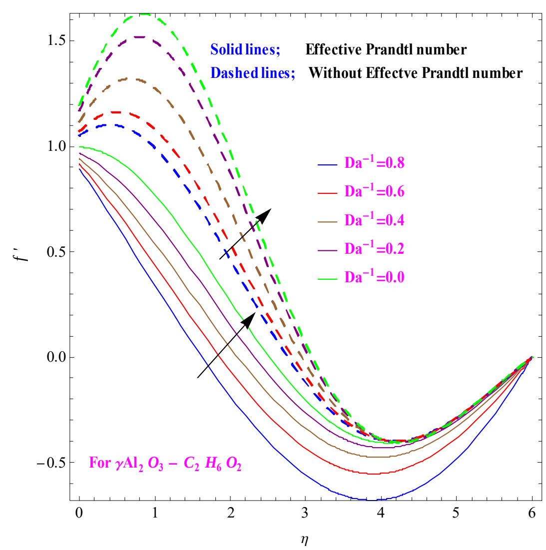

Fig. 4.2(b) : Da^{-1} on f'.

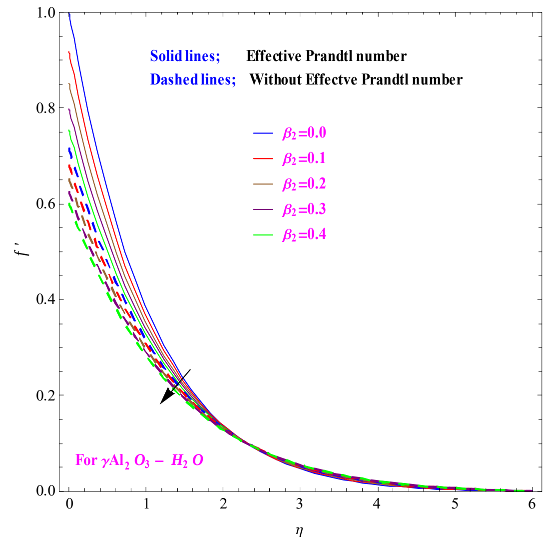

Fig. 4.3(a) : β_2 on f'.

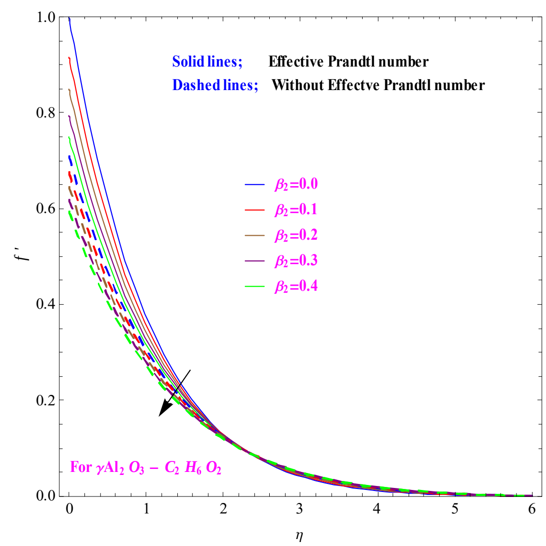

Fig. 4.3(b) : β_2 on f'.

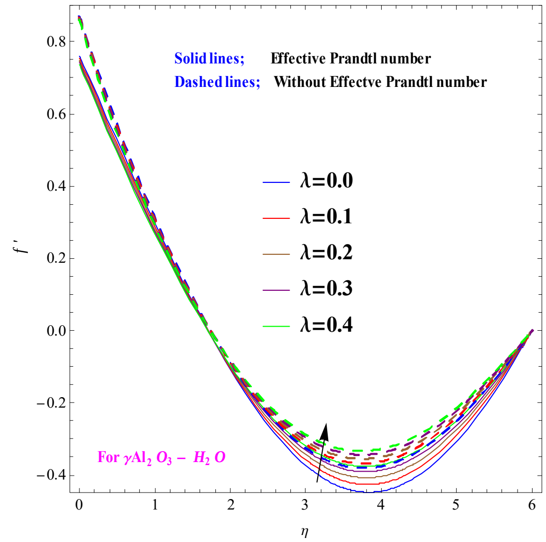

Fig. 4.4(a) : λ on f'.

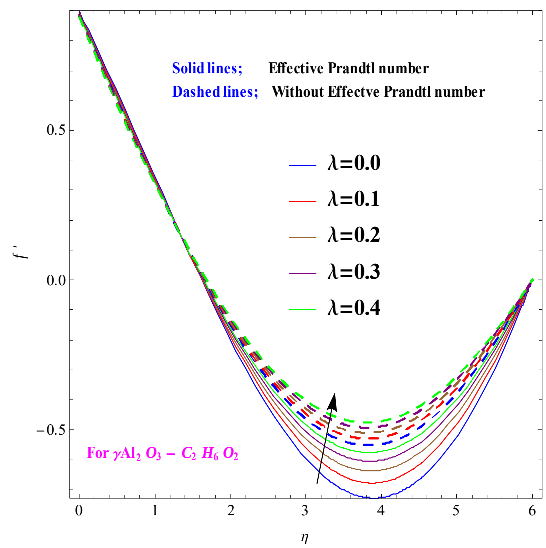

Fig. 4.4(b) : λ on f'.

4.6 Temperature field

Figs. 4.5(a, b) plots the temperature $t(\eta)$ for magnetic parameter $(M = 0.0, 0.2, 0.6, 0.8, 1.0)$ through both $(\gamma Al_2O_3 - H_2O$ and $\gamma Al_2O_3 - C_2H_6O_2)$ nanofluids. Lorentz force consequences through collision of fluid elements augmented $t(\eta)$. It is also shown via Fig . 4.6(a, b) that $(R_d = 0.0, 0.1, 0.2, 0.3, 0.4)$ always enhances $t(\eta)$ of the system due to provision of more heat. Influence of $t(\eta)$ through $(\Pr = 0.1, 0.2, 0.3, 0.4, 0.5)$ is plotted via Figs. 4.7(a, b). Increase in temperature distribution for $\gamma Al_2O_3 - H_2O$ is noted when compared with $\gamma Al_2O_3 - C_2H_6O_2$. It due the lower thermal conductivity of ethylene glycol than water.

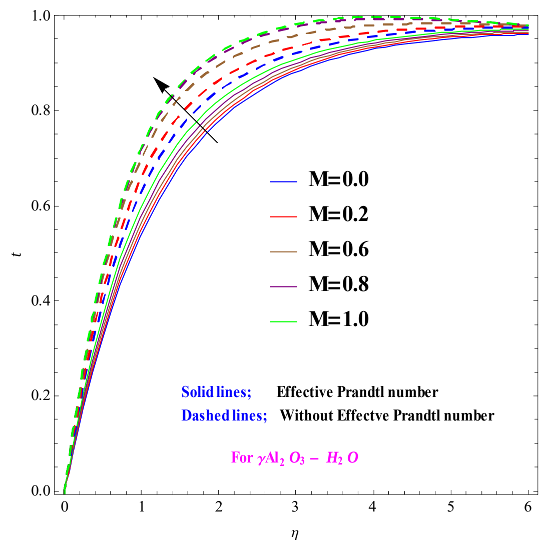

Fig. 4.5(a) : M on t.

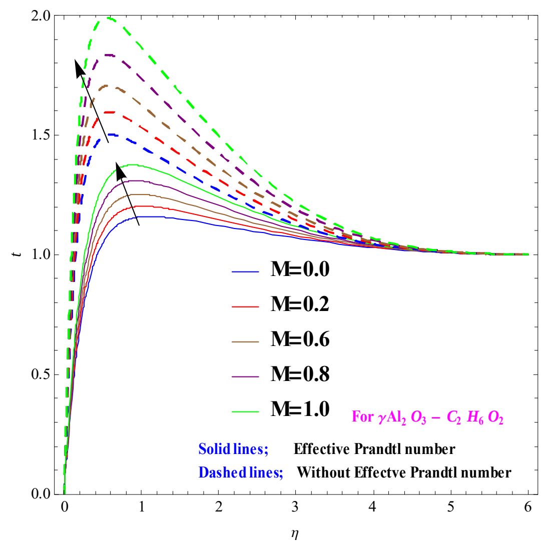

Fig. 4.5(b) : M on t.

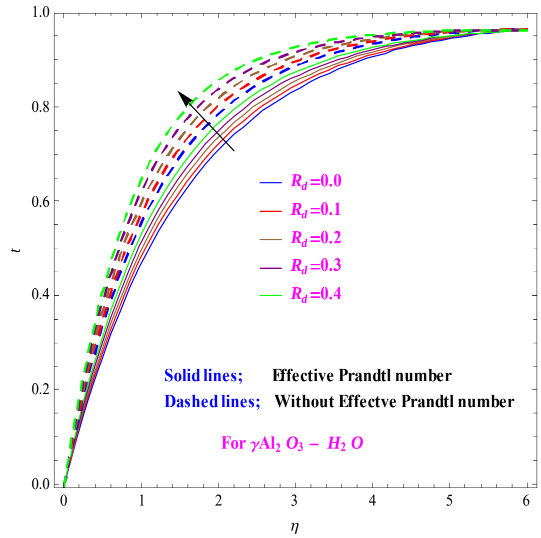

Fig. 4.6(a) : R_d on t.

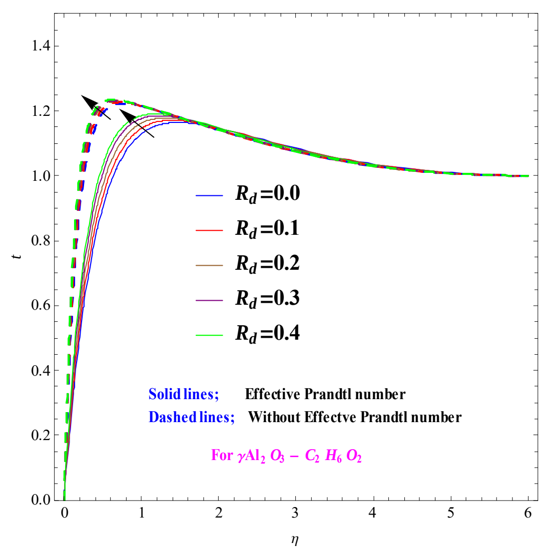

Fig. 4.6(b) : R_d on t.

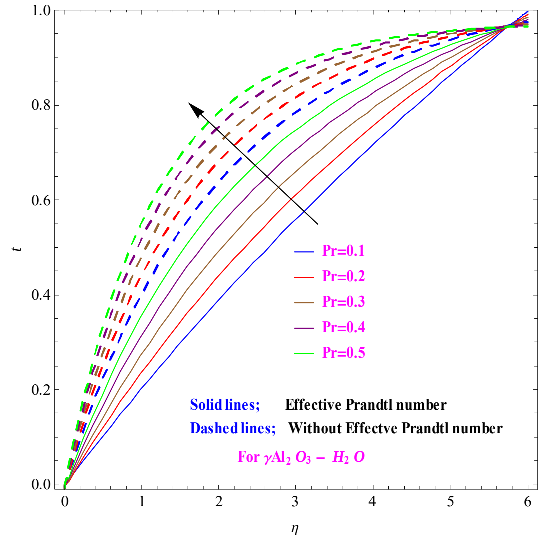

Fig. 4.7(a) : Pr on t.

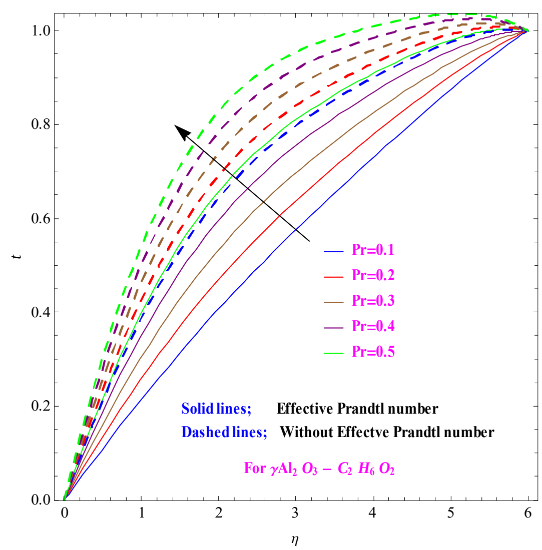

Fig. 4.7(b) : Pr on t.

4.7 Entropy and Bejan number

Entropy rate $(N_G(\eta))$ through $(M = 0.1, 0.2, 0.3, 0.4, 0.5)$ is given in Figs. 4.8(a, b). Lorentz force causes extra disturbance inside the system growing the entropy of the entire structure. Thermal entropy is less than total entropy which consequences a reduction in Bejan number as shown in Figs. 4.9(a, b) for both $(\gamma Al_2O_3 - H_2O$ and $\gamma Al_2O_3 - C_2H_6O_2)$ nanofluids. The performances of $N_G(\eta)$ as well as (Be) with respect to $(\mathrm{Re} = 0.1, 0.2, 0.3, 0.4, 0.5)$ are shown in

Figs. 4.10(a, b) and 4.11(a, b). Growing estimation of $(\text{Re} = 0.1, 0.2, 0.3, 0.4, 0.5)$ inclines for increasing $N_G(\eta)$ through Fig . 4.10(a, b). However reverse trend is perceived in case of (Be) for both $(\gamma Al_2O_3 - H_2O$ and $\gamma Al_2O_3 - C_2H_6O_2)$ nanofluids.

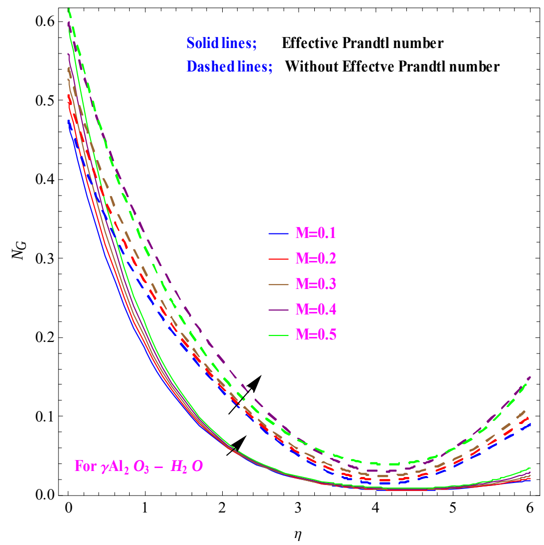

Fig. 4.8(a) : M on N_G.

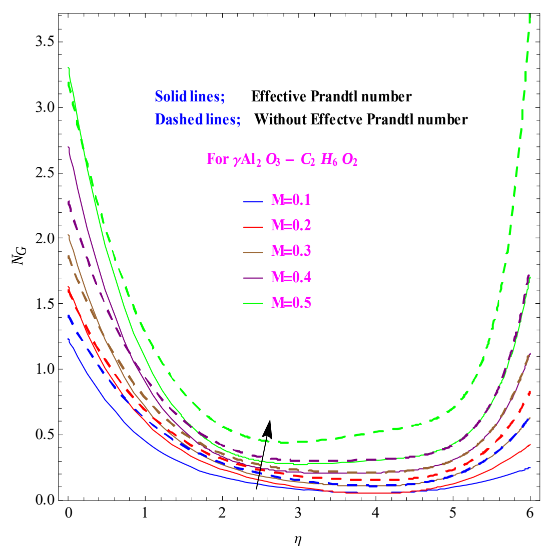

Fig. 4.8(b) : M on N_G.

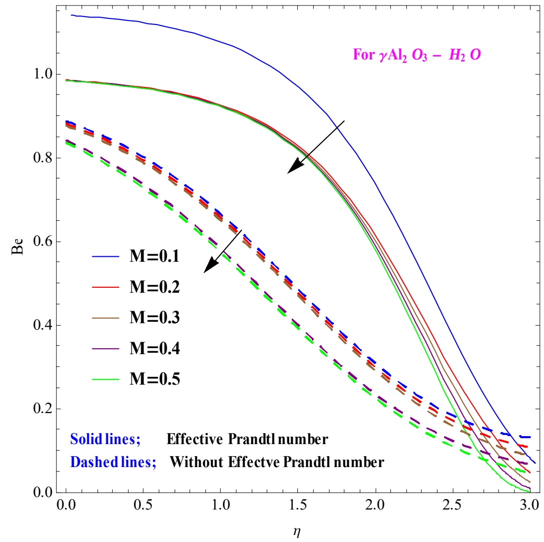

Fig. 4.9(a) : M on Be.

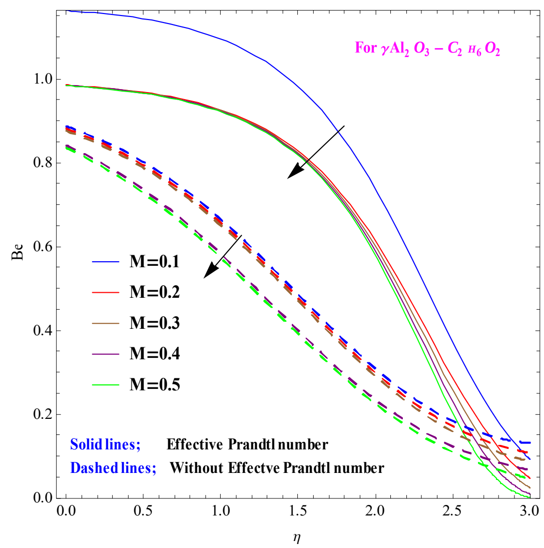

Fig. 4.9(b) : M on Be.

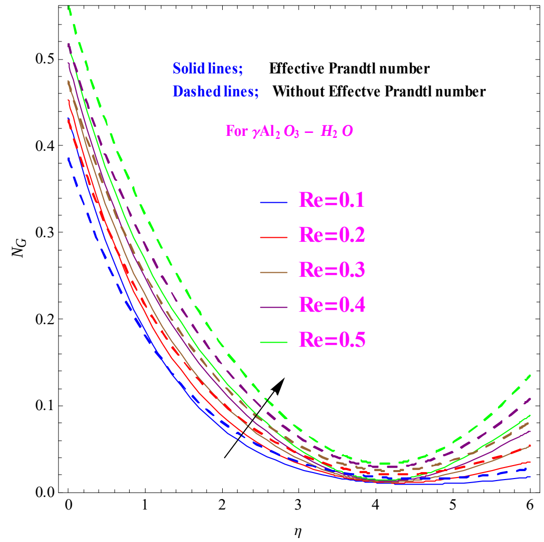

Fig. 4.10(a) : Re on N_G.

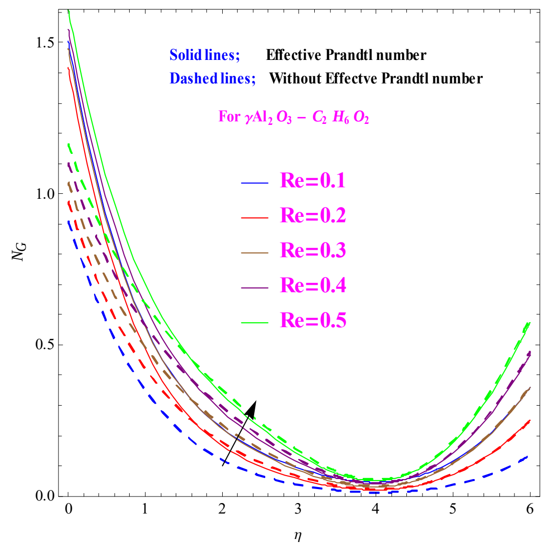

Fig. 4.10(b):Re on N_G.

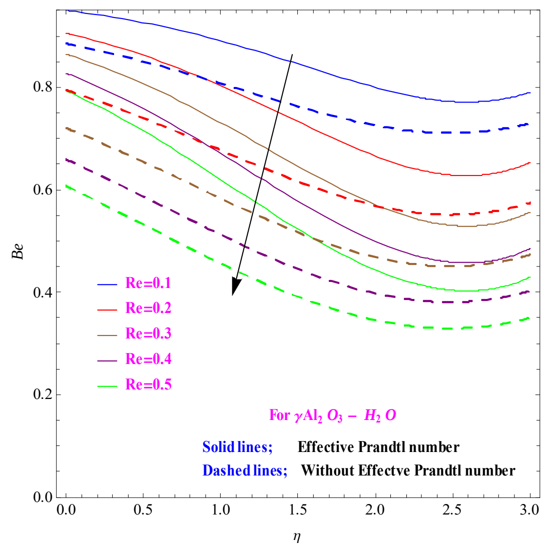

Fig. 4.11(a) : Re on Be.

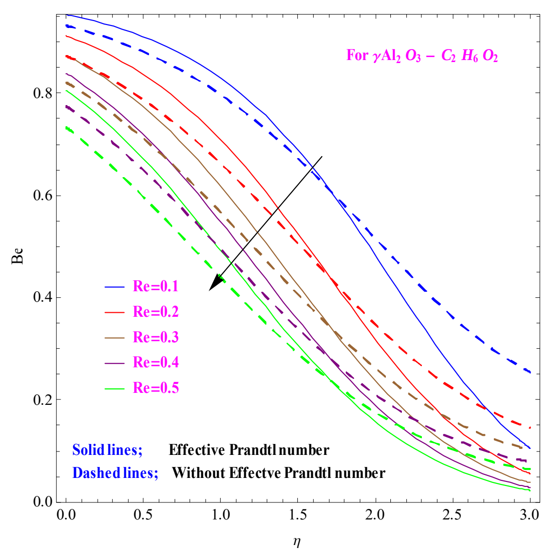

Fig. 4.11(b):Re on Be.

4.8 Skin friction and Nusselt number

Tables 4.2 and 4.3 show the influences of (M) and $\left(Da^{-1}\right)$ on (C_f). For $(M = 0.0, 0.1, 0.2)$ and $(Da^{-1} = 0.0, 0.1, 0.2)$, skin friction reduces for both $\gamma Al_2O_3 - H_2O$ and $\gamma Al_2O_3 - C_2H_6O_2$ nanofluids. Table 4.4 and 4.5 present the behaviors of (M), (Mn) and (R_d) on Nusselt number for both $\gamma Al_2O_3 - H_2O$ and $\gamma Al_2O_3 - C_2H_6O_2$ nanofluids. Nusselt number increases for higher values of $(M = 0.0, 0.1, 0.2)$, $(Mn = 0.1, 0.2, 0.3)$ and $(R_d = 0.1, 0.2, 0.3)$.

Table 4.2

M	Da^{-1}	Skin friction $C_f(\mathrm{Re}_x)^{-0.5}$ ($\gamma Al_2O_3 - H_2O$) With effective Prandtl number	Without effective Prandtl number
0.0	0.0	1.208	1.458
0.1	0.0	1.193	1.434
0.2	0.0	1.178	1.411
0.0	0.0	1.260	1.521
0.0	0.1	1.115	1.337
0.0	0.2	0.945	1.127

Table 4.3

M	Da^{-1}	Skin friction $C_f(\mathrm{Re}_x)^{-0.5}$ ($\gamma Al_2O_3 - C_2H_6O_2$) With effective Prandtl number	Without effective Prandtl number
0.0	0.0	1.878	1.866
0.1	0.0	1.874	1.862
0.2	0.0	1.874	1.862
0.0	0.0	1.648	1.633
0.0	0.1	1.290	1.277
0.0	0.2	0.848	0.829

Table 4.4

M	Mn	R_d	Nusselt number $Nu_x(\mathrm{Re}_x)^{-0.5}$ ($\gamma Al_2O_3 - H_2O$)	
			With effective Prandtl number	Without effective Prandtl number
0.0			1.471	1.214
0.1			1.512	1.247
0.2			1.555	1.282
	0.1		1.552	1.299
	0.3		1.603	1.320
	0.5		1.672	1.361
		0.1	1.603	1.320
		0.2	1.625	1.343
		0.3	1.647	1.365

Table 4.5

M	Mn	R_d	Nusselt number $Nu_x(\mathrm{Re}_x)^{-0.5}$ ($\gamma Al_2O_3 - C_2H_6O_2$)	
			With effective Prandtl number	Without effective Prandtl number
0.0			1.618	1.315
0.1			1.683	1.366
0.2			1.756	1.422
	0.1		1.791	1.449
	0.3		1.840	1.487
	0.5		1.904	1.539
		0.1	1.777	1.426
		0.2	1.798	1.447
		0.3	1.819	1.467

4.9 Final points

Major finding are given below.

- Velocity discriminant is absorbed for larger (M) as well as (β_2) for both $(\gamma Al_2O_3 - H_2O)$ and $(\gamma Al_2O_3 - C_2H_6O_2)$ nanofluids.
- Temperature is growing for larger magnetic and radiation parameters.
- Entropy enhances for $(\mathrm{Re} = 0.1, 0.2, 0.3, 0.4, 0.5)$ but reverse behavior is seen for (Be).
- (C_f) reduces for higher (Da^{-1}).
- (Nu) increases for larger (Mn) and (R_d).

Chapter 5

Thermal radiation and heat source/sink impacts in stagnation point flow of viscous nanomaterial

This chapter addresses the significances of stagnation point flow of nanomaterial towards non-linear stretching surface. Stretching surface of variable thickness is considered. Thermophoresis and Brownian movement impacts are accounted. Radiative heat and convective conditions are also analyzed. Inclined magnetic field is taken. Homotopy analysis method is employed to find the serious solution. Impacts of numerous physical variables are graphically discussed. Closing remarks are presented.

5.1 Modelling

We study MHD two-dimensional (2D) flow of viscous fluid past a stretching surface with velocity $(u_w = a(x+b)^n)$ where a and b denote positive constants. Stretching sheet is along $(x - axix)$ while $(y - axix)$ is normal to the sheet. Applied magnetic field is taken inclined. Induced magnetic field for small magnetic Reynolds number is ommitted. The related problems are

$$\frac{\partial u}{\partial x} + \frac{\partial v}{\partial y} = 0, \tag{5.1}$$

$$u\frac{\partial u}{\partial x}+v\frac{\partial u}{\partial y}=U_e\frac{\partial U_e}{\partial x}+\frac{\sigma}{\rho}B_o^2\sin^2\theta(U_e-u)+\nu\frac{\partial^2 u}{\partial y^2}, \tag{5.2}$$

$$u\frac{\partial T}{\partial x}+v\frac{\partial T}{\partial y}=\alpha^*\frac{\partial^2 T}{\partial y^2}+\tau D_B\left(\frac{\partial T}{\partial y}\frac{\partial C}{\partial y}\right)+\tau\frac{D_T}{T_\infty}\left(\frac{\partial T}{\partial y}\right)^2-\frac{1}{(\rho c_p)_f}\frac{\partial q_r}{\partial y}+\frac{Q(x)(T-T_\infty)}{(\rho c)_f}, \tag{5.3}$$

$$u\frac{\partial C}{\partial x}+v\frac{\partial C}{\partial y}+K(C-C_\infty)=D_B\left(\frac{\partial^2 C}{\partial y^2}\right)+\frac{D_T}{T_\infty}\left(\frac{\partial^2 T}{\partial y^2}\right), \tag{5.4}$$

$$u=U_w\left(x\right)=a(x+b^*)^n,\ \ -k_f\frac{\partial T}{\partial y}=h_f(T_f-T)\ \ D_B\frac{\partial C}{\partial y}+\frac{D_T}{T_\infty}\frac{\partial T}{\partial y}=0\text{ at } y=A(x+b^*)^{\frac{1-n}{2}}, \tag{5.5}$$

$$u\rightarrow U_e(x)=b(x+b^*)^n,\ T\rightarrow T_\infty\ C\rightarrow C_\infty\text{ when } y\rightarrow\infty. \tag{5.6}$$

The following transformation are used to reduce Eqs. $[5.2-5.6]$ into dimensionless expression;

$$\begin{aligned}\zeta &= \sqrt{\frac{n+1}{2}\frac{a}{\upsilon}(x+b^*)^{n-1}}y,\ \psi=\sqrt{2\left(n+1\right)^{-1}\upsilon a(x+b^*)^{n+1}}F(\zeta),\\ u &= a(x+b^*)^nF'(\zeta),\ v=-\sqrt{\frac{n+1}{2}\upsilon a(x+b^*)^{n-1}}[F(\zeta)+\zeta\frac{n-1}{n+1}F'(\zeta)],\end{aligned} \tag{5.7}$$

$$\Theta\left(\zeta\right)=\frac{T-T_\infty}{T_f-T_\infty},\ \Phi\left(\zeta\right)=\frac{C_\infty}{C-C_\infty} \tag{5.8}$$

The incompressibility condition (5.1) is trivially satisfied whereas Eqs. $[(5.2-5.6)]$ take following forms

$$F'''+FF''-(\frac{2n}{n+1})F'^2+(\frac{2}{n+1})M*M*\sin^2\theta(F'-S)+\left(\frac{2n}{n+1}\right)S^2=0, \tag{5.9}$$

$$\left(1+\frac{3}{4}R_d\right)[(1+(\Theta_w-1)\Theta)^3\Theta']'+\Pr F\Theta'+\Pr N_B\Theta'\Phi'+\Pr N_T(\Theta')^2+(\frac{2}{n+1})\Pr\delta\Theta=0, \tag{5.10}$$

$$\Phi''+ScF\Phi'-(\frac{2}{n+1})Sc\gamma_o\Phi+\left(\frac{Nt}{Nb}\right)\Theta''=0, \tag{5.11}$$

$$\left.\begin{array}{c} F(\alpha)=\zeta(\frac{1-n}{n+1}),\ F'(\alpha)=1,\ \Theta'(\alpha)=\gamma_2(1-\Theta(\alpha)),\ Nb\Phi'+Nt\Theta'=0,\\ F^{'}(\infty)=A,\ \Theta(\infty)=1,\ \Phi(\infty)=0. \end{array}\right\} \tag{5.12}$$

Here $\alpha=A\sqrt{\frac{n+1}{2}\frac{a}{v}}$, represents surface thickness parameter and $\zeta=\alpha=(A\sqrt{\frac{n+1}{2}\frac{a}{v}})$ the plate surface. We define $F(\zeta)=f(\zeta-\alpha)=f(\eta)$, $\Theta(\zeta)=t(\zeta-\alpha)=t(\eta)$ and $\Phi(\zeta)=J(\zeta-\alpha)=J(\eta)$ therefore governing Eqs. $(5.9-5.12)$ yield

$$f'''+ff''-(\frac{2n}{n+1})f'^2+(\frac{2}{n+1})M*M*\sin^2\theta(f'-S)+(\frac{2n}{n+1})S^2=0 \tag{5.13}$$

$$\left(1+\frac{3}{4}R_d\right)[(1+(\theta_w-1)t)^3t']'+\Pr Nbt'J'+(\frac{2}{n+1})\Pr\delta t+\Pr ft'+\Pr Nt(t')^2=0, \tag{5.14}$$

$$J''+ScfJ'-(\frac{2}{n+1})Sc\gamma_o J+\left(\frac{N_T}{N_B}\right)t''=0, \tag{5.15}$$

$$\left.\begin{array}{c} f(0)=\alpha(\frac{1-n}{n+1}),\ f'(0)=1,\ t'(0)=-\gamma_2(1-t(0)),\ N_BJ'+N_Tt'=0,\\ f^{'}(\infty)=S,\ t(\infty)=1,\ J(\infty)=0. \end{array}\right\} \tag{5.16}$$

5.2 Engineering curiosity

Skin friction and heat transfer rate (N_u) are

$$C_f=\frac{\tau_w}{\rho u_w^2/2},\ N_u=\frac{(x+b)q_w}{k_f(T_f-T_\infty)}. \tag{5.17}$$

Finally

$$C_f(\mathrm{Re}_x)^{\frac{1}{2}}=2\sqrt{\frac{n+1}{2}}f''(0), \tag{5.18}$$

$$\frac{Nu}{\sqrt{\mathrm{Re}_x}}=-\sqrt{\frac{n+1}{2}}\left(1+\frac{3}{4}R_d\right)[(1+(\theta_w-1)t(0))^3]t'(0). \tag{5.19}$$

5.2.1 Dimensionless parameter

$$\left.\begin{array}{c} \Pr=\frac{\nu}{\alpha},\ N_B=\frac{\tau D_BC_\infty}{\nu},\ M=\sqrt{\frac{\sigma}{\rho a}}B_0, N_T=\frac{\tau D_{T(T_f-T_\infty)}}{\nu T_\infty},\\ R_d=\frac{4\sigma^*T_\infty^3}{k_fk^*}\ \delta=\frac{Q_O}{a\rho c_p},\ \gamma_o=\frac{k}{a},\ Sc=\frac{\nu}{D_B},\\ \theta_w=\frac{T_f}{T_\infty},\ \gamma_2=\frac{h_f}{k_f\sqrt{\frac{a}{\nu}}(x+b^*)^{\frac{n-1}{2}}},\ \mathrm{Re}_x=\frac{a(x+b)}{\nu} \end{array}\right\}. \tag{5.20}$$

5.3 Methodology

We employed homotopic procedure to solve these Eqs. suggested by Liao [92]. The initial guesses and operators $((f_0,\, t_0, J_0),\, (\mathcal{L}_f,\, \mathcal{L}_t, \mathcal{L}_J))$ for the dimensionless equations are

$$\left.\begin{array}{c} f_0(\eta) = \left(\alpha(\frac{1-n}{1+n}) * A * \eta + (1-A) * (1-e^{-\eta})\right), \\ t_0(\eta) = \left(\left(\frac{\gamma_2}{(1+\gamma_2)}\right) * e^{-\eta}\right), \\ J_0(\eta) = \left(-(\frac{\gamma_2}{(1+\gamma_2)}) * e^{(-(\frac{N_T}{N_B})*\eta)}\right), \end{array}\right\} \tag{5.21}$$

with

$$\mathcal{L}_f = \left(f''' - f'\right),\ \mathcal{L}_t = \left(t'' - t\right),\ \mathcal{L}_J = \left(J'' - J\right), \tag{5.22}$$

5.3.1 Convergence analysis

The auxiliary parameters $\hbar_f$, $\hbar_t$ and $\hbar_J$ have key role in convergence analysis. Ultimate the values of assisting parameters for convergence are in the ranges $-2.2 \leq \hbar_f \leq 0.8$, $-2.0 \leq \hbar_t \leq -1.3$ and $-2.2 \leq \hbar_J \leq -1.5$.

Table (5.1): Convergence of series solutions when $\alpha = 0.1 = \gamma_2$, $n = 0.5$, $\Pr = 1.0$, $M = \gamma_o = 0.2$, $N_B = 0.2$, $N_T = 0.3$, $R = 0.3$, $\theta_w = 1.1$, $\delta = 0.2$, $\theta = \frac{\pi}{2}$, $S = 0.1$ and $Sc = 1$. From table it is noted that 28^{th} order of approximations is suitable for the convergence of function $f''(0)$ while 24^{th} and 20^{th} order of approximations are sufficient for the convergence of $t'(0)$ and $J'(0)$.

Order of approximation	$-f''(0)$	$-t'(0)$	$J'(0)$
1	0.8785	0.08708	0.05805
3	0.8753	0.08397	0.05598
8	0.8588	0.08045	0.05364
10	0.8493	0.07964	0.05309
15	0.8386	0.07851	0.05235
16	0.8365	0.07842	0.05230
20	0.8354	0.07815	0.05224
24	0.8341	0.07810	0.05224
28	0.8338	0.07810	0.05224
32	0.8338	0.07810	0.05224

5.4 Outcomes

Here we take $n = 0.5$, $\alpha = 0.4$, $\Pr = 1.2$, $S = 0.1 = R_d$, $M = 0.2 = \gamma_2$, $\theta_w = 1.1$, $N_T = 0.5$, $N_B = 0.5$, $\delta = 0.4$ and $\gamma_o = 0.2$.

Velocity profile: Fig. (5.1) is drawn for larger magnetic ($M = 0.0, 0.5, 1.0, 1.5, 2.0$) parameter on velocity profile ($f'(\eta)$). Here we observed that ($f'(\eta)$) decays against ($M = 0.0, 0.5, 1.0, 1.5, 2.0$). Fig. (5.2) demonstrated the features of ($\alpha = 0.0, 1.0, 2.0, 3.0, 4.0$) on $f'(\eta)$. Velocity declines against ($\alpha = 0.0, 1.0, 2.0, 3.0, 4.0$). Physically when we boost the values of (α), more instabilities arised in the material medium which produces resistance to the material properties. Therefore velocity declines. Fig. (5.3) is proposed to deliberate the impact of ($S = 1.0, 1.5, 2.0, 2.5, 3.0$) on $f'(\eta)$. Here $f'(\eta)$ boosts against ($S = 1.0, 1.5, 2.0, 2.5, 3.0$). Fig. (5.4) describes the variation of ($n = 0.0, 0.1, 0.2, 0.3, 0.4$) on $f'(\eta)$. Clearly $f'(\eta)$ boosts against larger ($n = 0.0, 0.1, 0.2, 0.3, 0.4$).

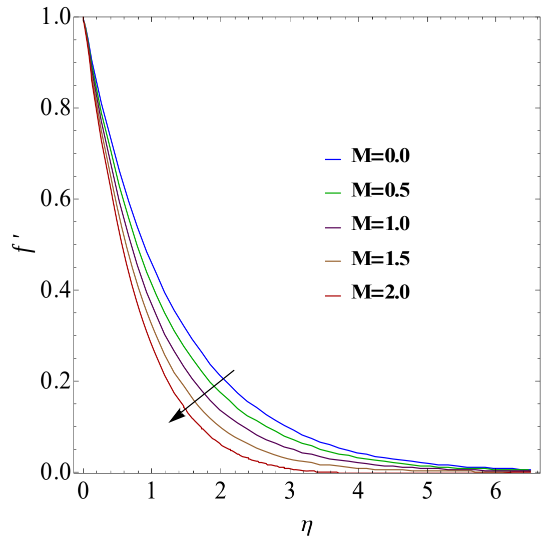

Fig. 5.1 : M on f'.

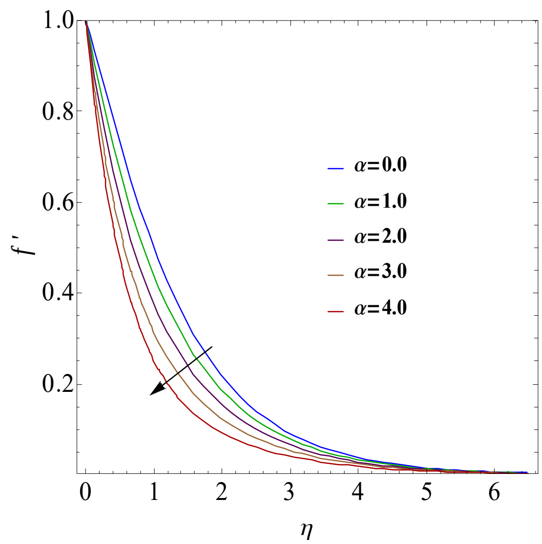

Fig. 5.2 : α on f'.

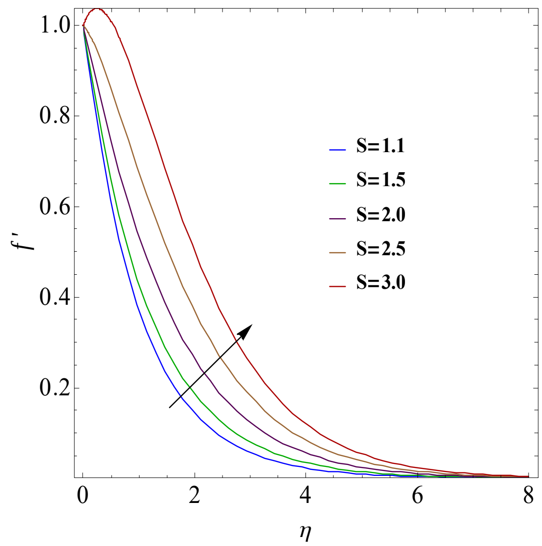

Fig. 5.3 : S on f'.

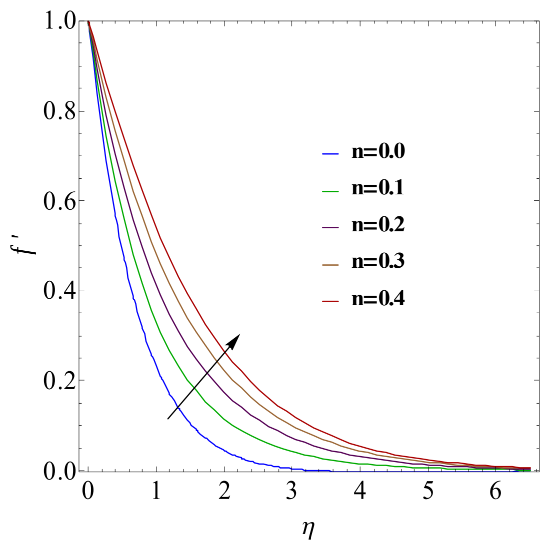

Fig. 5.4 : n on f'.

Temperature distribution: Fig. (5.5) is sketched the relevant features of (Pr) on $(t(\eta))$. For rising approximations of $(\mathrm{Pr} = 1.3, 1.5, 1.7, 1.9, 2.1)$ thermal diffusion rate declines and as a result thermal field reduces. Fig. (5.6) is depicted to deliberate the performance of (θ_w) on $(t(\eta))$. Here $(t(\eta))$ is increased via (θ_w). Since larger ratio variable $(\theta_w = 1.1, 2.0, 3.0, 4.0, 5.0)$ give more heat to the system. As a result the thermal field boosts. Outcomes of (R_d) on $(t(\eta))$ is depicted in Fig. (5.7). Since internal energy of system enhances for larger radiative variable. Therefore the temperature of entire system enhances. Fig. (5.8) shows the influence of (δ) on ($t(\eta)$). It is perceived that an increment in ($\delta = 0.0, 0.3, 0.6, 0.9, 1.2$) corresponds to improve the fluid temperature. Physically more heat is produced through larger (δ). Fig. (5.9) is described to explore the features of (γ_2) on ($t(\eta)$). Here ($t(\eta)$) boosts against larger ($\gamma_2 = 1.1, 1.3, 1.5, 1.7, 1.9$).

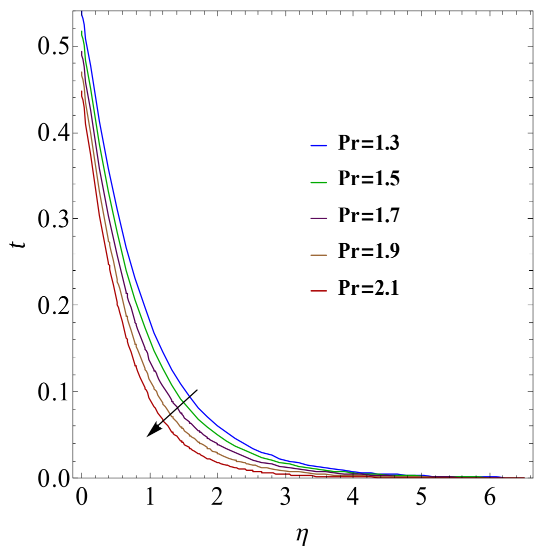

Fig. 5.5 : Pr on t.

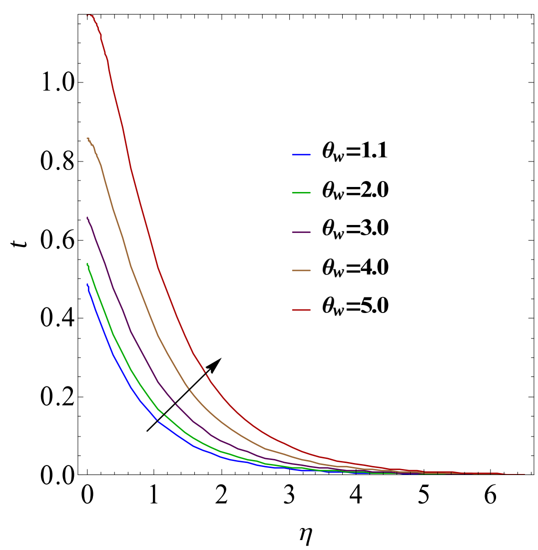

Fig. 5.6 : θ_w on t.

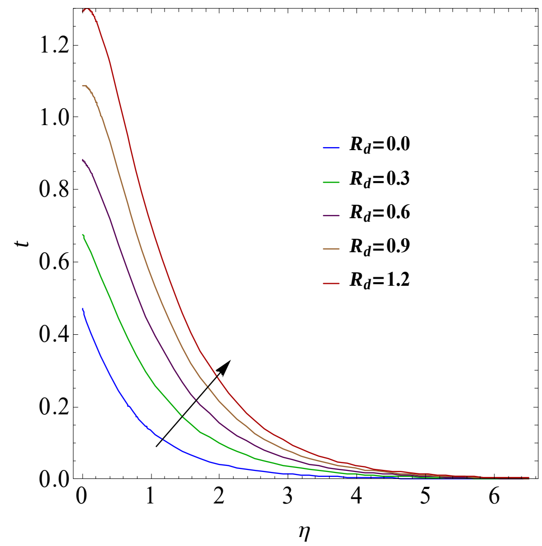

Fig. 5.7 : R_d on t.

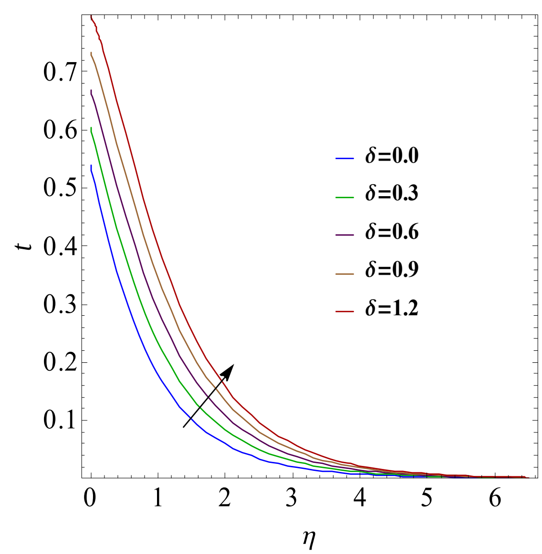

Fig. 5.8 : δ on t.

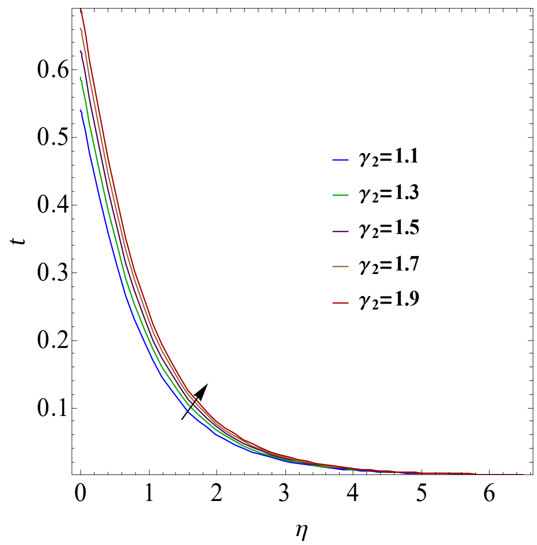

Fig. 5.9 : γ_2 on t.

Concentration profile: Figs. (5.10) and (5.11) represented the behaviors of ($N_T = 0.0, 0.1, 0.2, 0.3, 0.4$) and ($N_B = 0.5, 0.7, 0.9, 1.1, 1.3$) on concentration ($J(\eta)$). Here distinct impression is perceived for ($J(\eta)$) against larger (N_B) and (N_T). Fig. (5.12) is designated for (Sc) on ($J(\eta)$). For larger ($Sc = 0.0, 0.2, 0.4, 0.6, 0.8$), molecular diffusion rate reduces. That is why concentration enhances. Characteristic of (γ_0) on ($J(\eta)$) is emphasized in Fig. (5.13). Here both concentration field and associated layer thickness upsurge versus higher (γ_0).

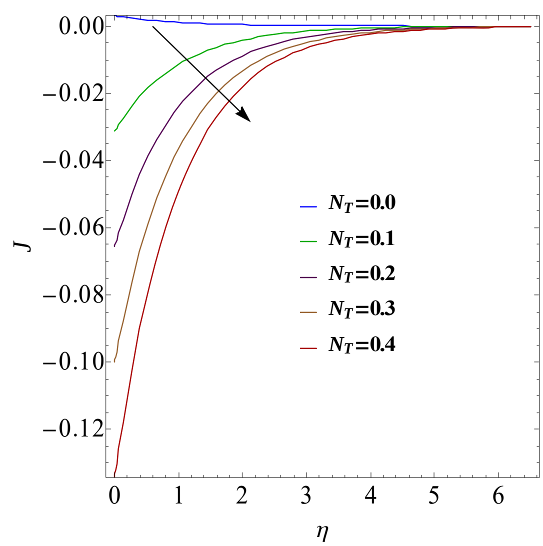

Fig. 5.10 : N_T on J.

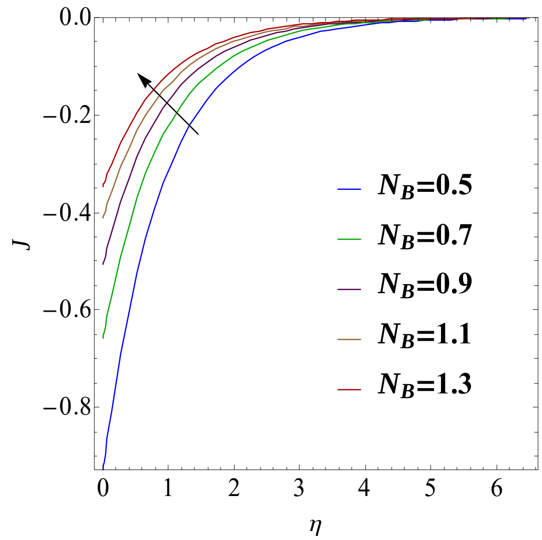

Fig. 5.11 : N_B on J.

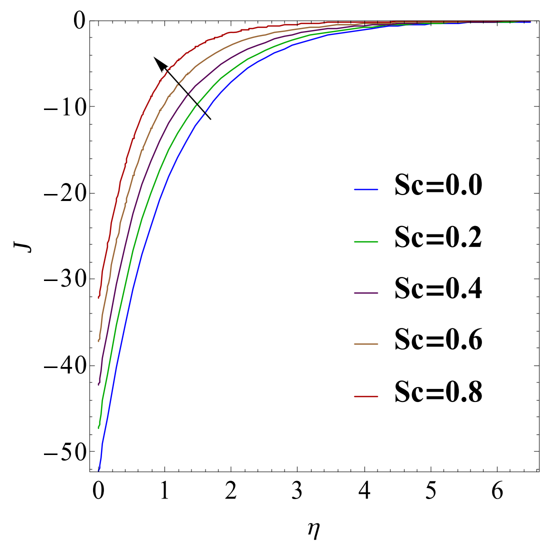

Fig. 5.12 : Sc on J.

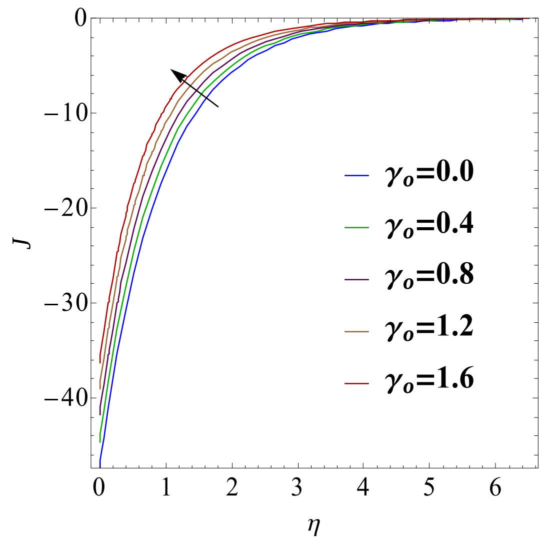

Fig. 5.13 : γ_o on J.

5.5 Engineering quantities

Table. (5.2) shows numerical values of skin friction (C_f) against $(M = 0.0, 0.1, 0.2)$, $(\alpha = 0.0, 0.1, 0.2)$ and $(n = 0.0, 0.5, 1.5)$. Here (C_f) enhances via (M), (α) and (n). Table. (5.3) characterizes (Nu) for larger $(\theta_w = 1.2, 1.4, 1.6)$, $(R_d = 0.1, 0.2, 0.3)$, $(\gamma_2 = 0.1, 0.3, 0.5)$, $(\Pr = 1.0, 1.5, 2.0)$ and $(\delta = 0.0, 0.1, 0.2)$. Clearly heat transfer rate enhances for larger (θ_w), (R_d) and (γ_2) and it reduces via $(\Pr)$ and (δ).

Table 5.2: Influence of (α), (S), (M) and (n) on (C_f).

α	S	M	n	$\sqrt{Re_x}C_f$
0.0				0.7521
0.1				0.7608
0.2				0.7695
	0.0			0.8285
	0.2			0.7851
	0.4			0.5666
		0.0		0.7469
		0.1		0.7504
		0.2		0.7695
			0.0	0.5172
			0.5	0.7608
			1.0	0.9520

Table 5.2: Influence of (Pr), (θ_w), (R_d), (δ) and (γ_2) on heat transfer rate

Pr	θ_w	R_d	δ	γ_2	$-Nu\sqrt{\mathrm{Re}_x}$
1.0					0.1535
1.5					0.1528
2.0					0.1520
	1.2				0.1638
	1.4				0.1866
	1.6				0.2115
		0.1			0.1532
		0.2			0.1628
		0.3			0.1723
			0.0		0.1578
			0.1		0.1566
			0.2		0.1555
				0.1	0.0842
				0.3	0.2101
				0.5	0.2971

5.6 Final remarks

Key observations include the following points.

- Velocity enhances against higher (n) and (S).
- There is decay in velocity versus (M) and (n).
- Thermal field decays via (Pr) and opposite result is seen for higher (R_d), (δ) and (θ_w).
- Concentration improves versus higher (Sc) and (γ_o) but it reduces for (N_T).
- Skin friction coefficient enhances for higher (α) and (S).

Chapter 6

Computational analysis of 3D radiative Darcy-Forchheimer flow subject to suction/injection

This chapter elaborates the three-dimensional (3D) radiative flow over non-linear stretched surface. Porous medium is taken into account. Porous medium is characterized by Darcy-Forchheimer relation. Radiation, convective condition and slip effect are addressed. Stagnation point flow is examined. Non-linear ordinary differential system are solved through shooting method. Graphical results are portrayed and scrutinized with distinct values of dimensionless variables. Drag force and Nusselt number are computed and evaluated through Tables.

6.1 Mathematical description

We consider $(3D)$ stagnation point Darcy- Forchheimer flow subject to permeable stretched surface. The (x, y) axes are chosen parallel to stretched sheet and $(z - axis)$ normal to flow. Let (v_w) is shrinking/stretching velocity, $(w_w(x, y))$ the mass flux velocity and $T_w(x, y)$ the surface temperature. The boundary layer equations and corresponding boundary condition are $[89 - 91]$

$$\frac{\partial u}{\partial x}+\frac{\partial v}{\partial y}+\frac{\partial w}{\partial z}=0, \tag{6.1}$$

$$\left.u\frac{\partial u}{\partial x}+v\frac{\partial u}{\partial y}-w\frac{\partial u}{\partial z}=U_e\frac{\partial U_e}{\partial x}+\nu\frac{\partial^2 u}{\partial z^2}+g\beta_1(T-T_\infty)-\frac{\nu}{k^*}u-\frac{c_p}{x\sqrt{k^*}}u^2\right\}, \tag{6.2}$$

$$\left.u\frac{\partial v}{\partial x}+v\frac{\partial v}{\partial y}-w\frac{\partial v}{\partial z}=\nu\frac{\partial^2 v}{\partial z^2}-\frac{\nu}{k^*}u-\frac{c_p}{x\sqrt{k^*}}u^2\right\}, \tag{6.3}$$

$$\left(u\frac{\partial T}{\partial x}+v\frac{\partial T}{\partial y}+w\frac{\partial T}{\partial z}\right)=\left(k_f+\frac{16\sigma^* T_1^3}{3k_1^*}\right)\frac{\partial^2 T}{\partial z^2}, \tag{6.4}$$

$$\left.\begin{array}{r} u=0,\quad v=v_w+\beta_1\frac{\partial v}{\partial z},\quad w=w_w,\\ -k\frac{\partial T}{\partial z}=h_f(T_f-T)\text{ at } z=0,\\ u=u_e,\quad v\to 0,\quad T\to T_\infty \text{ at } z\to\infty, \end{array}\right\}. \tag{6.5}$$

We set the quantities as follows.

$$\left.\begin{array}{c} v_w=b(x+y)^n,\;\; w_w=-\sqrt{a\nu}s\left(\frac{n+1}{2}\right)(x+y)^{\frac{n-1}{2}},\quad u_e=a(x+y)^n\\ A_1=\sqrt{\frac{\nu}{a}}(x+y)^{\frac{1-n}{2}}A_o,\;\; T_w=T_\infty+T_o(x+y)^{2n-1} \end{array}\right\}. \tag{6.6}$$

Letting

$$\left.\begin{array}{c} u=a(x+y)^n f'(\eta),\quad v=a(x+y)^n h'(\eta),\quad w=-2h\Omega_1 f(\eta),\\ w=-\sqrt{a\nu_f}(x+y)^{\frac{n-1}{2}}[\left(\frac{n+1}{2}\right)(f+h)+\left(\frac{n-1}{2}\right)(f'+h')]\;\; t=\frac{T-T_\infty}{T_w-T_\infty},\; \eta=\sqrt{\frac{a}{\nu_f}}(x+y)^{\frac{n-1}{2}}z, \end{array}\right\}. \tag{6.7}$$

The continuity equation is trivially satisfied while momentum, energy and corresponding boundary conditions take the following forms

$$\left.f'''+\left(\frac{n+1}{2}\right)[f+h]f''-n[f'+h']f'+n+\lambda t+[Da^{-1}-\beta f']f'=0\right\}, \tag{6.8}$$

$$\left.h'''+\left(\frac{n+1}{2}\right)[f+h]h''-n[f'+h']h'-[Da^{-1}-\beta h']h'=0\right\}, \tag{6.9}$$

$$\left.\left(1+\frac{3}{4}R_d\right)t''+\Pr\left[\frac{n+1}{2}[f+h]t'-(2n-1)(f'+h')t\right]=0\right\}, \tag{6.10}$$

$$\left.\begin{cases} f(0)=0,\ f(1)=0,\ f'(0)=0,\ f'(\infty)=1 \\ h(0)=V_o,\ h'(0)=\varepsilon+\beta_2 h''(0),\ h'(\infty)=0 \\ t'(0)=-\gamma_2[1-t(0)],\ t'(\infty)=0 \end{cases}\right\}. \tag{6.11}$$

6.1.1 Drag force

The drag force coefficients (C_f) are defined below i.e

$$C_{fx}=\left(\frac{\tau_{zx}}{\rho_f\,(u_w)^2}\right)_{z=0}. \tag{6.12}$$

$$C_{fy}=\left(\frac{\tau_{zy}}{\rho_{f(u_w)^2}}\right)_{z=0}. \tag{6.13}$$

The nondimensional form of skin friction coefficients are

$$\sqrt{\mathrm{Re}_x}C_{fx}=f''(0). \tag{6.14}$$

$$\sqrt{\mathrm{Re}_y}C_{fy}=h''(0). \tag{6.15}$$

6.1.2 Nusselt number

Magnitude of heat transfer rate is

$$Nu_{x1}=\left(\frac{(x+y)q_w}{k_f\,(T_w-T_\infty)}\right). \tag{6.16}$$

Nondimensional form gives

$$\frac{Nu_x}{(\mathrm{Re}_x)}=-\left(1+\frac{4}{3}R_d\right)t'(0) \tag{6.17}$$

where $\mathrm{Re}_x\left(=\frac{u_w(x+y)}{\nu_f}\right)$ and $\mathrm{Re}_y\left(=\frac{v_w(x+y)}{\nu_f}\right)$ denote the local Reynold number along $x\_$.and $y\_$ directions respectively.

6.1.3 Dimensionless parameters

$$\left.\begin{array}{c} Da^{-1}(=\frac{\nu_f}{ak^*(x+b)n-1}),\ R_d(=\frac{4\sigma^* T_\infty^3}{k_f k}),\ \beta(=F(x+y)) \\ \gamma_2(=\frac{h}{k}\sqrt{\frac{\nu}{a}}),\ \lambda=(\frac{g\beta_1 T_o}{a^2}),\ \Pr=\left(\frac{\mu C_p}{k}\right) \\ \varepsilon(=\frac{b}{a}),\ \beta_2\left(=\beta_1\sqrt{\frac{a}{\nu}}\right), \end{array}\right\}. \tag{6.18}$$

6.2 Results and discussion

6.2.1 Velocity profile

Figs. $[6.1-6.4]$ describe the outcomes of suction ($V_o > 0$) and injection parameters ($V_o < 0$) on both velocities (($f'(\eta)$) and $h'(\eta)$)). In suction case ($V_o > 0$) both velocities ($f'(\eta)$) and $h'(\eta)$) develop whereas inverse behavior is apparent for injection case ($V_o < 0$). In fact for suction variable the liquid film thickness declines on the extended sheet. Due to this inadequate quantity of liquid moving faster past the stretching sheet. In case of injection ($V_o < 0$) constant development of fluid mass decelerates the motion of liquid film. Figs. (6.5) and (6.6) reveal the features of (β) on ($f'(\eta)$) and $h'(\eta)$). Clearly the velocities ($f'(\eta)$) and $h'(\eta)$) reduce for larger values of ($\beta = 0.0, 0.1, 0.2, 0.3, 0.4$). Because resistive forces enhance in fluid movement in the presence of permeable medium. Therefore both velocities ($f'(\eta)$) and $h'(\eta)$) reduce. Similar result has been seen for $\left(Da^{-1} == 0.0, 0.1, 0.2, 0.3, 0.4\right)$ on velocities ($f'(\eta)$) and $h'(\eta)$) see Figs. (6.7) and (6.8) . Figs. (6.9) and (6.10) show the behavior of (ϵ) on ($f'(\eta)$) and $h'(\eta)$). Fluid velocity $(f'(\eta))$ and $h'(\eta))$ enhances for higher values of $(\epsilon = 0.0, 0.1, 0.2, 0.3, 0.4)$

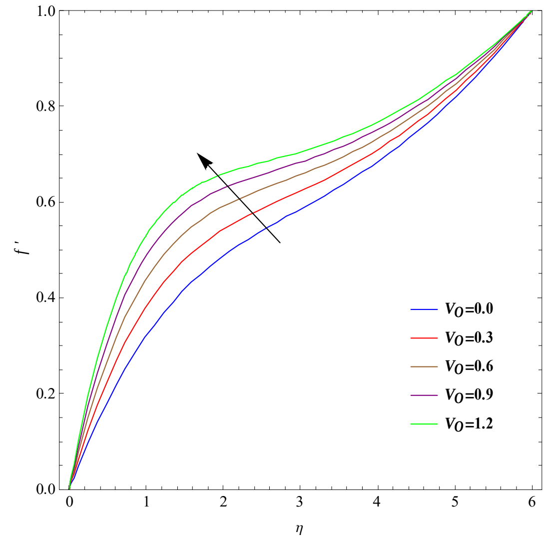

Fig. 6.1 : $(V_o > 0)$ on f'.

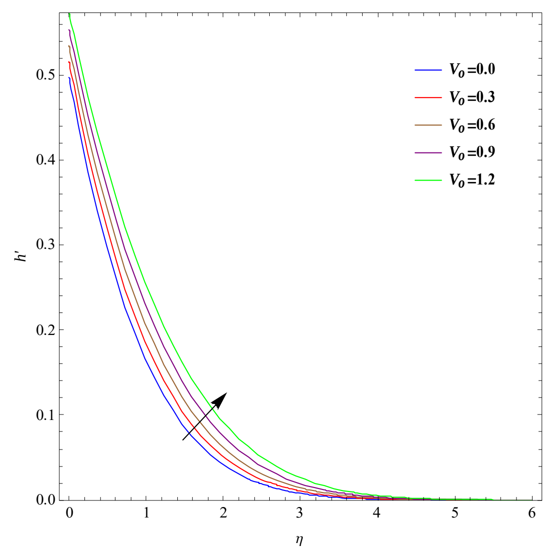

Fig. 6.2 : $(V_o > 0)$ on h'.

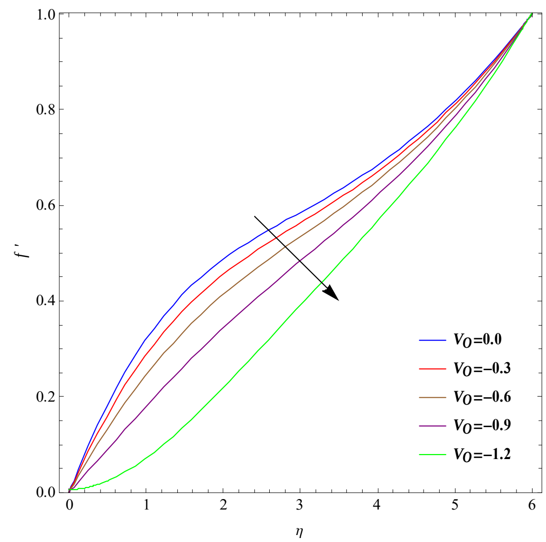

Fig. 6.3 : ($V_o < 0$) on f'.

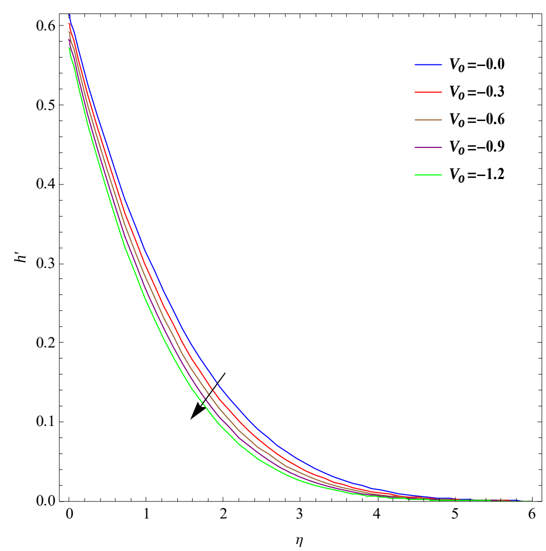

Fig. 6.4 : ($V_o < 0$) on h'.

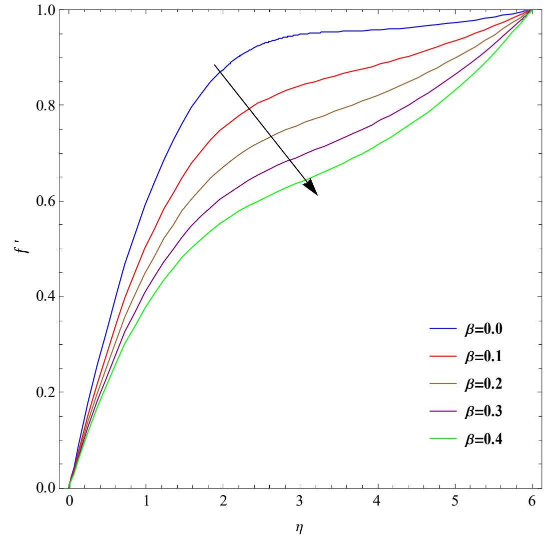

Fig. 6.5 : β on f'.

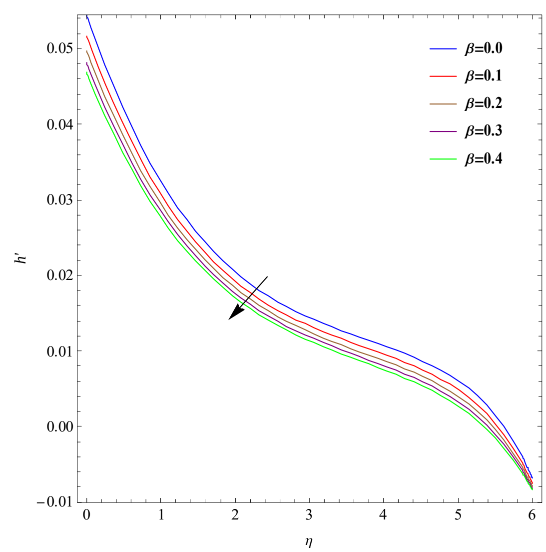

Fig. 6.6 : β on h'.

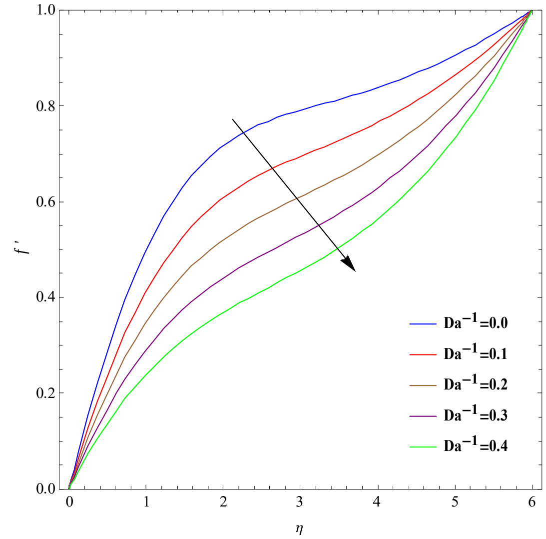

Fig. 6.7 : Da^{-1} on f'.

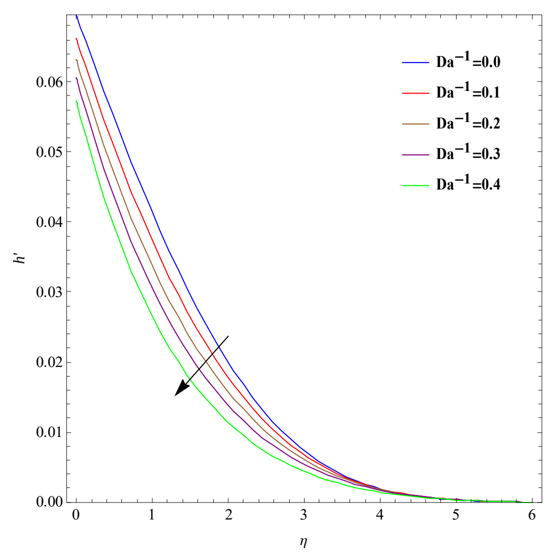

Fig. 6.8 : Da^{-1} on h'.

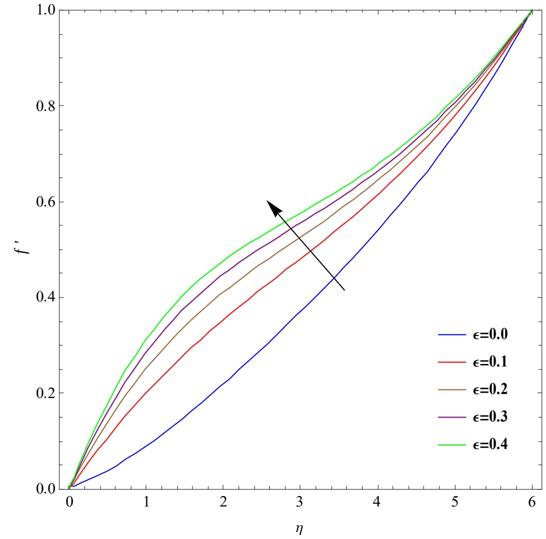

Fig. 6.9 : ϵ on f'.

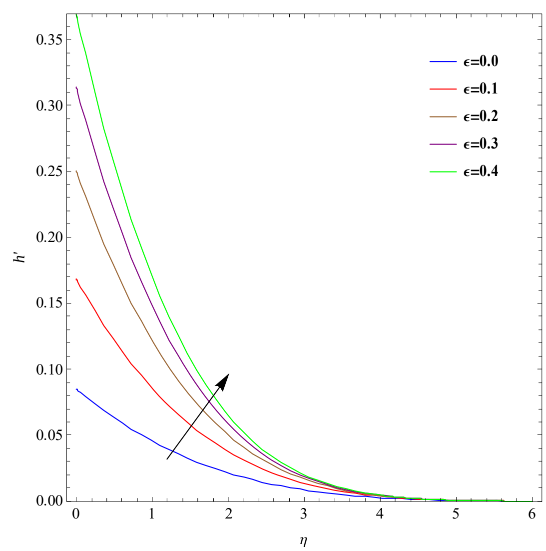

Fig. 6.10 : ϵ on h'.

6.2.2 Temperature

Figs. (6.11) and (6.12) explain temperature $(t(\eta))$ against suction $(V_o > 0)$/injection $(V_o < 0)$ variable. When $(V_o > 0)$ then $(t(\eta))$ rises but converse behavior is seen for $(V_o < 0)$. Fig. (6.13) shows that an increase in (R_d) leads to enhance $(t(\eta))$. Due to improvement in radiation more heat is discharged by the liquid that leads to boost the thermal field. Features of (γ_2) on $t(\eta)$ is explained in Fig. (6.14) . For rising estimations of $(\gamma_2 = 0.0, 0.2, 0.4, 0.6, 0.8)$ rate of convective heat transport enhances. It leads to an enhancement of $t(\eta)$. Fig. (6.15) describes effect of (Pr) on $t(\eta)$. Higher values of $(\mathrm{Pr} = 1.0, 1.1, 1.2, 1.3, 1.4)$ results in decays of temperature. Fig. (6.16) shows the impact of $(\lambda = 0.0, 1.0, 2.0, 3.0, 4.0)$ on $t(\eta)$. Temperature decreases via (λ). As expected the cooling effects increases when $(\lambda = 0.0, 1.0, 2.0, 3.0, 4.0)$ enhances and hence temperature reduces.

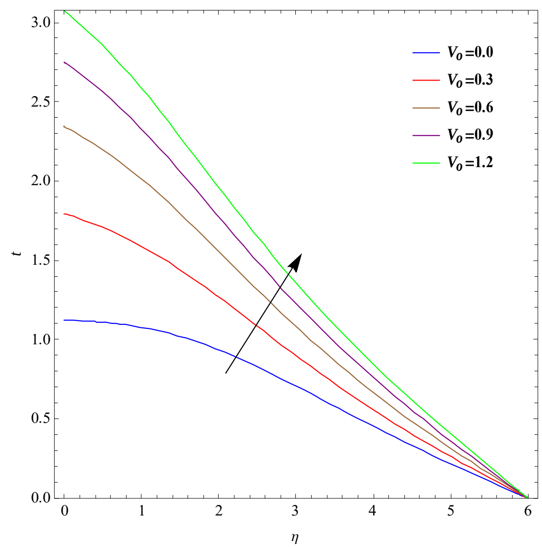

Fig. 6.11 : $(V_o > 0)$ on t.

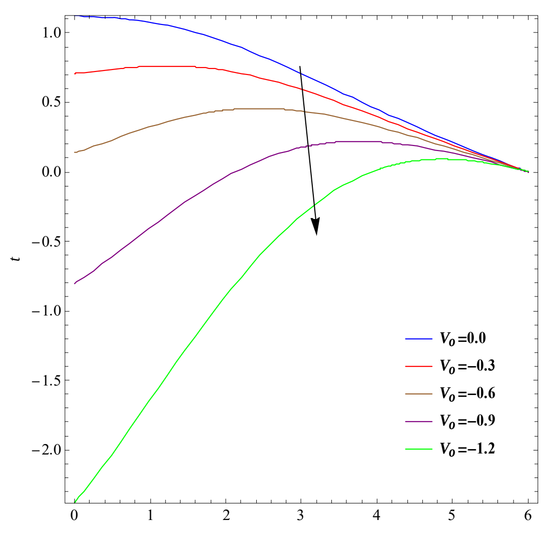

Fig. 6.12 : $(V_o < 0)$ on t.

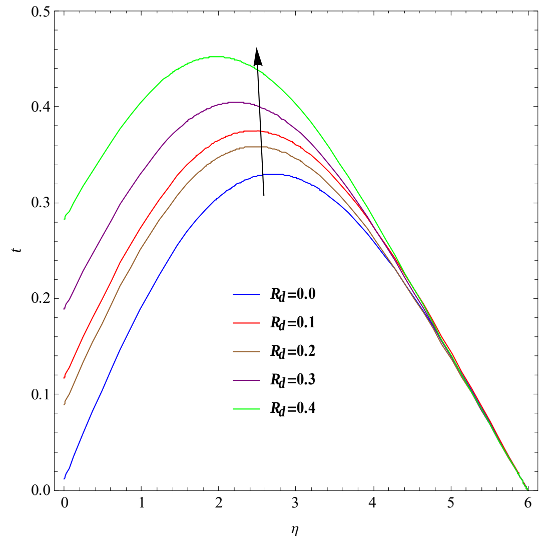

Fig. 6.13 : R_d on t.

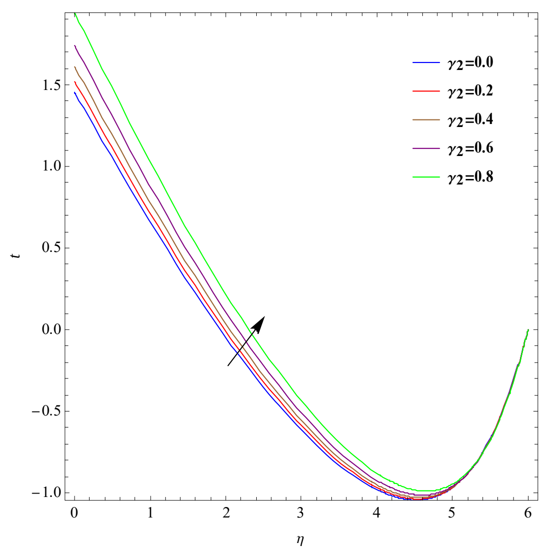

Fig. 6.14 : γ_2 on t.

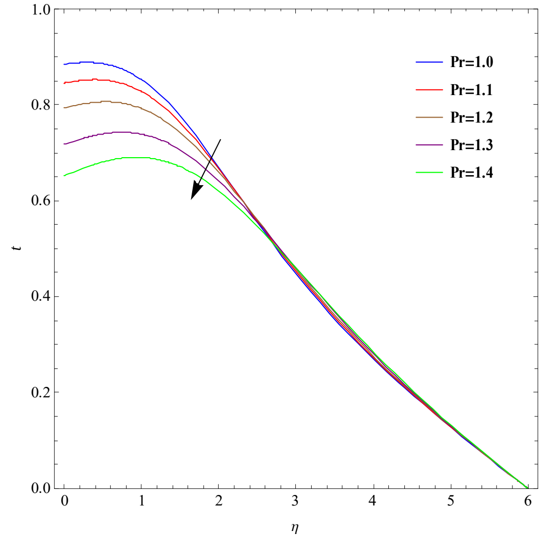

Fig. 6.15 : Pr on t.

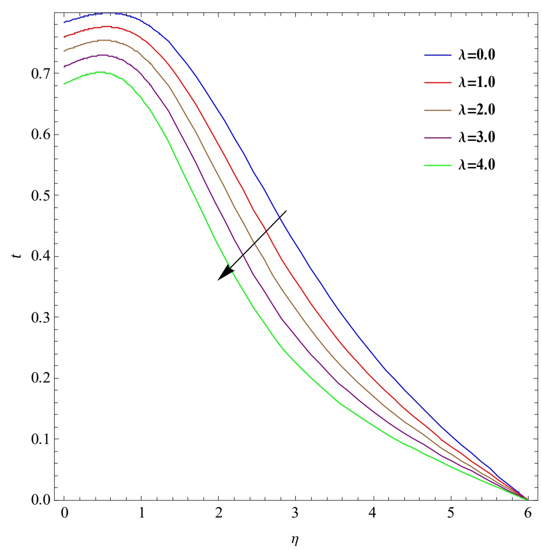

Fig. 6.16 : λ on t.

6.2.3 Analysis of engineering quantities

Table (6.1) is for impact drag force coefficient $((\mathrm{Re}_x)^{0.5} C_{fx}$ and $(\mathrm{Re}_x)^{0.5} C_{fy})$ against varying (β), (Da^{-1}), $(V_o > 0)$, $(V_o < 0)$ and (λ). It is noticed that $(\mathrm{Re}_x)^{0.5} C_{fx}$ and $(\mathrm{Re}_x)^{0.5} C_{fy}$ enhance for larger (β), (Da^{-1}), $(V_o > 0)$, and (λ) but it decreases for $(V_o < 0)$. Table (6.2) demonstrates numerical values of Nusselt number via (R_d, Pr γ_2 and V_o). It has been observed that $(-(Re_x)^{-0.5} Nu_x)$ increases for larger (R_d γ_2 and V_o) but opposite behavior is seen for $(Pr = 1.5,\ 2.0,\ 2.5)$

Table 6.1

β	Da^{-1}	$V_o > 0$	$V_0 < 0$	λ	$(\mathrm{Re}_x)^{0.5}\, C_{fx}$	$(\mathrm{Re}_x)^{0.5}\, C_{fy}$
0.0					0.59711	0.04711
0.1					0.65634	0.55861
0.2					0.76648	0.55870
	0.0				0.467954	0.16205
	0.1				0.55073	0.16591
	0.2				0.66817	0.16807
		0.0			0.42298	0.33105
		0.3			0.54724	0.34001
		0.6			0.67533	0.35428
			-0.1		0.36358	0.31633
			-0.2		0.29043	0.30129
			-0.3		0.18129	0.28490
				0.0	0.27428	0.16807
				0.1	0.37041	0.17036
				0.2	0.46795	0.18549

Table 6.2

R_d	Pr	γ_2	V_0	$-(Re_x)^{-0.5} Nu_x$
0.0				0.12117
0.1				0.15697
0.2				0.23068
	1.5			0.09221
	2.0			0.06391
	2.5			0.05776
		0.0		0.04037
		0.1		0.11968
		0.2		0.44349
			0.3	0.18016
			0.6	0.30414
			0.9	0.39672

6.2.4 Concluding remarks

The key finding of this chapter are listed below.

- Both velocities ($f'(\eta)$) and $h'(\eta)$) are decreasing functions of $\left(Da^{-1}\right)$ and (β).

- For suction case ($f'(\eta)$ and $h'(\eta)$) enhance and for injection case both ($f'(\eta)$) and $h'(\eta)$) are reduced.

- Larger values of (R_d) and (γ_2) lead to temperature enhancement.

- Drag force reduces via injection parameter.

- Nusselt number enhances for larger (R_d).

Chapter 7

Utilization of entire modern aspect of Cattaneo-Christov model in mixed convective entropy optimized flow by Riga wall

Present chapter investigates the steady mixed convective nanoliquid flow due to a stretchable Riga wall. Porous medium is considered. stagnation point flow is addressed. Brownian motion and thermophoresis are adopted. Cattaneo-Christove model for heat and mass fluxes are used to examine the heat and mass transfer. Entropy generation is modeled. Convective condition of heat transfer is addressed. Zero mass flux condition is imposed. Suitable transformation are employed to model the relevant ordinary differential systems. The governing systems are solved by ND solve technique. The impacts of sundry parameters are graphically examined.

7.1 Modeling

We discuss MHD two-dimensional (2D) flow of viscous liquid over a stretchable Riga wall. Heat and mass transfer are examined through Cattaneo-Christov (CC) heat and mass fluxes. Analysis of entropy production is considered according to the second thermodynamic law. The plate is stretching along $(x-axis)$ while $(y-axis)$ is normal to the surface. Here $(U_e = bx)$ ambient fluid velocity. Heat generation/absorption and radiation are also taken into account.

The velocity, temperature and concentration fields are defined as

$$V = [u(x,y), v(x,y), 0], \tag{7.1}$$

$$T = T(x,y), \tag{7.2}$$

$$C = C(x,y). \tag{7.3}$$

Heat and mass diffusion equations are

$$\mathbf{q} + \delta_E(\frac{\partial q}{\partial t} + \mathbf{V}\cdot\triangledown\mathbf{q} - \mathbf{q}\cdot\triangledown\mathbf{V} + (\triangledown\cdot\mathbf{V})\mathbf{q}) = -k\triangledown\mathbf{T}. \tag{7.4}$$

$$\mathbf{C} + \delta_F(\frac{\partial C}{\partial t} + \mathbf{V}\cdot\triangledown\mathbf{C} - \mathbf{C}\cdot\triangledown\mathbf{V} + (\triangledown\cdot\mathbf{V})\mathbf{C}) = -D_B\triangledown\mathbf{C}. \tag{7.5}$$

For incompressible steady flow one has

$$q + \delta_E(\mathbf{V}\cdot\triangledown\mathbf{q} - \mathbf{q}\cdot\triangledown\mathbf{V}) = -k\triangledown\mathbf{T}. \tag{7.6}$$

$$C + \delta_F(\mathbf{V}\cdot\triangledown\mathbf{C} - \mathbf{C}\cdot\triangledown\mathbf{V}) = -D_B\triangledown\mathbf{C}. \tag{7.7}$$

The governing expressions for the problems under consideration are

$$\frac{\partial u}{\partial x} + \frac{\partial v}{\partial y} = 0, \tag{7.8}$$

$$\left. u\frac{\partial u}{\partial x} + v\frac{\partial u}{\partial y} = U_e\frac{\partial U_e}{\partial x} + \nu\frac{\partial^2 u}{\partial y^2} + \frac{\pi J_o Q}{8\rho}Exp[-\frac{\pi}{a_1}y] + g\beta_t(T - T_\infty) - \frac{\nu\epsilon}{k^*}(u - u_e), \right\} \tag{7.9}$$

$$
\left.\begin{array}{c}
u\frac{\partial T}{\partial x}+v\frac{\partial T}{\partial y}=-\nabla .q+\tau\left[D_B\frac{\partial C}{\partial y}\frac{\partial T}{\partial y}+\frac{D_T}{T_\infty}\left(\frac{\partial T}{\partial y}\right)^2\right]+\\
\frac{Q}{\rho C_p}(T-T_\infty)+\frac{\mu}{\rho C_p}\left(\frac{\partial u}{\partial y}\right)^2-\frac{16\sigma^* T^3}{3\rho c_p k^*}\frac{\partial^2 T}{\partial y^2}
\end{array}\right\} \tag{7.10}
$$

$$
\left. u\frac{\partial C}{\partial x}+v\frac{\partial C}{\partial y}=-\nabla .C+D_B\frac{\partial^2 C}{\partial y^2}+\frac{D_T}{T_\infty}\frac{\partial^2 T}{\partial y^2}\right\} \tag{7.11}
$$

Eliminating q and C from equations $(7.6, 7.10)$ and $(7.7, 7.11)$ we get

$$
\left.\begin{array}{c}
u\frac{\partial T}{\partial x}+v\frac{\partial T}{\partial y}+\delta_E\Omega_E=\alpha\frac{\partial^2 T}{\partial y^2}+\tau\left[D_B\frac{\partial C}{\partial y}\frac{\partial T}{\partial y}+\frac{D_T}{T_\infty}\left(\frac{\partial T}{\partial y}\right)^2\right]\\
+\frac{Q}{\rho C_p}(T-T_\infty)+\frac{\mu}{\rho C_p}\left(\frac{\partial u}{\partial y}\right)^2-\frac{16\sigma^* T^3}{3\rho c_p k^*}\frac{\partial^2 T}{\partial y^2}
\end{array}\right\}, \tag{7.12}
$$

$$
\left. u\frac{\partial C}{\partial x}+v\frac{\partial C}{\partial y}+\delta_F\Omega_F=D_B\frac{\partial^2 C}{\partial y^2}+\frac{D_T}{T_\infty}\frac{\partial^2 T}{\partial y^2}\right\} \tag{7.13}
$$

In the above equations Ω_E and Ω_F are

$$
\left.\begin{array}{c}
\Omega_E=u\frac{\partial u}{\partial x}\frac{\partial T}{\partial x}+v\frac{\partial u}{\partial y}\frac{\partial T}{\partial y}+u\frac{\partial v}{\partial x}\frac{\partial T}{\partial y}+v\frac{\partial u}{\partial y}\frac{\partial T}{\partial x}+2uv\frac{\partial^2 T}{\partial y\partial x}+u^2\frac{\partial^2 T}{\partial x^2}+v^2\frac{\partial^2 T}{\partial y^2}\\
-\frac{Q}{\rho C_p}\left(u\frac{\partial T}{\partial x}+v\frac{\partial T}{\partial y}\right)-\frac{\mu}{\rho C_p}\left(2u\frac{\partial u}{\partial y}\frac{\partial^2 u}{\partial x\partial y}+2v\frac{\partial u}{\partial y}\frac{\partial^2 u}{\partial y^2}\right)\\
-\tau D_B\left(v\frac{\partial T}{\partial y}\frac{\partial^2 C}{\partial y^2}+v\frac{\partial C}{\partial y}\frac{\partial^2 T}{\partial y^2}+u\frac{\partial^2 C}{\partial x\partial y}\frac{\partial T}{\partial y}+u\frac{\partial C}{\partial y}\frac{\partial^2 T}{\partial x\partial y}\right)\\
+2\frac{\tau D_T}{T_\infty}\left(v\frac{\partial T}{\partial y}\frac{\partial^2 T}{\partial y^2}+u\frac{\partial T}{\partial y}\frac{\partial^2 T}{\partial x\partial y}\right)+R_d\left(u\frac{\partial^2 T}{\partial x\partial y}+v\frac{\partial^2 T}{\partial y^2}\right)
\end{array}\right\} \tag{7.14}
$$

$$
\left.\begin{array}{c}
\Omega_F=u^2\frac{\partial^2 C}{\partial x^2}+u\frac{\partial u}{\partial x}\frac{\partial C}{\partial x}+u\frac{\partial v}{\partial x}\frac{\partial C}{\partial y}+2uv\frac{\partial^2 C}{\partial x\partial y}\frac{\partial T}{\partial x}+v\frac{\partial u}{\partial y}\frac{\partial C}{\partial x}+v^2\frac{\partial^2 C}{\partial y^2}+\\
v\frac{\partial v}{\partial y}\frac{\partial C}{\partial y}-D_B\left(u\frac{\partial^3 C}{\partial x\partial y^2}+v\frac{\partial^3 C}{\partial y^3}\right)-\frac{D_T}{T_\infty}\left(v\frac{\partial^3 T}{\partial y^3}+u\frac{\partial^3 T}{\partial x\partial y^2}\right)
\end{array}\right\}. \tag{7.15}
$$

The subjected boundary conditions satisfy

$$
\left.\begin{array}{c}
u=U_w=ax,\quad v=0,\quad -k\frac{\partial T}{\partial y}=h_f(T_f-T),\ D_B\frac{\partial C}{\partial y}+D_T\frac{\partial T}{\partial y}=0 \text{ at } y=0,\\
u=U_e=bx,\quad T\to T_\infty,\quad C\to C_\infty \text{ at } y\to\infty,
\end{array}\right\}. \tag{7.16}
$$

The suitable transformations are

$$
\left. u=axf'(\eta),\quad v=-\sqrt{a\nu}f(\eta),\quad t=\frac{T-T_\infty}{T_w-T_\infty},\ J=\frac{C-C_\infty}{C_w-C_\infty},\ \eta=\sqrt{\frac{a}{\nu}}y\right\}. \tag{7.17}
$$

The non-dimensional form of governing equations are as follows.

$$f''' + f'' - f'^2 + S^2 + MExp[-B\eta] + \lambda t + Da^{-1} f' = 0 \Big\} , \tag{7.18}$$

$$\left. \begin{array}{c} (1+R_d)t'' + \Pr ft' + \Pr\gamma_1(ff't' + f'^2t'' - \delta ft' - 2ff't'') + \\ \Pr\gamma_1 Ec(2f'f'f'' - ff''f''') - (\Pr)(\gamma_1)(N_B)(ft'J'' - fJ't') \\ -\Pr(\gamma_1)(N_t)J''t' - \Pr\gamma_1 R_d ft'' + N_B t'J' + N_t t'^2 + \Pr Ecf''^2 + \Pr\delta t] = 0, \end{array} \right\} \tag{7.19}$$

$$J'' + LefJ' + \frac{N_B}{N_t}t'' - Le\gamma_3[f^2J'' + ff'J'] - \gamma_3\frac{N_B}{N_t}t'' = 0 \Big\} , \tag{7.20}$$

$$\left\{ \begin{array}{c} f(0) = 0,\ f'(0) = 1,\ f'(\infty) = S \\ t'(0) = -\gamma_2(1 - t(0)),\ t(\infty) = 0, \\ N_B t'(0) + N_t J'(0) = 0, J(\infty) = 0 \end{array} \right\} . \tag{7.21}$$

7.2 Entropy generation rate

Entropy generation rate here is given by

$$\left. \begin{array}{c} N'''_{gen} = \underbrace{\frac{k}{T_\infty^2}\left(\frac{\partial T}{\partial y}\right)^2 + \frac{16\sigma^*}{T_\infty^2}\left(\frac{\partial T}{\partial y}\right)^2}_{\text{Heat Transfer irreversibility}} + \underbrace{\frac{\mu}{T_\infty}\left(\frac{\partial u}{\partial y}\right)^2}_{\text{Fluid friction irreversibility}} \\ + \underbrace{\frac{R_D}{T_\infty}\left(\frac{\partial T}{\partial y}\frac{\partial C}{\partial y}\right) + \frac{R_D}{T_\infty}\left(\frac{\partial C}{\partial y}\right)^2}_{\text{Mass transfer irreversibility}} \end{array} \right\} , \tag{7.22}$$

Characteristic entropy rate is defined as follows

$$N'''_0 = \frac{k(\nabla T)^2}{L^2 T_\infty^2} \tag{7.23}$$

Using transformations the non-dimensional form of entropy generation satisfies

$$N_G = \frac{N'''_{gen}}{N'''_0} = \mathrm{Re}(1+R_d)t'^2 + \frac{\mathrm{Re}\,Br}{\Omega}f''^2 + \frac{\mathrm{Re}\,\chi\gamma_4}{\Omega}t'J' + \mathrm{Re}\,\chi\gamma_4 J'^2. \tag{7.24}$$

Bejan number satisfies

$$B_e = \frac{\mathrm{Re}(1+R_d)t'^2 + \frac{\mathrm{Re}\,\chi\gamma_4}{\Omega}t'J' + \mathrm{Re}\,\chi\gamma_4 J'^2}{\mathrm{Re}(1+R_d)t'^2 + \frac{\mathrm{Re}\,Br}{\Omega}f''^2 + \frac{\mathrm{Re}\,\chi\gamma_4}{\Omega}t'J' + \mathrm{Re}\,\chi\gamma_4 J'^2}, \tag{7.25}$$

7.3 Skin friction coefficient

Drag force coefficient (C_f) is defined below as

$$C_{fx} = \left(\frac{\tau_{yx}}{\rho_f \left(U_w\right)^2} \right), \tag{7.26}$$

and non-dimensional form of skin friction is

$$\sqrt{\mathrm{Re}_x} C_{fx} = f''(0), \tag{7.27}$$

7.3.1 Dimensionless parameters

$$\left.\begin{array}{c} M\left(=\frac{\pi J_o M_o}{8\rho a^2}\right),\ Da^{-1}\left(=\frac{\nu\epsilon}{k}\right),\ \lambda\left(=\frac{g\beta_t(T_w-T_\infty)}{a}\right),\ B\left(=\frac{\pi}{a_1}\sqrt{\frac{\nu}{a}}\right),\ S\left(=\frac{b}{a}\right), \\ \gamma_1\left(=a\delta_E\right),\ \gamma_2\left(=\frac{h_f\nu}{a}\right),\ \gamma_3\left(=a\delta_F\right),\ \gamma_4=\left(\frac{\nabla C}{C_\infty}\right),\ N_B\left(=\frac{\tau D_B(C_w-C_\infty)}{\nu}\right), \\ N_T\left(=\frac{\tau D_T(T_w-T_\infty)}{\nu T_\infty}\right),\ Ec\left(=\frac{U_w^2}{C_P(T_w-T_\infty)}\right),\ Le\left(=\frac{\nu}{D_B}\right),\ \delta\left(=\frac{Q}{\rho C_p}\right), \\ \Pr\left(=\frac{\mu C_p}{k}\right),\ \left(Br=\left(\frac{\mu U_w^2}{k\nabla T}\right)\right),\ \left(\Omega=\left(\frac{\nabla T}{T_\infty}\right)\right),\ \chi=\left(\frac{R_D C_\infty}{k}\right),\ \mathrm{Re}_x\left(=\frac{U_w x}{\nu_f}\right), \end{array}\right\}. \tag{7.28}$$

Table :1. Numerical values of (C_f) for $\left(Da^{-1}\right)$, (λ) and (M).

Da^{-1}	M	λ	$\sqrt{\mathrm{Re}}C_{fx}$
0.5	0.2	0.4	0.36808
0.6			0.29513
0.7			0.21928
0.3	0.01	0.4	0.79609
	0.02		0.78710
	0.03		0.77817
0.3	0.2	0.2	0.58065
		0.3	0.52983
		0.4	0.47967

7.4 Outcomes

In this section, the effect of various physical variables on $f'(\eta)$, $t(\eta)$, $J(\eta)$, N_G and Be are discussed. The values are selected as follows: $S = 0.1$, $M = 0.2$, $Ec = 0.6$, Pr =1.2, $Sc = 1.0$, $\mathrm{Re} = 0.1$, $\frac{1}{Da} = 0.2$, $\Gamma = 0.2$, $E = 0.1$, $Br = 0.1$, $\Omega = 0.4$, $N_t = 0.5$, $N_B = 1.0$, $R_d = 0.2$ and χ $= 0.5$.

7.5 Velocity profile

Fig. (7.1) shows the development of (M) on velocity. For larger $(M = 0.0, 0.1, 0.2, 0.3, 0.4)$ the $f'(\eta)$ enhances. In fact Lorentz force produces due to applied magnetic field. Fig. (7.2) demonstrates the impact of $\left(\frac{1}{Da}\right)$ on $f'(\eta)$. Velocity is reduced for larger $\left(\frac{1}{Da}\right)$. Here the resistive force in the permeable medium enhances during fluid motion. Thus velocity decays rapidly. Influence of (λ) on $f'(\eta)$ is depicted in Fig. (7.3). For $(\lambda = 0.0, 0.2, 0.4, 0.6, 0.8)$ the $f'(\eta)$ enhances. In fact higher (λ) correspond to decrease of viscous forces and so velocity enhances. Fig. 7.4 illustrates that for larger (S) the velocity increases. Physically higher values of (S) convince a supporting ambient velocity that often tends to increase velocity.

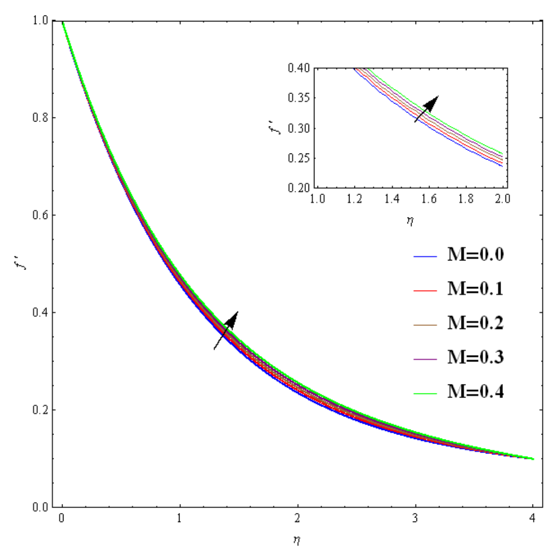

Fig. 7.1 : M on f'.

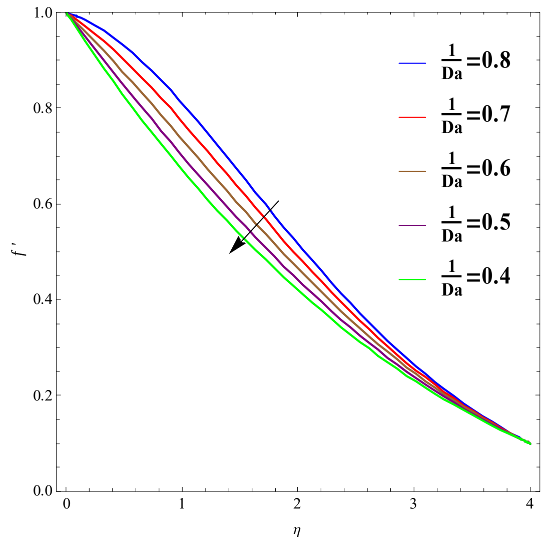

Fig. 7.2 : Da^{-1} on f'.

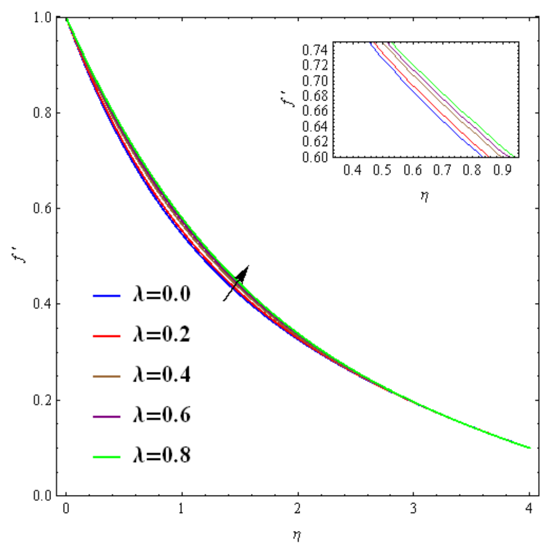

Fig. 7.3 : λ on f'.

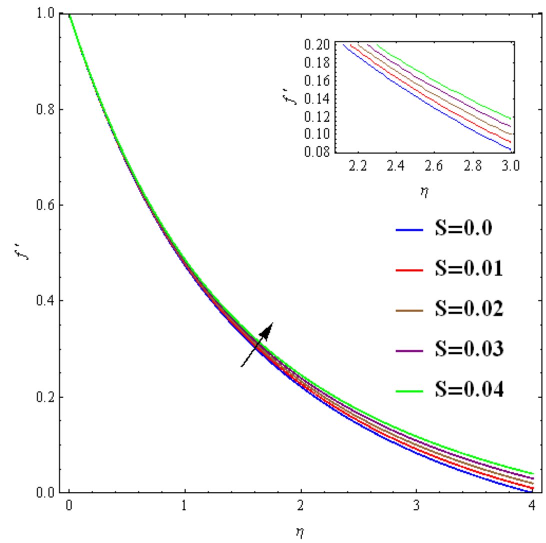

Fig. 7.4 : S on f'.

7.6 Temperature distribution

Impact of (M) on $t(\eta)$ is discloses in Fig. (7.5). Clearly $t(\eta)$ has decreasing trend against (M) . Impact of $(\gamma_1 = 0.0, 0.1, 0.2, 0.3, 0.4)$ on $t(\eta)$ is depicted in Fig. (7.6). For larger (γ_1) fluid particles take extra time for transfer heat from heated region to cold one. Thus $t(\eta)$ is reduced. Influence of (δ) on $t(\eta)$ is inspected in Fig. (7.7). Higher $(\delta = 0.0, 0.1, 0.2, 0.3, 0.4)$ yield more heat in the fluid which enhances $t(\eta)$. Fig. (7.8) reveals the impact of (Ec) on $t(\eta)$. Physically for higher (Ec) more heat produces in fluid due to high friction forces between fluid particle. Hence $t(\eta)$ enhances. Fig. (7.9) demonstrates that temperature enhances for larger Biot number. Impact of (R_d) on $t(\eta)$ is discussed in Fig. (7.10). Obviously $t(\eta)$ is increased via R_d. Physically working fluid creates more heat which causes in the temperature rise. Impact of (N_B) on $t(\eta)$ is presented in Fig. (7.11). Temperature $t(\eta)$ enhances for $(N_B = 1.0, 1.1, 1.2, 1.3, 1.4)$. This is because an uplift in the base fluid thermal conductivity exists with greater$(N_B = 1.0, 1.1, 1.2, 1.3, 1.4)$. Therefore boundary layer becomes thicker and thus rises in temperature $t(\eta)$. Opposite trend is seen for larger values of N_T (see Fig. 7.12).

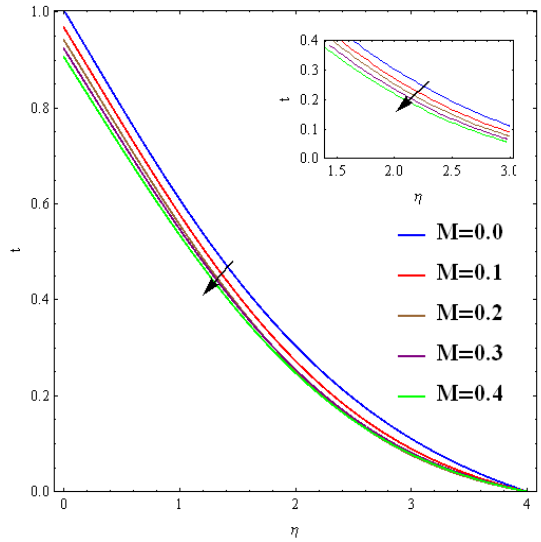

Fig. 7.5 : M on t.

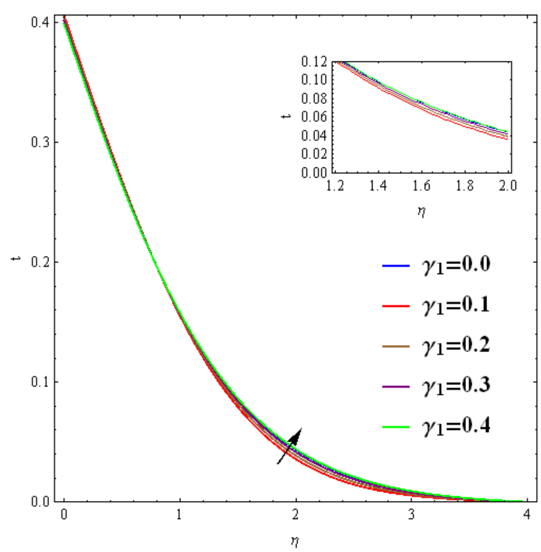

Fig. 7.6 : γ_1 on t.

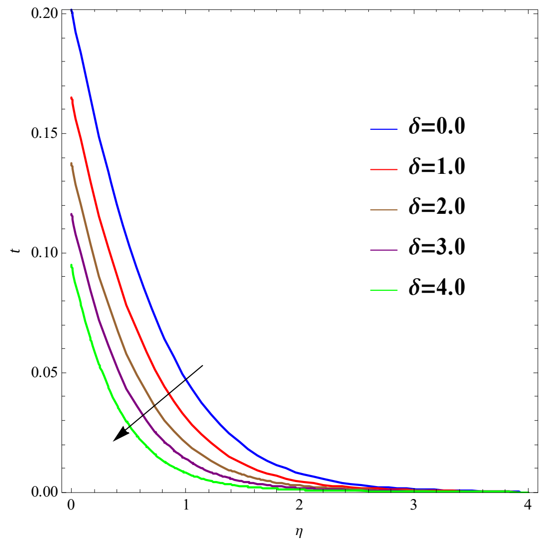

Fig. 7.7 : δ on t.

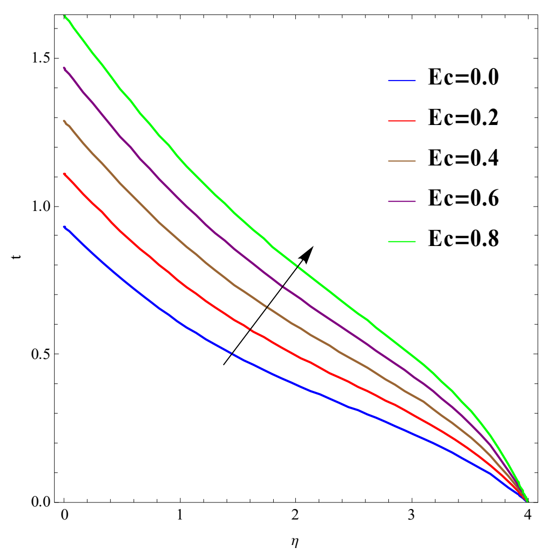

Fig. 7.8 : Ec on t.

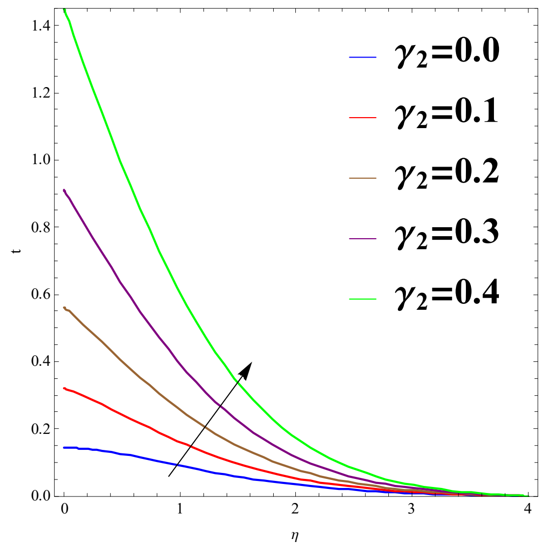

Fig. 7.9 : γ_2 on t.

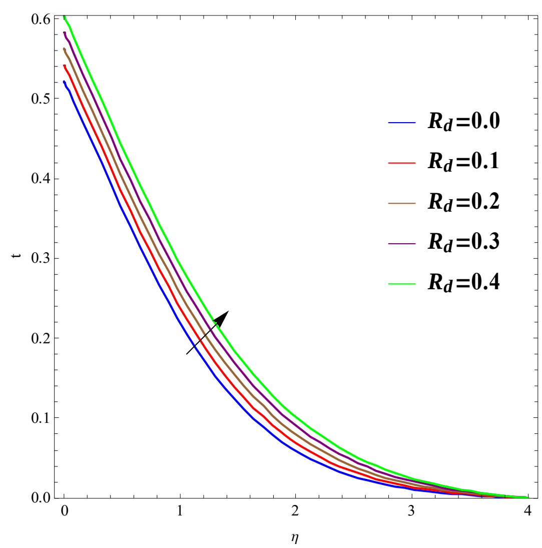

Fig. 7.10 : R_d on t.

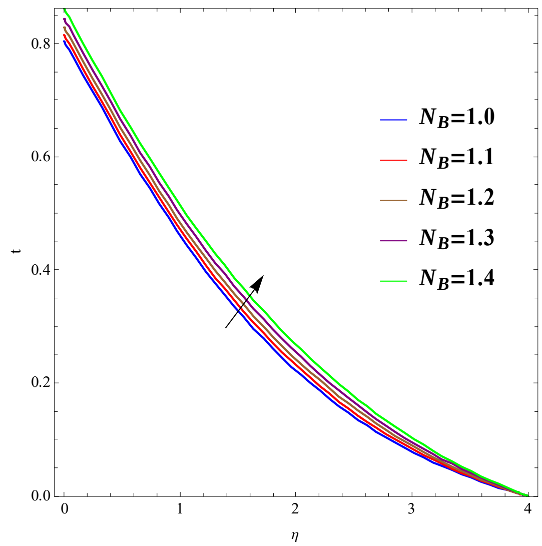

Fig. 7.11 : N_B on t.

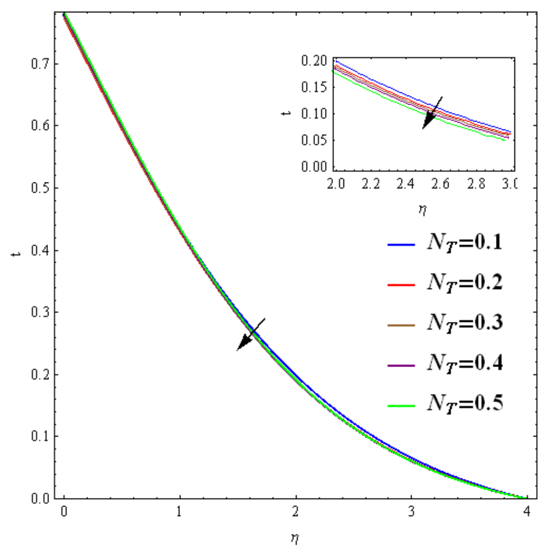

Fig. 7.12 : N_T on t.

7.7 Concentration

Fig. (7.13) shows that the increasing behavior of ($N_B = 1.0, 1.1, 1.2, 1.3, 1.4$) reduces concentration. For higher (N_B) the collision between nanoparticles occur fastly in fluid Thus more heat is emitted and therefore concentration decreases. Fig. (7.14) scrutinized the impact of ($N_t = 0.1, 0.2, 0.3, 0.4, 0.5$) on $J(\eta)$. Here thermophoresis parameter is directly related with temperature gradient. Hence fluid temperature enhances for ($N_t = 0.1, 0.2, 0.3, 0.4, 0.5$) so $J(\eta)$

increases.

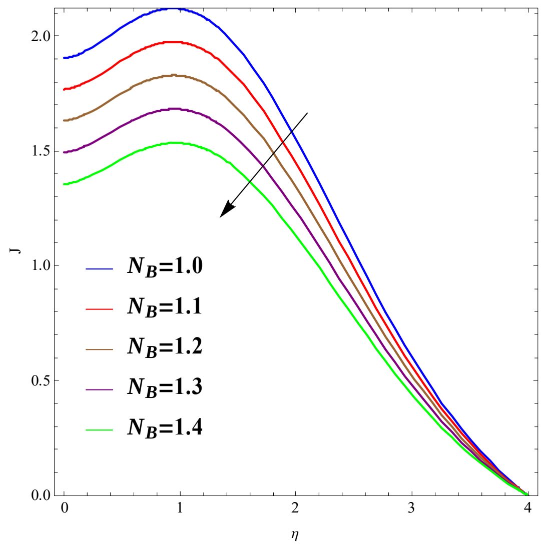

Fig. 7.13 : N_B on J.

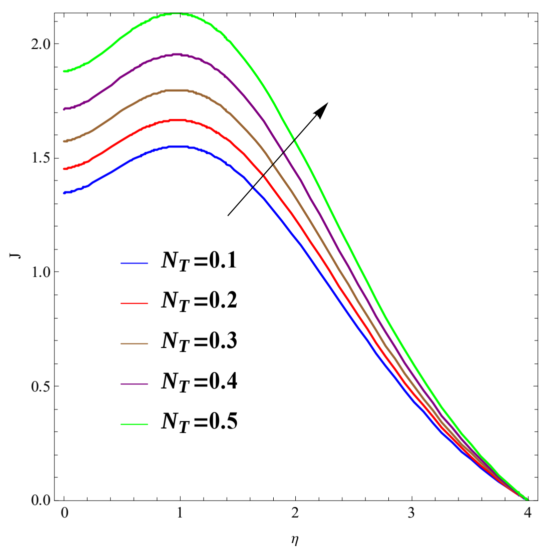

Fig. 7.14 : N_T on J.

7.8 Entropy (N_G) and Bejan number (Be)

Impact of (N_G) and (Be) for variation of (R_d) is seen in Figs. $[7.15-7.16]$. A increment in (N_G) and (Be) is accompanied by varying $(R_d = 0.0, 0.1, 0.2, 0.3, 0.4)$. Higher estimation of $(\chi = 0.1, 0.2, 0.3, 0.4, 0.5)$ on (N_G) and (Be) is seen in Figs. $[7.17-7.18]$. N_G is enhanced for larger (χ). Since for $(\chi = 0.1, 0.2, 0.3, 0.4, 0.5)$ the diffusivity of fluid increases which enhance the disorderness in the fluid particles and thus entropy (N_G) increases. Entropy (N_G) and (Be) via $(\Omega = 0.2, 0.3, 0.4, 0.5, 0.6)$ are discussed in Figs [7.19 − 7.20]. More disorderness occurs for larger $(\Omega = 0.2, 0.3, 0.4, 0.5, 0.6)$ therefore (N_G) enhances. However decaying behavior is seen for (Be) via Ω. Fig. [7.21 − 7.22] revealed the impact of (γ_4) on (N_G) and (Be). Here an reverse trend is seen for (N_G) and (Be) respectively. Figs. [7.23 − 7.24] show result of (Br) on entropy and Bejan number. For higher $(Br = 0.0, 0.1, 0.2, 0.3, 0.4)$ the (N_G) enhances while opposite result is observed for (Be). (Br) has direct relationship with heat through molecular conduction produced by fluid friction and heat transfer. Therefore the system produces more heat via higher (Br) which increases the systems disorderliness. Hence (N_G) is enhanced. Fig. (7.24) shows that(Be) is decreased via (Br).

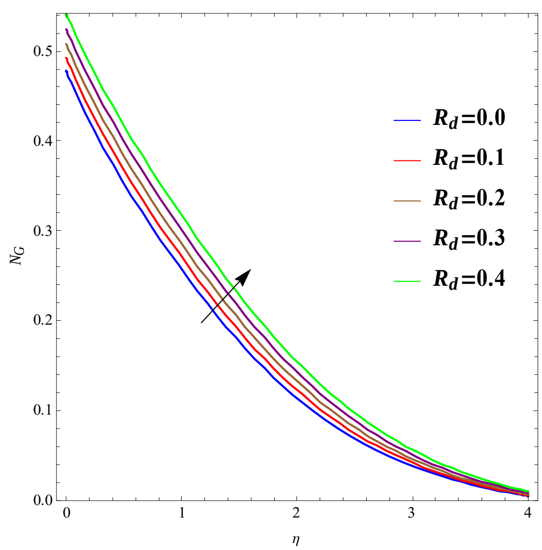

Fig. 7.15 : R_d on N_G.

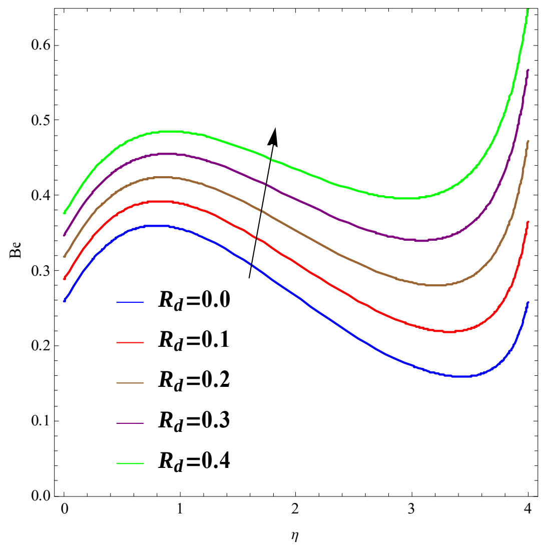

Fig. 7.16 : R_d on Be.

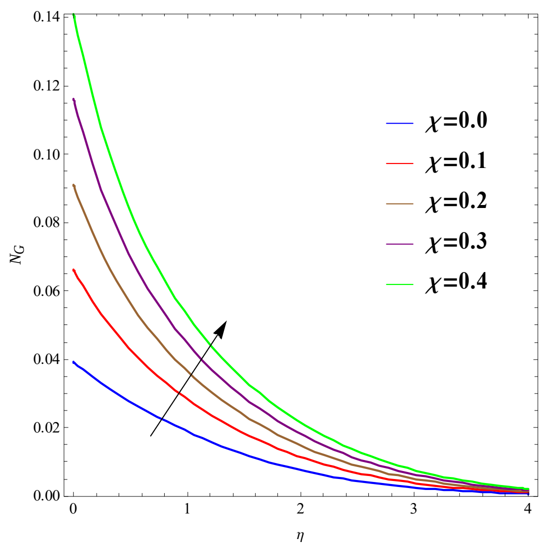

Fig. 7.17 : χ on N_G.

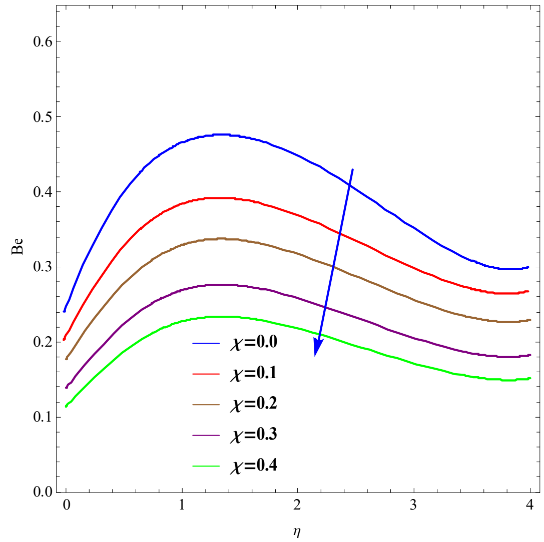

Fig. 7.18 : χ on Be.

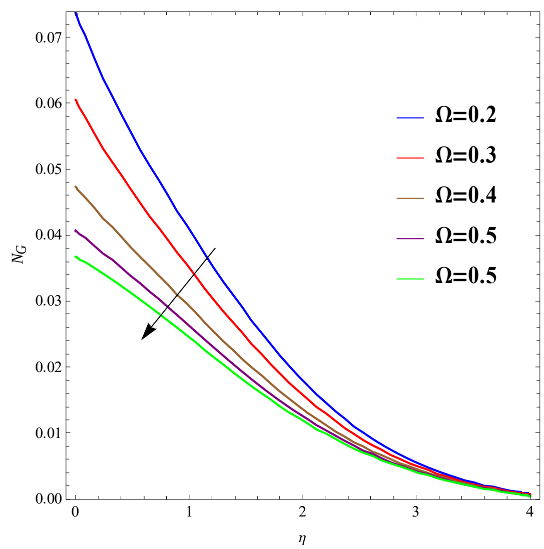

Fig. 7.19 : Ω on N_G.

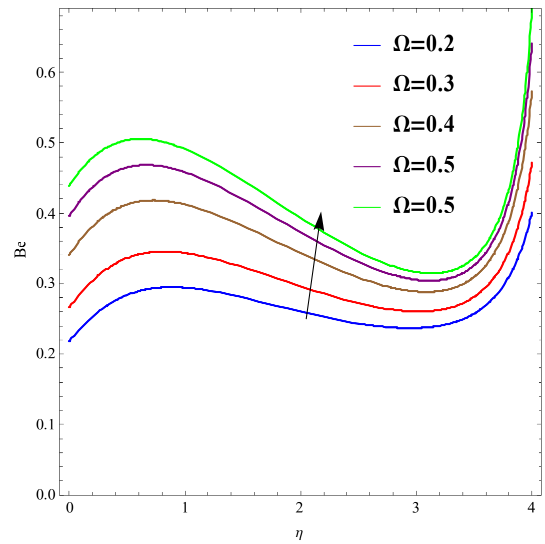

Fig. 7.20 : Ω on Be.

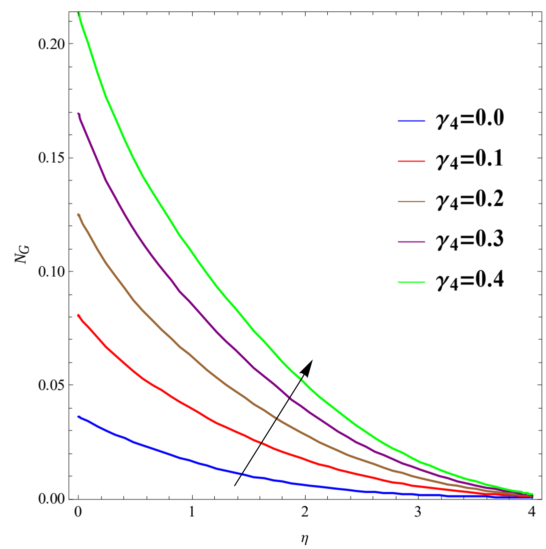

Fig. 7.21 : γ_4 on N_G.

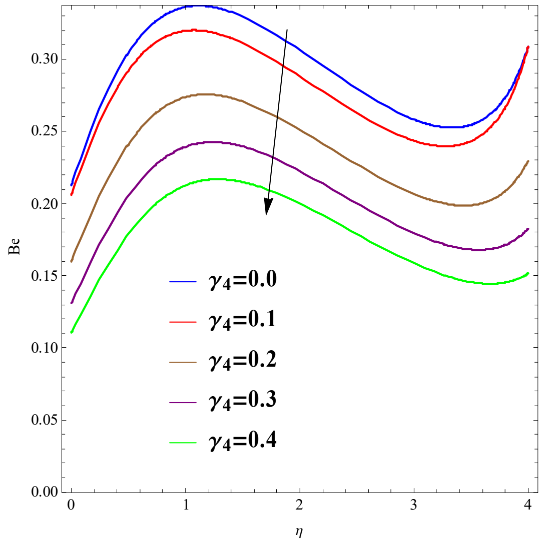

Fig. 7.22 : γ_4 on Be.

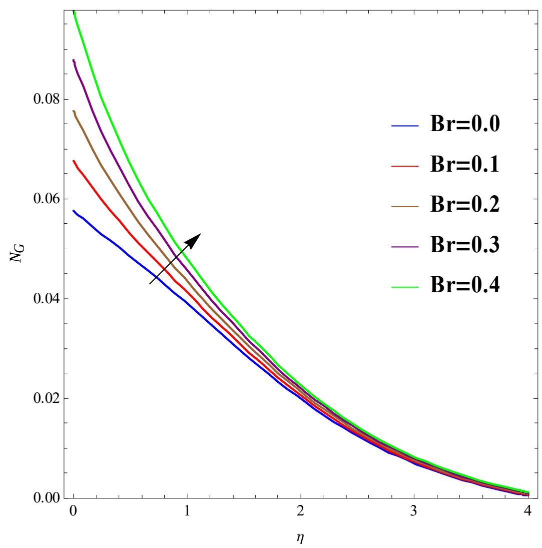

Fig. 7.23 : Br on N_G.

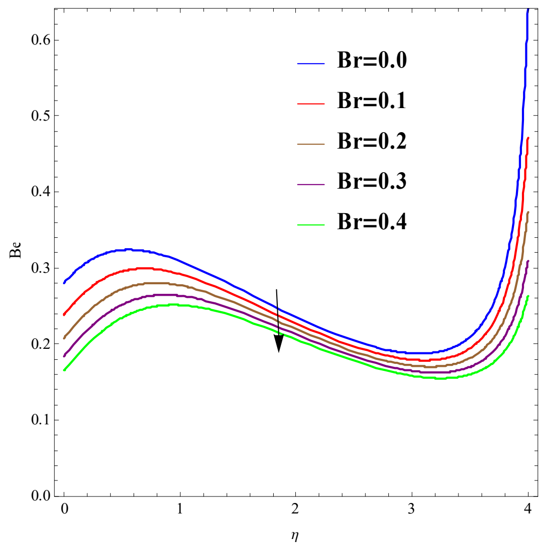

Fig. 7.24 : Br on Be.

7.9 Main points

The main outcomes are summarized as follows;

- $f\,'(\eta)$ enhances for larger (M), (λ) and (S).
- $t(\eta)$ reduces via (M), $(\Pr)$ and (Sc).
- Concentration is an increasing of N_t.
- For higher diffusion and temperature difference parameters there is a rise in entropy generation.
- For larger (M) and $\left(Da^{-1}\right)$ the (C_f) reduces.

Chapter 8

A novel perspective of Cattaneo-Christov double diffusions in MHD second grade nanofluid flow

MHD flow of second grade nano-fluid flow towards a stretched Riga wall is examined in this chapter. Heat and mass transfer are based upon Cattaneo-Christov (CC) theory. These considerations are totally different than classical heat and mass fluxes by Fourier and Fick's laws. The fundamental concept of the development of entropy is illustrated. Temperature expression consists of radiation, heat generation and mixed convection. Governing equations are solved through (OHAM).

8.1 Mathematical description

We study MHD two-dimensional mixed convective steady flow of second grade liquid towards a stretchable Riga wall. Heat and mass transporation are examined through Cattaneo-Christov (CC) flux model. Entropy generation is also taken into account. The plate is stretching along $(x-axis)$ with stretching velocity $(U_w = ax)$. $(U_e = bx)$ is the free stream velocity. Here $y-axis$ is perpendicular to $x-axis$. The problems statement are

$$\frac{\partial u}{\partial x} + \frac{\partial v}{\partial y} = 0. \tag{8.1}$$

$$
\left.\begin{array}{c}
u\frac{\partial u}{\partial x}+v\frac{\partial u}{\partial y}=U_e\frac{\partial U_e}{\partial x}+\frac{\alpha_1}{\rho}\left(\frac{\partial u}{\partial x}\frac{\partial^2 u}{\partial y^2}+u\frac{\partial^3 u}{\partial x\partial y^2}+\frac{\partial u}{\partial y}\frac{\partial^2 u}{\partial x\partial y}+v\frac{\partial^3 u}{\partial y^3}\right)\\
+\nu\frac{\partial^2 u}{\partial y^2}+\frac{\pi J_o Q_o}{8\rho}Exp[-\frac{\pi}{a_1}y]+g\beta_t(T-T_\infty)
\end{array}\right\}. \tag{8.2}
$$

Corresponding boundary conditions are

$$
\left.\begin{array}{c}
u=U_w=ax,\quad v=0 \text{ at } y=0,\\
u=U_e=bx \text{ when } y\to\infty
\end{array}\right\}. \tag{8.3}
$$

According to Cattaneo-Christove (CC) theory the heat flux satisfies

$$
\mathbf{q}+\delta_E*\left(\frac{\partial\mathbf{q}}{\partial t}+\mathbf{V}^*\cdot\nabla\mathbf{q}-\mathbf{q}\cdot\nabla\mathbf{V}^*+(\nabla\cdot\mathbf{V}^*)\mathbf{q}\right)=-k\nabla\mathbf{T}. \tag{8.4}
$$

For steady flow of an incompressible fluid Eq. [8.4] is reduced to

$$
\mathbf{q}+\delta_E(\mathbf{V}^*\cdot\nabla\mathbf{q}-\mathbf{q}\cdot\nabla\mathbf{V}^*)=-k\nabla\mathbf{T}. \tag{8.5}
$$

Energy expression in present situation satisfies

$$
\left.\begin{array}{c}
u\frac{\partial T}{\partial x}+v\frac{\partial T}{\partial y}=-\nabla.\mathbf{q}+\tau\left[D_B\frac{\partial C}{\partial y}\frac{\partial T}{\partial y}+\frac{D_T}{T_\infty}\left(\frac{\partial T}{\partial y}\right)^2\right]+\\
\frac{Q}{\rho c_p}(T-T_\infty)-\frac{16\sigma^*T^3}{3\rho c_p k_1}\frac{\partial^2 T}{\partial y^2}
\end{array}\right\} \tag{8.6}
$$

Eliminating $\mathbf{q}$ from Eqs. (8.5) and (8.6) yields to the following relation for the temperature field

$$
\left.\begin{array}{c}
u\frac{\partial T}{\partial x}+v\frac{\partial T}{\partial y}+\delta_E\Omega_E=\alpha\frac{\partial^2 T}{\partial y^2}+\tau\left[D_B\frac{\partial C}{\partial y}\frac{\partial T}{\partial y}+\frac{D_T}{T_\infty}\left(\frac{\partial T}{\partial y}\right)^2\right]\\
+\frac{Q}{\rho C_p}(T-T_\infty)-\frac{16\sigma^*T^3}{3\rho c_p k_1}\frac{\partial^2 T}{\partial y^2}
\end{array}\right\}, \tag{8.7}
$$

where Ω_E is given by

$$
\left.\begin{array}{c}
\Omega_E=u\frac{\partial u}{\partial x}\frac{\partial T}{\partial x}+v\frac{\partial u}{\partial y}\frac{\partial T}{\partial y}+u\frac{\partial v}{\partial x}\frac{\partial T}{\partial y}+v\frac{\partial u}{\partial y}\frac{\partial T}{\partial x}+2uv\frac{\partial^2 T}{\partial y\partial x}+u^2\frac{\partial^2 T}{\partial x^2}+v^2\frac{\partial^2 T}{\partial y^2}\\
-\frac{Q}{\rho C_p}\left(u\frac{\partial T}{\partial x}+v\frac{\partial T}{\partial y}\right)-\frac{\mu}{\rho C_p}\left(2u\frac{\partial u}{\partial y}\frac{\partial^2 u}{\partial x\partial y}+2v\frac{\partial u}{\partial y}\frac{\partial^2 u}{\partial y^2}\right)\\
-\tau D_B\left(v\frac{\partial T}{\partial y}\frac{\partial^2 C}{\partial y^2}+v\frac{\partial C}{\partial y}\frac{\partial^2 T}{\partial y^2}+u\frac{\partial^2 C}{\partial x\partial y}\frac{\partial T}{\partial y}+u\frac{\partial C}{\partial y}\frac{\partial^2 T}{\partial x\partial y}\right)\\
+2\frac{\tau D_T}{T_\infty}\left(v\frac{\partial T}{\partial y}\frac{\partial^2 T}{\partial y^2}+u\frac{\partial T}{\partial y}\frac{\partial^2 T}{\partial x\partial y}\right)+R_d\left(u\frac{\partial^2 T}{\partial x\partial y}+v\frac{\partial^2 T}{\partial y^2}\right)
\end{array}\right\}. \tag{8.8}
$$

The imposed boundary conditions are

$$\left.\begin{array}{c} -k\frac{\partial T}{\partial y} = h_f(T_f - T) \text{ at } y = 0, \\ T \to T_\infty \text{ when } y \to \infty \end{array}\right\}. \tag{8.9}$$

According to Cattaneo-Christove model the mass flux obeys following expression

$$\mathbf{j} + \delta_F * \left(\frac{\partial j}{\partial t} + \mathbf{V}^* \cdot \triangledown \mathbf{j} - \mathbf{j} \cdot \triangledown \mathbf{V}^* + (\triangledown \cdot \mathbf{V}^*)\mathbf{j}\right) = -D_B \triangledown \mathbf{C}. \tag{8.10}$$

For steady flow of an incompressible fluid the Eq. (8.10) yields

$$\mathbf{j} + \delta_F(\mathbf{V}^* \cdot \triangledown \mathbf{j} - \mathbf{j} \cdot \triangledown \mathbf{V}^*) = -D_B \triangledown \mathbf{C}. \tag{8.11}$$

Here concentration field satisfies

$$\left. u\frac{\partial C}{\partial x} + v\frac{\partial C}{\partial y} = -\nabla.\mathbf{j} + \frac{D_T}{T_\infty}\frac{\partial^2 T}{\partial y^2} \right\}. \tag{8.12}$$

Eliminating $\mathbf{j}$ from Eqs. (8.11) and (8.12) one arrives at

$$\left. u\frac{\partial C}{\partial x} + v\frac{\partial C}{\partial y} + \delta_F \Omega_F = D_B\frac{\partial^2 C}{\partial y^2} + \frac{D_T}{T_\infty}\frac{\partial^2 T}{\partial y^2} \right\}, \tag{8.13}$$

in which Ω_F is given by

$$\left.\begin{array}{c} \Omega_F = u^2\frac{\partial^2 C}{\partial x^2} + u\frac{\partial u}{\partial x}\frac{\partial C}{\partial x} + u\frac{\partial v}{\partial x}\frac{\partial C}{\partial y} + 2uv\frac{\partial^2 C}{\partial x \partial y}\frac{\partial T}{\partial x} + v\frac{\partial u}{\partial y}\frac{\partial C}{\partial x} + v^2\frac{\partial^2 C}{\partial y^2} + \\ v\frac{\partial v}{\partial y}\frac{\partial C}{\partial y} - D_B\left(u\frac{\partial^3 C}{\partial x \partial y^2} + v\frac{\partial^3 C}{\partial y^3}\right) - \frac{D_T}{T_\infty}\left(v\frac{\partial^3 T}{\partial y^3} + u\frac{\partial^3 T}{\partial x \partial y^2}\right) \end{array}\right\}. \tag{8.14}$$

The relevant boundary conditions are

$$\left.\begin{array}{c} C \to C_w \text{ at } y = 0, \\ C \to C_\infty \text{ as } y \to \infty, \end{array}\right\}. \tag{8.15}$$

By considering transformations

$$\left. u = axf'(\eta), \quad v = -\sqrt{a\nu}f(\eta), \quad t = \frac{T - T_\infty}{T_w - T_\infty}, \; J = \frac{C - C_\infty}{C_w - C_\infty}, \; \eta = \sqrt{\frac{a}{\nu}}y \right\}, \tag{8.16}$$

the incompressibility condition is satisfied and problems now become

$$\left.\begin{array}{c} f''' + f'' - f'^2 + \alpha^*\left(2f'f''' - (f'')^2 - f''''f\right) \\ +S^2 + MExp[-B\eta] + \lambda t = 0 \end{array}\right\}, \tag{8.17}$$

$$\left.\begin{array}{c} (1+R_d)t'' + \Pr\gamma_1(ff't' + f'^2t'' - \delta ft' - 2ff't'') - (\Pr)(\gamma_1)(N_B)(ft'J'' - fJ't') \\ -\Pr\gamma_1 N_t J''t' - \Pr\gamma_1 R_d ft'' + N_B t'J' + N_T t'^2 + \Pr\delta t] + \Pr ft' = 0, \end{array}\right\} \tag{8.18}$$

$$\left. J'' + LefJ' + \frac{N_B}{N_T}t'' - Le\gamma_3[f^2J'' + ff'J'] - \gamma_3\frac{N_B}{N_T}t'' = 0\right\}, \tag{8.19}$$

$$\left\{\begin{array}{c} f(0) = 0,\ f'(0) = 1,\ f^{'}(\infty) = S \\ t'(0) = -\gamma_2(1 - t(0)),\ t(\infty) = 0, \\ J(0) = 1,\ J(\infty) = 0 \end{array}\right\}. \tag{8.20}$$

8.1.1 Entropy generation

Entropy generation rate here is given by

$$\left.\begin{array}{c} N_{gen}^{'''} = \frac{R_D}{T_\infty}\left(\frac{\partial T}{\partial y}\frac{\partial C}{\partial y}\right) + \frac{R_D}{T_\infty}\left(\frac{\partial C}{\partial y}\right)^2 \\ +\frac{k}{T_\infty^2}\left(\frac{\partial T}{\partial y}\right)^2 + \frac{16\sigma^*}{T_\infty^2}\left(\frac{\partial T}{\partial y}\right)^2 \end{array}\right\}. \tag{8.21}$$

Characteristic entropy $\left(N_0^{'''}\right)$ rate is defined as follows

$$N_0^{'''} = \frac{k(\nabla T)^2}{L^2T_\infty^2}, \tag{8.22}$$

non-dimensional form of entropy generation

$$N_G = \frac{N_{gen}^{'''}}{N_0^{'''}} = \mathrm{Re}(1+R_d)t'^2 + \frac{\mathrm{Re}\,\chi\gamma_4}{\Omega}t'J' + \mathrm{Re}\,\chi\gamma_4 J'^2. \tag{8.23}$$

The skin friction coefficient is

$$C_{fx} = \left(\frac{\tau_w}{\rho_f\left(U_w\right)^2}\right), \tag{8.24}$$

or

$$\sqrt{\mathrm{Re}_x} C_{fx} = f''(0) + \alpha^* \left(3f'(0)f''(0) - f(0)f'''(0)\right). \tag{8.25}$$

8.1.2 Dimensionless parameters

$$\left.\begin{array}{c} M\left(=\frac{\pi J_o M_o}{8\rho a^2}\right),\ Da^{-1}\left(=\frac{\nu\epsilon}{k}\right),\ \lambda\left(=\frac{g\beta_t(T_w-T_\infty)}{a}\right),\ B\left(=\frac{\pi}{a_1}\sqrt{\frac{\nu}{a}}\right), \\ S\left(=\frac{b}{a}\right),\ \alpha^*\left(=\frac{\alpha_1 a}{\mu}\right),\ R_d\left(=\frac{16\sigma^* T_\infty^3}{3k_1 k}\right),\ \gamma_1\left(=a\delta_E\right), \\ \gamma_4=\left(\frac{\nabla C}{C_\infty}\right),\ N_B\left(=\frac{\tau D_B(C_w-C_\infty)}{\nu}\right),\ N_T\left(=\frac{\tau D_T(T_w-T_\infty)}{\nu T_\infty}\right), \\ Ec\left(=\frac{U_w^2}{C_P(T_w-T_\infty)}\right),\ Le\left(=\frac{\nu}{D_B}\right),\ \delta\left(=\frac{Q}{\rho C_p}\right),\ \Pr\left(=\frac{\mu C_p}{k}\right), \\ \chi=\left(\frac{R_D C_\infty}{k}\right),\ \mathrm{Re}_x\left(=\frac{U_w x}{\nu_f}\right),\ \left(\Omega=\left(\frac{\nabla T}{T_\infty}\right)\right), \\ \left(Br=\left(\frac{\mu U_w^2}{k\nabla T}\right)\right), \gamma_2\left(=\frac{h_f \nu}{a}\right), \gamma_3\left(=a\delta_F\right), \end{array}\right\}. \tag{8.26}$$

8.2 Methodology (OHAM)

The series solutions are determined using the optimal method of homotopy (OHAM) analysis.

$$\varepsilon_{k^*}^f(h_f) = \frac{1}{N+1}\sum_{j=0}^{N} * \left[\sum_{i=0}^{k}(f_i)_{\eta=j\Pi\eta}\right]^2, \tag{8.27}$$

$$\varepsilon_{k^*}^t(h_f,h_t,h_J) = \frac{1}{N+1}\sum_{j=0}^{N} * \left[\sum_{i=0}^{k^*}(f_i)_{\eta=j\Pi\eta}, \sum_{i=0}^{k^*}(t_i)_{\eta=j\Pi\eta}, \sum_{i=0}^{k^*}(J_i)_{\eta=j\Pi\eta}\right]^2, \tag{8.28}$$

$$\varepsilon_{k^*}^J(h_f,h_t,h_J) = \frac{1}{N+1}\sum_{j=0}^{N} * \left[\sum_{i=0}^{k^*}(f_i)_{\eta=j\Pi\eta}, \sum_{i=0}^{k^*}(t_i)_{\eta=j\Pi\eta}, \sum_{i=0}^{k^*}(J_i)_{\eta=j\Pi\eta}\right]^2, \tag{8.29}$$

$$\varepsilon_{k^*}^{t^*} = \varepsilon_{k^*}^f + \varepsilon_{k^*}^t + \varepsilon_{k*}^J, \tag{8.30}$$

The optimal values of convergence-control parameters are $h_f = -1.79862$, $h_t = -0.755535$ and $h_J = -1.3454$. Total residual error is $\varepsilon_{k^*}^{t^*} = 0.0535156$.

Table; 8.1 Individual averaged squared residual errors considering optimal values of auxiliary parameters. It is observed that the averaged squared residual error reduces with higher order approximations.

k^*	$\varepsilon_{k^*}^{f}$	$\varepsilon_{k^*}^{t}$	$\varepsilon_{k^*}^{J}$
2	0.0357456	0.0100224	0.137
6	0.0336475	0.00184235	0.0180257
8	0.0323631	0.000687534	0.00631931
10	0.0307158	0.000145842	0.00189651
14	0.0295988	0.0000438513	0.00124949
16	0.0291453	0.0000269803	0.00121365

8.3 Discussion

This subsection consists of impacts of physical variables for the velocity $f'(\eta)$, temperature $t(\eta)$, concentration $J(\eta)$ and entropy N_G. These values selected in computations are $S = 0.1$, $M = 0.2$, $N_T = 0.1$, Pr =1.2, $N_B = 0.5$, Re $= 0.1$, $\alpha^* = 0.1$, $\gamma_1 = \gamma_2$= 0.2, $\gamma_3 = 0.3$, $\chi = 0.1$ and Ω = 0.4.

8.4 Velocity profile

Fig. (8.1) shows the variation of $(M = 0.0, 0.1, 0.2, 0.3, 0.4, 0.5)$ on $f'(\eta)$. For larger (M) the velocity enhances. In fact due to applied magnetic field Lorentz force produce. This force provides resistance to fluid particles and thus velocity reduces. Influence of (α^*) on $f'(\eta)$ is considered in Fig. (8.2). There is an increase in velocity via (α). Fig. (8.3) illustrates (S) against $f'(\eta)$. Here $f'(\eta)$ is increased for larger of $(S = 0.7, 0.8, 0.9, 1.0, 1.1, 1.2, 1.3)$. Influence of (λ) on $f'(\eta)$ is depicted in Fig. (8.4). $f'(\eta)$ enhances via $(\lambda = 0.0, 0.2, 0.4, 0.6, 0.8, 1.0)$. In fact higher (λ) correspond to decay of viscous forces and so velocity increases.

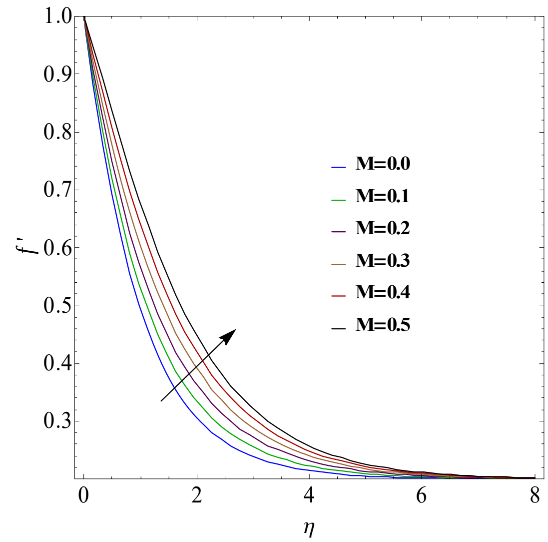

Fig. 8.1 : M on f'.

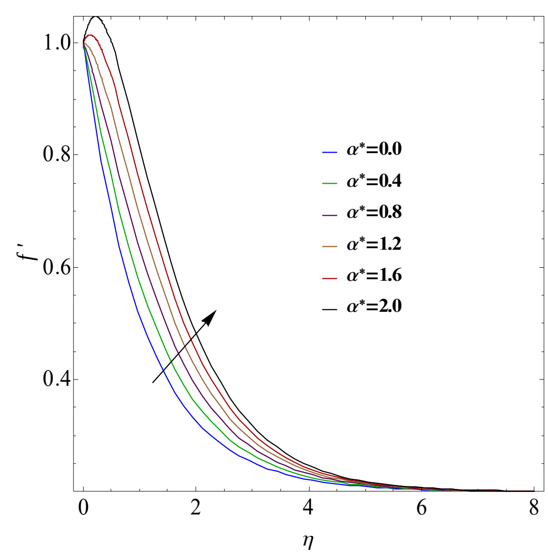

Fig. 8.2 : α^* on f'.

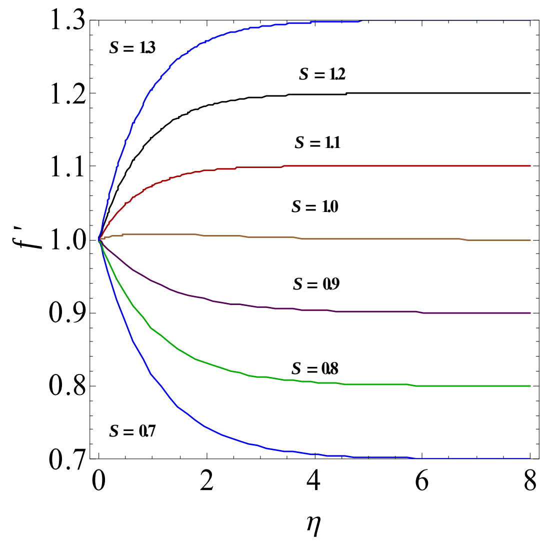

Fig. 8.3 : S on f'.

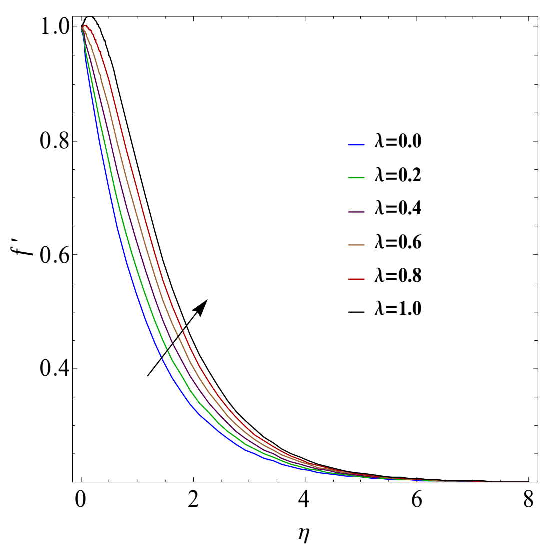

Fig. 8.4 : λ on f'.

8.5 Temperature

Influence of ($\gamma_1 = 0.0, 0.2, 0.4, 0.6, 0.8, 1.0$) on $t(\eta)$ is represented in Fig. (8.5). Particles of fluids take more time to transfer heated region to cold one. Therefore $t(\eta)$ is decays for larger (γ_1). Fig. (8.6) exhibits that $t(\eta)$ reduces for larger ($\gamma_3 = 0.0, 0.5, 1.0, 1.5, 2.0, 2.5$). Fig. 8.7 witnesses that ($\Pr = 1.0, 2.0, 3.0, 4.0, 5.0, 6.0$) leads to decline $t(\eta)$. For higher ($\Pr$) the momentum diffusivity dominates the thermal diffusivity. Therefore temperature decays. Influence of ($\delta =$

$0.1, 0.3, 0.6, 0.9.1.2, 1.5)$ on $t(\eta)$ is inspected in Fig. (8.8). Higher (δ) produce more heat in the fluid which enhances temperature. Variation of (R_d) on $t(\eta)$ is discussed in Fig. (8.9). Obviously $t(\eta)$ is increased via $(R_d = 0.1, 0.3, 0.6, 0.9.1.2, 1.5)$. Impact of $t(\eta)$ for (N_B) is presented in Fig. (8.10). $t(\eta)$ upsurges for larger $(N_B = 0.1, 0.5, 1.0, 1.2, 2.0, 2.5)$. Opposite result is seen for larger $(N_t = 0.1, 0.5, 1.0, 1.2, 2.0, 2.5)$ (see Fig. 8.11).

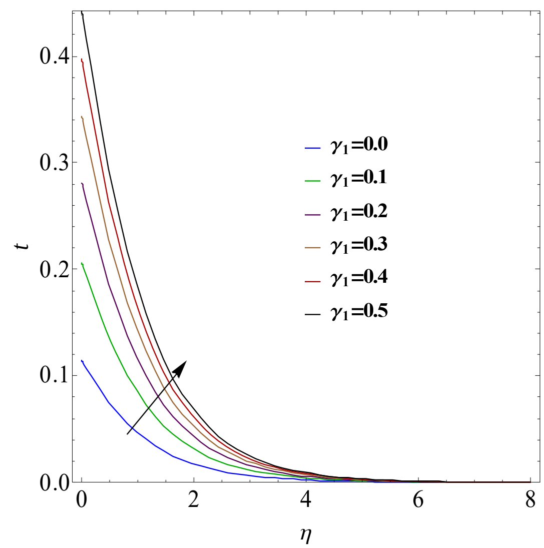

Fig. 8.5 : γ_1 on t.

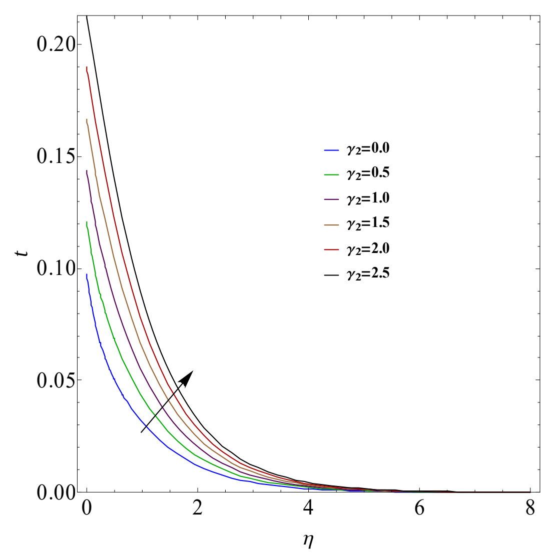

Fig. 8.6 : γ_2 on t.

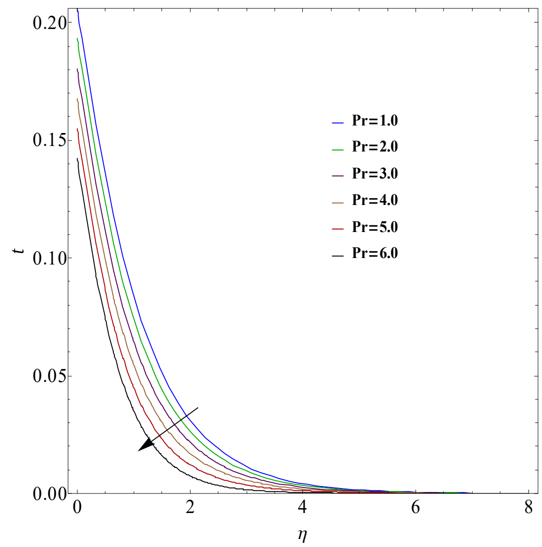

Fig. 8.7 : Pr on t.

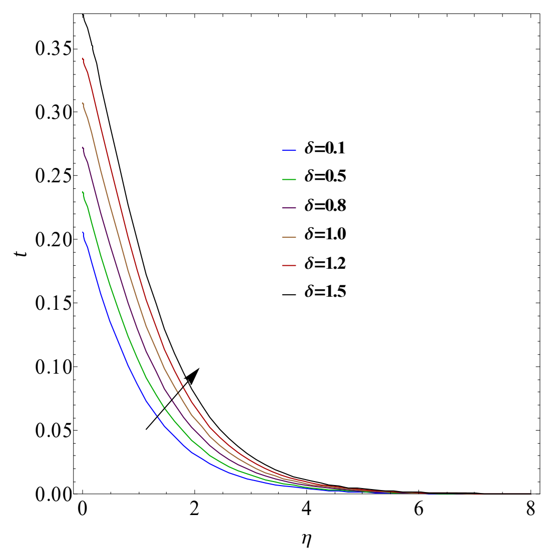

Fig. 8.8 : δ on t.

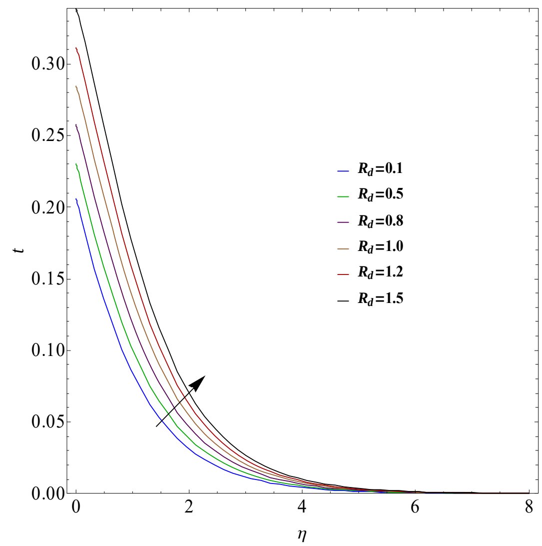

Fig. 8.9 : R_d on t.

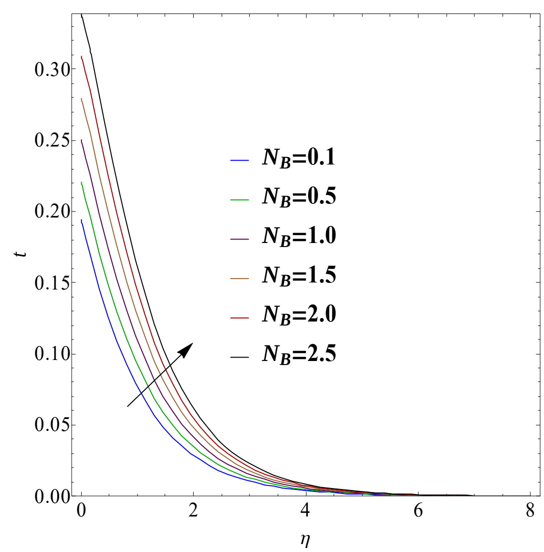

Fig. 8.10 : N_B on t.

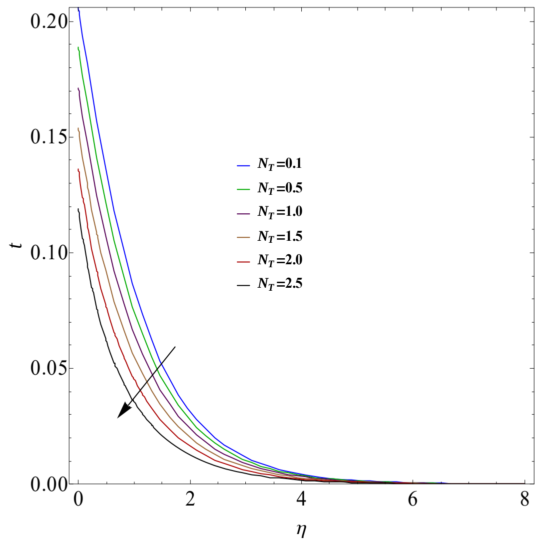

Fig. 8.11 : N_T on t.

8.6 Concentration

Fig. (8.12) demonstrates the impact of (γ_3) on $J(\eta)$. Clearly $J(\eta)$ is reduced for larger $(\gamma_3 = 0.0, 0.2, 0.4, 0.6, 0.8, 1.0)$. Physically for higher (γ_3) the mass transfer diminishes from fluid to surface. Impact of (Le) on $J(\eta)$ is discussed in Fig. (8.13). The concentration reduces with higher (Le). Fig. (8.14) shows that the increasing behavior of $(N_B = 0.1, 0.5, 1.0, 1.5, 2.0, 2.5)$ reduces concentration. Fig. (8.15) analyzed impact of $(N_T = 0.1, 0.5, 1.0, 1.5, 2.0, 2.5)$ on $J(\eta)$. Here $J(\eta)$ increases. In fact thermophoresis parameter is directly related with temperature gradient. Therefore temperature of fluid enhances for $(N_T = 0.1, 0.5, 1.0, 1.5, 2.0, 2.5)$ so $J(\eta)$ increases.

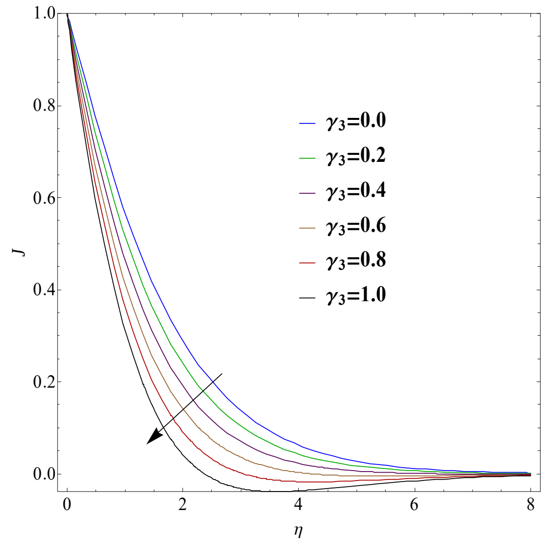

Fig. 8.12 : γ_3 on J.

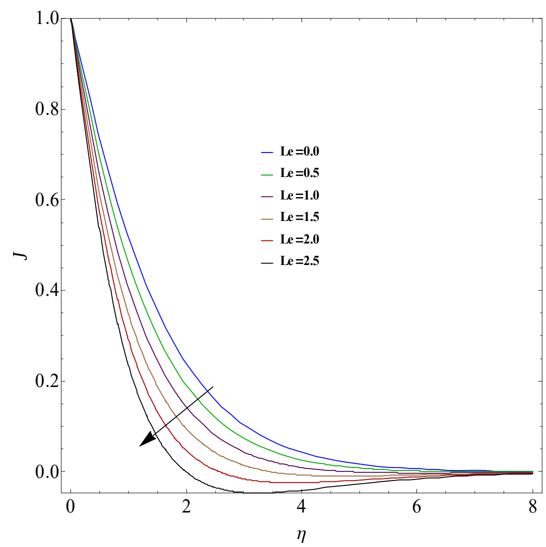

Fig. 8.13 : Le on J.

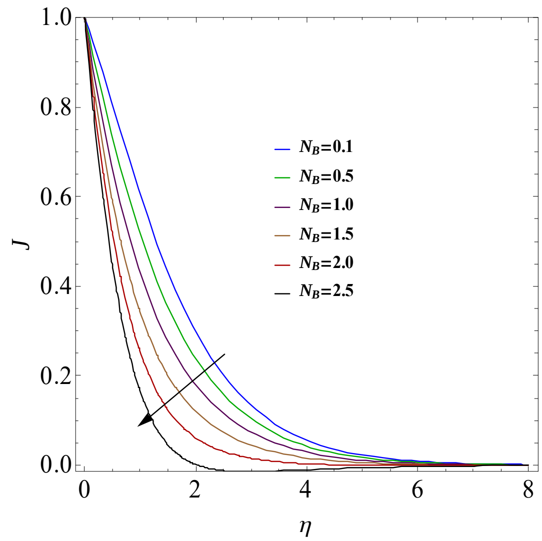

Fig. 8.14 : N_B on J.

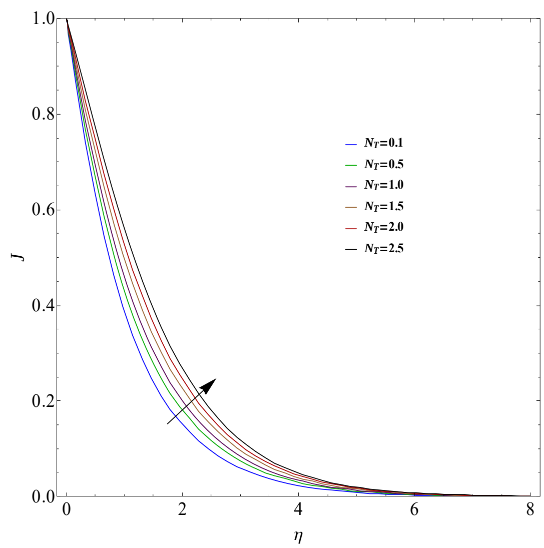

Fig. 8.15 : N_T on J.

8.7 Entropy

Fig. (8.16) shows the outcome of (χ) on $N_G(\eta)$. For higher $(\chi = 0.1, 0.5, 1.0, 1.5, 2.0, 2.5)$ the $N_G(\eta)$ boosts. Physically the higher fluid diffusivity increase the disorderness in the fluid particles and therefore entropy enhances. The effect of $(\mathrm{Re} = 0.1, 0.2, 0.3, 0.4, 0.5, 0.6)$ on $N_G(\eta)$ is discussed in Fig. (8.17). Our simulation shows that entropy is improved by the greater estimation of (Re). Here viscous effects here are dominated by inertial forces.

$(R_d = 0.1, 0.2, 0.3, 0.4, 0.5, 0.6)$ via entropy $(N_G(\eta))$ is plotted in Fig. (8.18). Clearly $N_G(\eta)$ increased by varying $(R_d = 0.1, 0.2, 0.3, 0.4, 0.5, 0.6)$. Entropy generation rate $(N_G(\eta))$ via (Ω) is deliberated in Fig. 8 (.19). More disorderness occurs for higher $(\Omega = 0.1, 0.2, 0.3, 0.4, 0.5, 0.6)$ and so $N_G(\eta)$ increases. Fig. (8.20) disclosed the impact of $(\gamma_4 = 0.1, 0.2, 0.3, 0.4, 0.5, 0.6)$ on $N_G(\eta)$. Here entropy is increased via (γ_4).

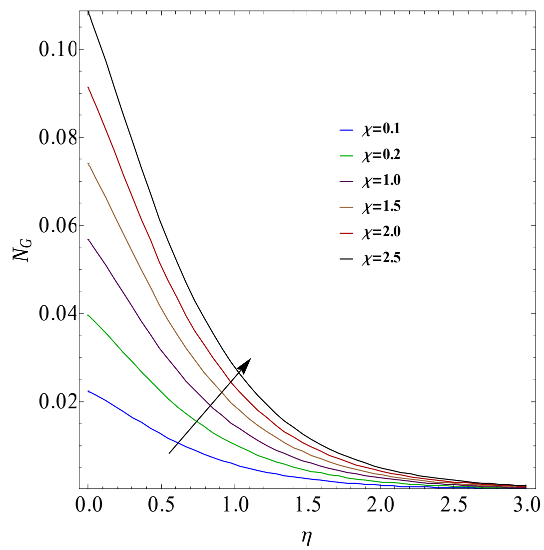

Fig. 8.16 : χ on N_G.

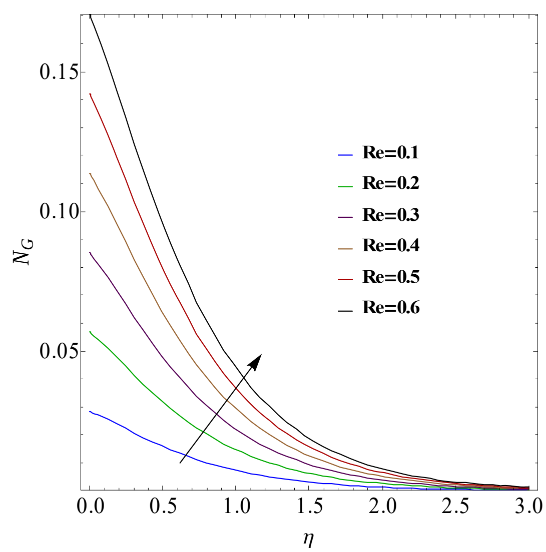

Fig. 8.17 : Re on N_G.

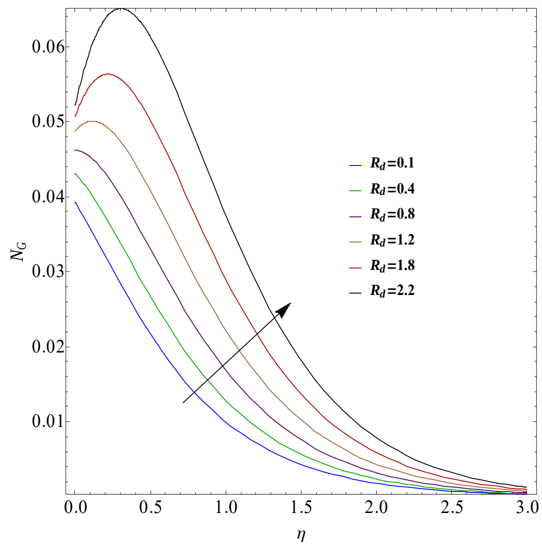

Fig. 8.18 : R_d on N_G.

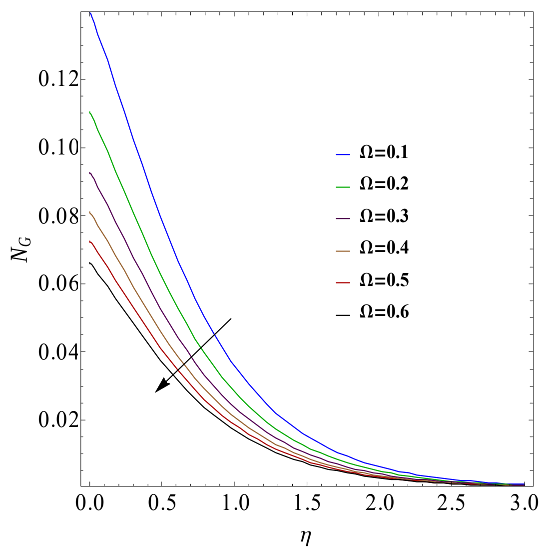

Fig. 8.19 : Ω on N_G.

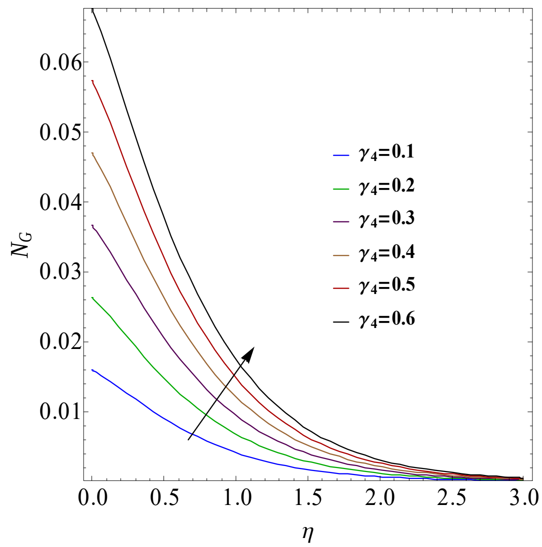

Fig. 8.20 : γ_4 on N_G.

8.8 Concluding remarks

- An increasing trend of velocity holds for (M), (α^*) and (S).
- $t(\eta)$ is enhanced for larger (R_d) and (γ_1).
- For larger (N_B) temperature enhances however opposite trend is noticed for concentration.
- Concentration is reduced via (γ_2) and (Le).
- Effects of (R_d) and (γ_4) on (N_G) are opposite to that of (Ω).

Chapter 9

Melting heat in Jeffrey fluid flow through permeable space

This chapter examines MHD Jeffrey nano-fluid bounded by a non-linear stretching surface with variable thickness. Permeable medium is also taken into account. Darcy-Forchheimer flow is investigated. Energy equation is considered in the existence of melting heat and heat absorption/ generation. The governing PDEs (partial differential equations) are converted into ODEs (ordinary differential equations) by using transformation. These non-dimensional equations are solved through Optimal homotopy method. Outcomes of involved parameters are sketched through graphs and analyzed.

9.1 Mathematical modeling

We consider steady two dimensional (2D) flow of an incompressible Jeffrey nano-fluid past a non-linear stretching sheet. Flow is due to stretching sheet at $y = \delta^*(x+b)^{\frac{1-n}{2}}$. Flow along the $(x - axis)$ has stretching velocity $(U_w = a(x+b)^n)$. MHD and heat generation concepts are utilized. Melting heat is examined. Brownian diffusion and thermophoresis are explained. The problems statements are

$$\frac{\partial u}{\partial x} + \frac{\partial v}{\partial y} = 0, \tag{9.1}$$

$$\left.\begin{array}{c} u\frac{\partial u}{\partial x} + v\frac{\partial u}{\partial y} = \frac{\nu}{1+\lambda_2}\left[\frac{\partial^2 u}{\partial y^2} + \lambda_1\left\{u\frac{\partial^3 u}{\partial x \partial y^2} + v\frac{\partial^3 u}{\partial y^3} - \frac{\partial u}{\partial x}\frac{\partial^2 u}{\partial y^2} + \frac{\partial u}{\partial y}\frac{\partial^3 u}{\partial x \partial y}\right\}\right] \\ -\frac{\sigma}{\rho}B^2(x)u - \frac{\nu\epsilon}{k}u - \frac{c_b\epsilon}{\sqrt{k}}u^2 \end{array}\right\}, \tag{9.2}$$

$$u\frac{\partial T}{\partial x}+v\frac{\partial T}{\partial y}=\alpha\frac{\partial^2 T}{\partial y^2}+\tau\left(D_B\frac{\partial C}{\partial y}\frac{\partial T}{\partial y}+\frac{D_T}{T_\infty}(\frac{\partial T}{\partial y})^2\right)+\frac{Q(x)(T_\infty-T)}{(\rho c)_p}, \tag{9.3}$$

$$u\frac{\partial C}{\partial x}+v\frac{\partial C}{\partial y}=D_B\frac{\partial^2 C}{\partial y^2}+\frac{D_T}{T_\infty}(\frac{\partial^2 T}{\partial y^2}), \tag{9.4}$$

$$u=U_w\left(x\right)=a(x+b)^n,\ v=0,\, T=T_w, C=C_w \text{ at } y=\delta^*(x+b)^{\frac{1-n}{2}}, \tag{9.5}$$

$$u\to 0,\ T\to T_\infty,\ C\to C_\infty \text{ when } y\to\infty. \tag{9.6}$$

$$k(\frac{\partial T}{\partial y})=\rho[\lambda^*+C_S(T_m-T_0)]v(x,0) \text{ at } y=\delta^*(x+b)^{\frac{1-n}{2}}, \tag{9.7}$$

where $Q(x)=Q_0(x+b)$ the nonuniform heat generation/absorption, and $B(x)=B_0(x+b)$ the nonuniform magnetic field.

Consider

$$\left.\begin{array}{c}\xi=\sqrt{\frac{n+1}{2}\frac{a}{v}(x+b)^{n-1}}y,\ \psi=\sqrt{2a\left(n+1\right)^{-1}v(x+b)^{n+1}}F(\xi),\\ u=a(x+b)^nF'(\xi),\ v=-\sqrt{\frac{n+1}{2}va(x+b)^{n-1}}[F(\xi)+\xi\frac{n-1}{n+1}F'(\xi)],\end{array}\right\} \tag{9.8}$$

$$\Theta\left(\xi\right)=\frac{T-T_m}{T_\infty-T_m},\ G(\xi)=\frac{C-C_\infty}{C_\infty}, \tag{9.9}$$

equation (9.1) is trivially satisfied while Eqs. $[(9.2-9.6)]$ take the following forms

$$\left.\begin{array}{c}F'''+(1+\lambda_2)FF''-(\frac{2n}{n+1})(1+\lambda_2)F'^2+K[(\frac{n+1}{2})F'F^{iv}-(\frac{3n-1}{2})F''^2-(n-1)F'F''']\\ -(\frac{2}{n+1})(1+\lambda_2)(M)^2F'-(\frac{2}{n+1})(1+\lambda_2)Da^{-1}F'-(\frac{2}{n+1})(1+\lambda_2)\beta F'^2=0\end{array}\right\}, \tag{9.10}$$

$$\Theta''+\Pr F\Theta'+\Pr N_B\Theta'\Phi'+\Pr N_T\Theta'^2+(\frac{2}{n+1})\Pr\delta\Theta=0, \tag{9.11}$$

$$\Phi''+Le\Pr F\Phi'+\frac{N_T}{N_B}\Theta''=0, \tag{9.12}$$

$$\left.\begin{array}{c}F'\left(\alpha\right)=1,\quad \Theta\left(\alpha\right)=0,\quad \left(Mn\right)\Theta^{'}(\alpha)+\Pr F(\alpha)+\Pr\xi(\frac{n-1}{n+1})=0,\\ \Phi(\alpha)=0, F^{'}(\infty)=0,\ \Theta(\infty)=1,\ \Phi(\infty)=0\end{array}\right\}, \tag{9.13}$$

Here $\alpha=\delta_1\sqrt{\frac{n+1}{2}\frac{a}{v}}$, represents surface thickness parameter and $\xi=\alpha=(\delta\sqrt{\frac{n+1}{2}\frac{a}{v}})$ represents the plate surface. we define $F(\xi)=f(\xi-\alpha)=f(\eta), \Theta(\xi)=t(\xi-\alpha)=t(\eta)$, $\Phi(\xi)=J(\xi-\alpha)=$

$J(\eta)$ therefore governing Eqs. $(9.10-9.13)$ yield

$$\left.\begin{array}{c} f''' + (1+\lambda_2) f f'' - (\frac{2n}{n+1})(1+\lambda_2) f'^2 + K[(\frac{n+1}{2}) f' f^{iv} - (\frac{3n-1}{2}) f''^2 - (n-1) f' f'''] \\ -(\frac{2}{n+1})(1+\lambda_2)(M)^2 f' - (\frac{2}{n+1})(1+\lambda_2) Da^{-1} f' - (\frac{2}{n+1})(1+\lambda_2)\beta f'^2 = 0 \end{array}\right\}, \tag{9.14}$$

$$t'' + \Pr N_T t'^2 + (\frac{2}{n+1}) \Pr \delta t + \Pr f t' + \Pr N_B t' J' = 0, \tag{9.15}$$

$$J'' + Le \Pr f J' + \frac{Nt}{Nb} t'' = 0, \tag{9.16}$$

$$\left.\begin{array}{c} f'(0) = 1, \quad t(\alpha) = 0, \quad (Mn)\, t'(0) + \Pr f(0) + \Pr \alpha (\frac{n-1}{n+1}) = 0, \; J(0) = 0, \\ f'(\infty) = 0, \; t(\infty) = 1, \; J(\infty) = 0 \end{array}\right\}. \tag{9.17}$$

9.2 Engineering curiosity

The skin friction, Nusselt number and local Sherwood number are define as

$$C_f = \frac{\tau_w}{\rho u_w^2/2}, \; N_u = \frac{(x+b) q_w}{k(T_\infty - T_m)}, Sh = \frac{(x+b) q_m}{D_B (C_\infty)}. \tag{9.18}$$

In non-dimensional form we get

$$C_f \sqrt{\mathrm{Re}_x} = 2\sqrt{\frac{n+1}{2}} \frac{1}{1+\lambda_2} (f''(0) + K f''(0)), \tag{9.19}$$

$$\frac{Nu}{\sqrt{\mathrm{Re}_x}} = -\sqrt{\frac{n+1}{2}} t'(0), \tag{9.20}$$

$$\frac{Sh}{\sqrt{\mathrm{Re}_{xq}}} = -\sqrt{\frac{n+1}{2}} J'(0). \tag{9.21}$$

9.2.1 Dimensionless parameters

$$\left.\begin{array}{c}\Pr\left(=\frac{\nu}{\alpha}\right),\ K\left(=\lambda_1 a(x+b^1)^{n-1}\right),\ M\left(=\sqrt{\frac{\sigma}{\rho a}}B_0\right),\ Da^{-1}\left(=\frac{\varepsilon\upsilon}{ka^1(x+b^1)^{n-1}}\right),\\ \delta\left(=\frac{Q_O}{a\rho c_p}\right),\ \beta\left(=\frac{C_b\varepsilon(x+b^1)}{\sqrt{k}}\right),\ Mn\left(=\frac{C_p(T_\infty-T_m)}{\lambda^*+C_s(T_m-T_0)}\right),\mathrm{Re}\ =\frac{a(x+b)^{n+1}}{\nu}\\ N_T\left(=\frac{\tau D_T(T_w-T_0)}{\nu T_\infty}\right),\ N_B\left(=\frac{\tau D_B(C_w-C_0)}{\nu}\right),\ Le\left(=\frac{\alpha}{D_B}\right),\end{array}\right\} \tag{9.22}$$

in which (Mn) is the melting heat.

9.3 Methodology

Optimal homotopy method (OHAM) is used to evaluate the series solutions.

$$\varepsilon_k^f(h_f)=\frac{1}{N+1}\sum_{j=0}^{N}*\left[\sum_{i=0}^{k}(f_i)_{\eta=j\Pi\eta}\right]^2, \tag{9.23}$$

$$\varepsilon_k^t(h_f,h_t,h_J)=\frac{1}{N+1}\sum_{j=0}^{N}*\left[\sum_{i=0}^{k}(f_i)_{\eta=j\Pi\eta},\sum_{i=0}^{k}(t_i)_{\eta=j\Pi\eta},\sum_{i=0}^{k}(J_i)_{\eta=j\Pi\eta}\right]^2, \tag{9.24}$$

$$\varepsilon_k^J(h_f,h_t,h_J)=\frac{1}{N+1}\sum_{j=0}^{N}*\left[\sum_{i=0}^{k}(f_i)_{\eta=j\Pi\eta},\sum_{i=0}^{k}(t_i)_{\eta=j\Pi\eta},\sum_{i=0}^{k}(J_i)_{\eta=j\Pi\eta}\right]^2, \tag{9.25}$$

$$\varepsilon_k^t=\varepsilon_k^f+\varepsilon_k^t+\varepsilon_k^J \tag{9.26}$$

The values of convergence-control parameters are $(h_f=-0.967169, h_t=-0.518451, h_J=-1.36582)$. The total residual error is $\left(\varepsilon_k^{t^*}=7.15033\times 10^8\right)$. Table (9.1) show that the averaged squared residual error reduces with higher order approximations.

Table; 9.1

k	ε_k^f	ε_k^t	ε_k^J
2	8.4516×10^{-5}	6.81238×10^{-4}	4.4501×10^{-7}
6	3.2315×10^{-9}	4.1032×10^{-6}	3.39785×10^{-7}
10	1.9392×10^{-11}	1.1216×10^{-9}	2.03086×10^{-9}
16	3.71564×10^{-15}	3.51569×10^{-10}	3.80485×10^{-13}
22	5.12567×10^{-19}	7.42344×10^{-12}	4.58971×10^{-16}
26	6.23623×10^{-26}	9.94954×10^{-16}	5.97298×10^{-19}

9.4 Discussion

We fixed the values of non-dimensional variables for numerical solutions as $n = 0.5$,$\delta = 0.1$,$\beta = 0.1$,$Da^{-1} = 0.1,\ \alpha = 2,\ \lambda_2 = 0.1, K = 0.4, M = 0.3, N_B = 0.2, N_T = 0.4, M = 0.2, Pr = 1.0$ and $Le = 1.0$.

Velocity profile: Fig. (9.1) describe the impact of (n) on $f'(\eta)$. Velocity enhances against higher power index (n). It is due to the fact that stretching velocity increases by higher (n) which produces more deformation in fluid. Fig. (9.2) shows $f'(\eta)$ for different values of (Mn). $f'(\eta)$ increases through (Mn). Impact of $\left(Da^{-1}\right)$ on velocity is shown in Fig. (9.3). In fact the resistive force enhances for larger $\left(Da^{-1} = 0.0, 0.3, 0.5, 0.8, 1.2\right)$ and so $f'(\eta)$ declines rapidly. Fig. (9.4) designates the impact of inertial coefficient parameter (β). Velocity $f'(\eta)$ reduces for an increase of $(\beta = 0.0, 0.4, 0.8, 1.2, 1.6)$. Effect of (K) on $f'(\eta)$ gradient is sketched in Fig. (9.5). Deborah number (K) is directly related to the retardation time. Larger $(K = 0.0, 0.5, 1.0, 1.5, 2.0)$ has higher retardation time. Such higher retardation time gives upsurge to the fluid flow due to which the velocity boosted. Fig. (9.6) illustrates the impact of (λ_2) on $f'(\eta)$. Velocity enhances for larger (λ_2).

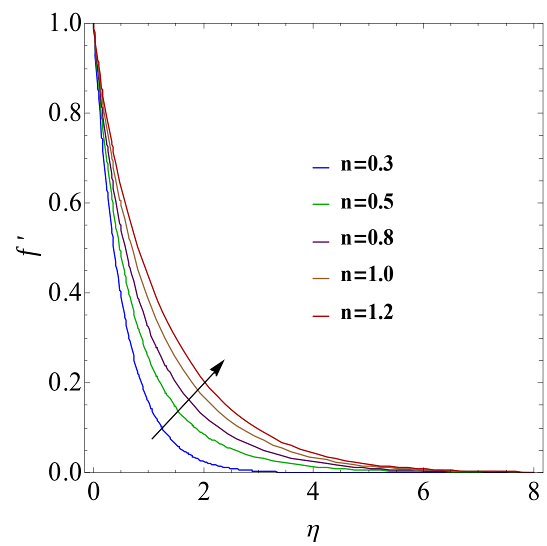

Fig. 9.1 : n on f'.

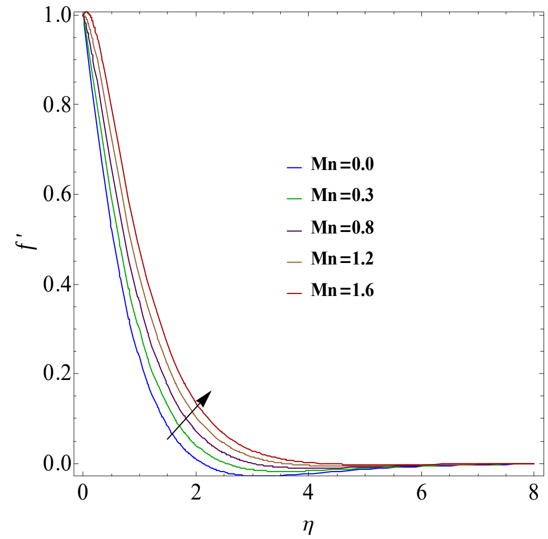

Fig. 9.2 : Mn on f'.

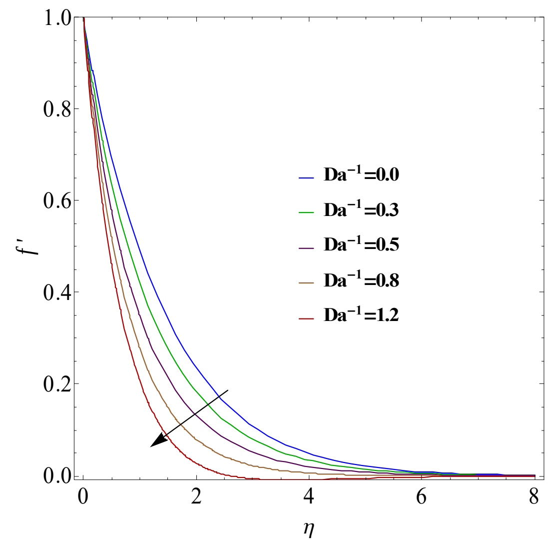

Fig. 9.3 : Da^{-1} on f'.

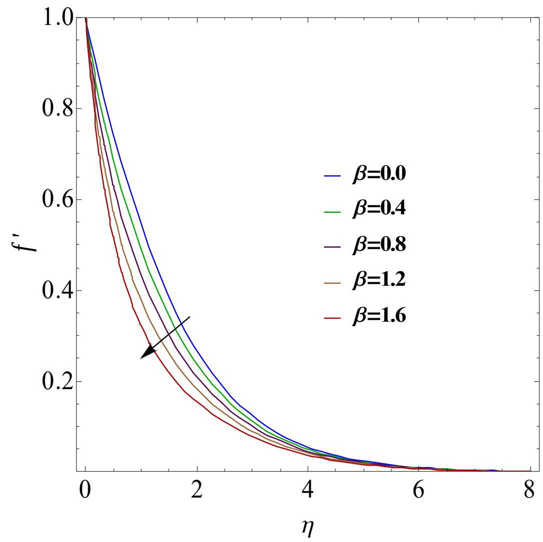

Fig. 9.4 : β on f'.

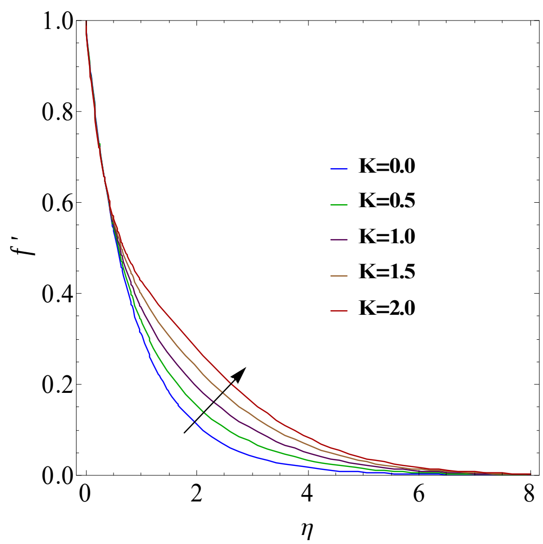

Fig. 9.5 : K on f'.

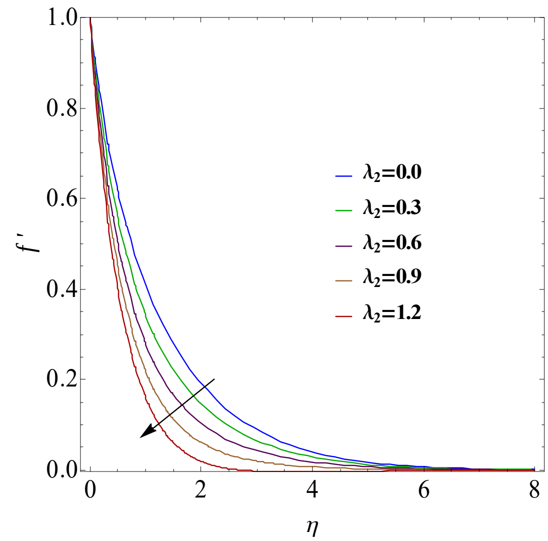

Fig. 9.6 : λ_2 on f'.

Temperature: Fig. (9.7) shows the significance of (δ) on $t(\eta)$. An increment in $(\delta = 0.0, 0.5, 1.0, 1.5, 2.0)$ corresponds to an increase of $t(\eta)$. Fig. (9.8) portrays that variation of melting parameter (Mn) yields enhancement in temperature. Fig. (9.9) indicates that $t(\eta)$ reduced for higher Prandtl number. In fact thermal diffusivity reduces by increasing $(\Pr = 0.2, 0.8, 1.6, 2.5, 3.0)$ and thus the heat diffuses away gradually from the heated body. Fig. (9.10) depicts $t(\eta)$ for various values of $(N_B = 0.5, 1.0, 1.5, 2.0, 2.5)$ which shows that temperature enhanced when we increase the value of (N_B). Larger (N_B) has higher brownian diffusion coefficient and smaller viscous forces that increase $t(\eta)$. Behavior of (Nt) on temperature distribution is similar to that of (N_B) (see Fig. 9.11).

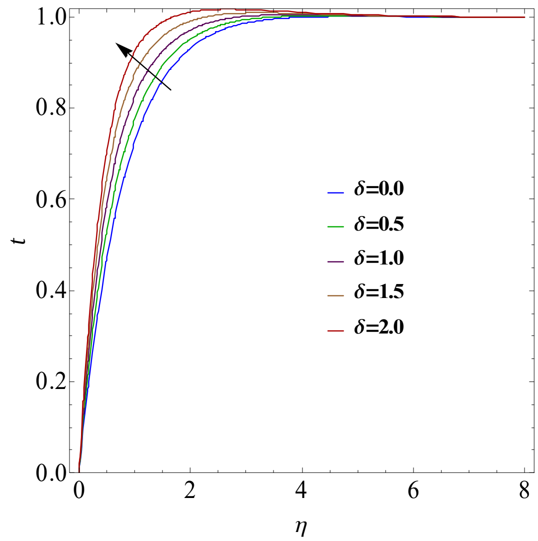

Fig. 9.7 : δ on t.

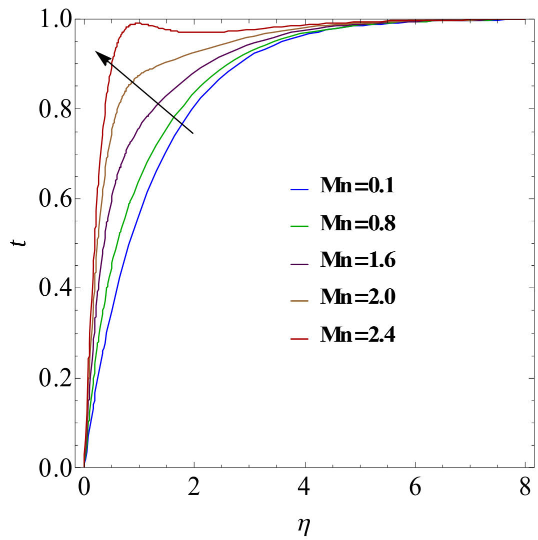

Fig. 9.8 : Mn on t.

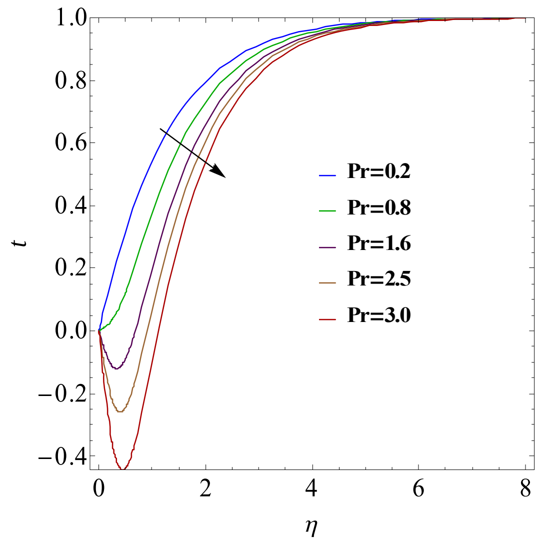

Fig. 9.9 : Pr on t.

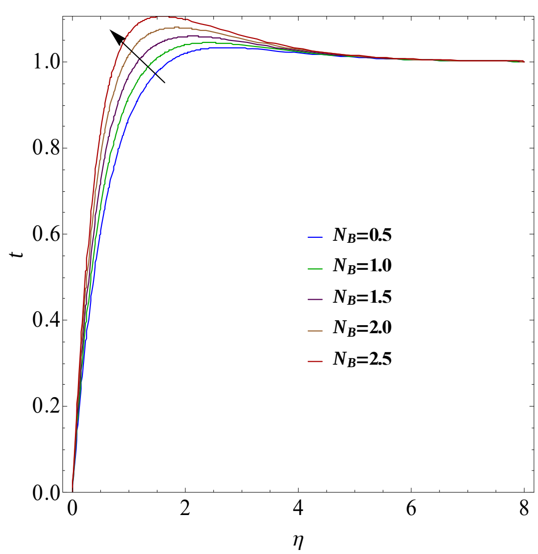

Fig. 9.10 : N_B on t.

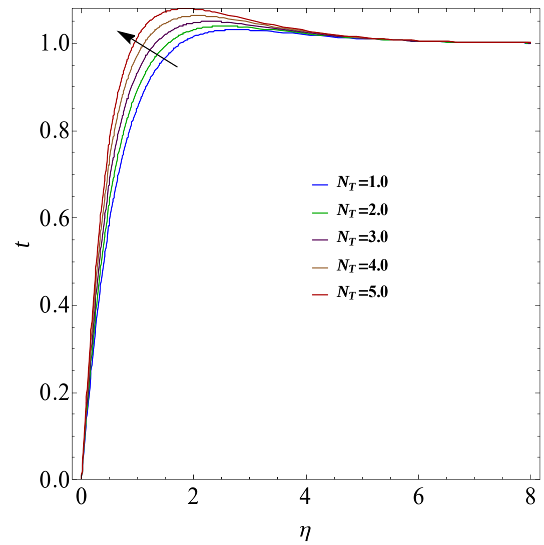

Fig. 9.11 : N_T on t.

Concentration distribution: Fig. (9.12) shows that concentration $(J(\eta))$ is an increasing function of melting parameter (Mn) . Fig. (9.13) addressed that higher values of $(Le = 0.0, 0.5, 1.0, 1.5, 2.0)$ reduce the concentration. Lewis number (Le) depends upon the Brownian diffusion coefficient. An increase in the values of (Le) leads to lower Brownian diffusion coefficient which shows a weaker concentration. Fig. (9.14) illustrates that an upsurge in the thermophoresis parameter leads to reduction of concentration.

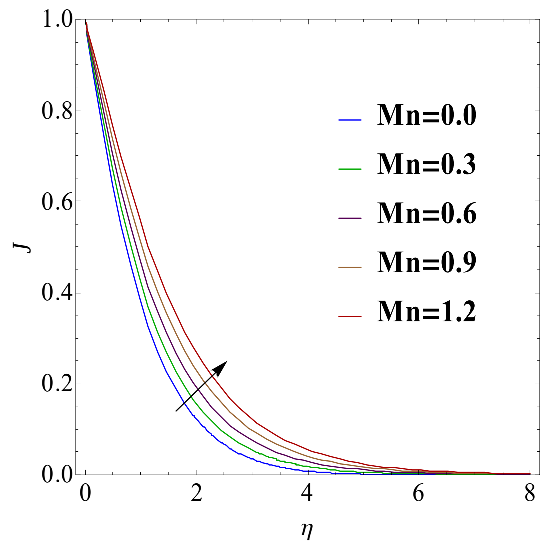

Fig. 9.12 : Mn on J.

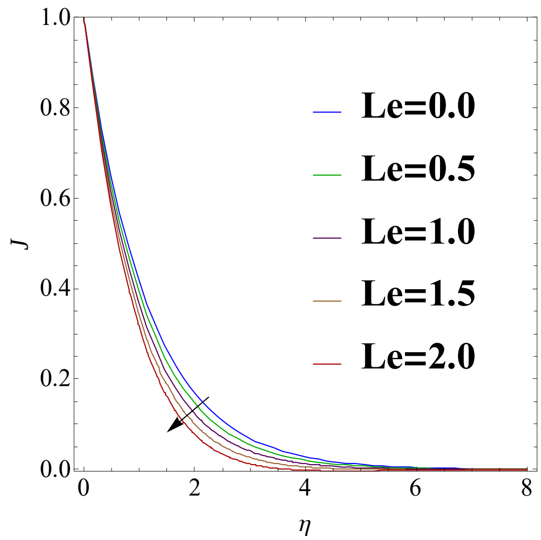

Fig. 9.13 : Le on J.

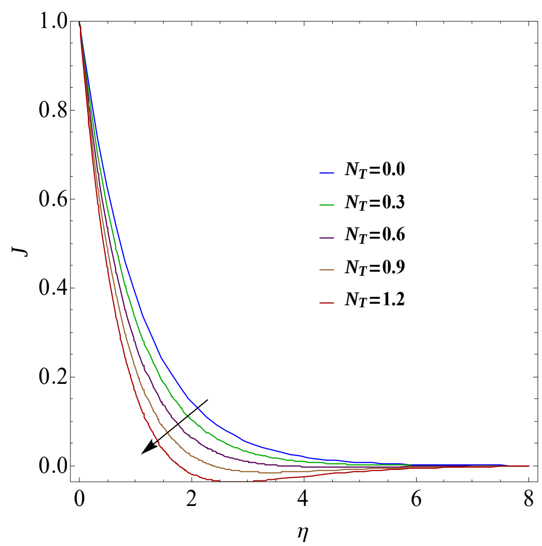

Fig. 9.14 : N_T on J.

Fig. (9.15) illustrate the effect of (n) and (M) on (C_f). It is clear that for increasing (n) and (M) the skin-friction coefficient reduces. Fig. (9.16) shows the performance of Deborah number (K) and ratio of relaxation to retardation times (λ_2) on skin friction coefficient. (C_f) has decreasing trend for larger (K) and (λ_2). Impact of (δ) and $(\Pr)$ on (Nu) is illustrated in Fig. (9.17). Nusselt number enhances via (δ) and $(\Pr)$. Fig. (9.18) shows the impact of (Nu) against (N_T) and (N_B). Nusselt number increases for higher thermophoresis parameter (N_T) while opposite trend is noticed for higher values of (N_B). Fig. (9.19) illustrate the effect of thermophoresis (N_T) and Brownian motion variable (N_B) on local Sherwood number. It is cleared that Sherwood number reduced for larger (N_T) and (N_B). Fig. (9.20) shows the magnitude of mass transfer against (Pr) and (Le). Magnitude of mass transfer increases for higher values of (Pr) while opposite trend is noticed for higher (Le).

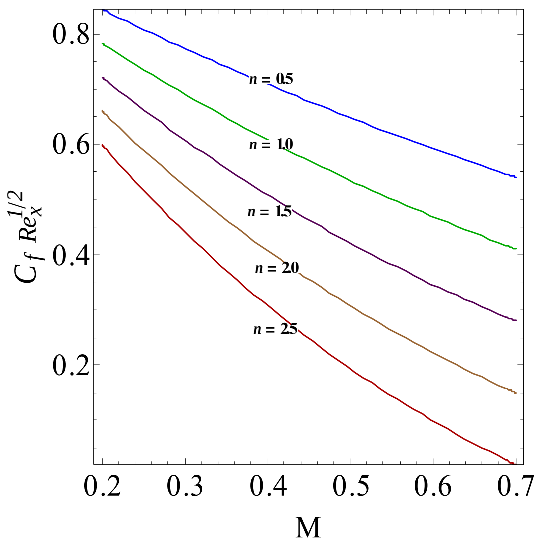

Fig. 9.15 : n and M on C_f.

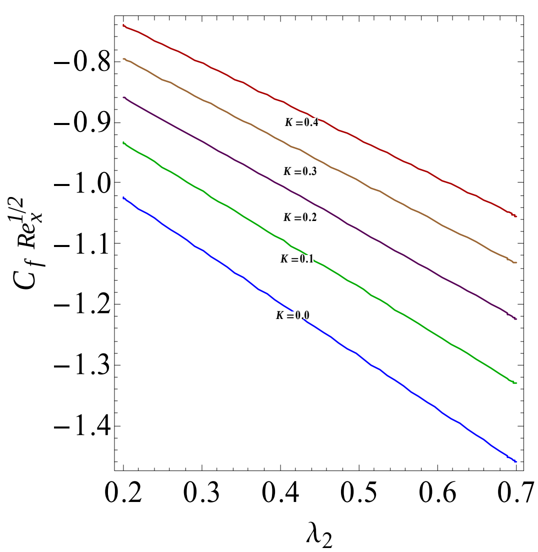

Fig. 9.16 : K and λ_2 on C_f.

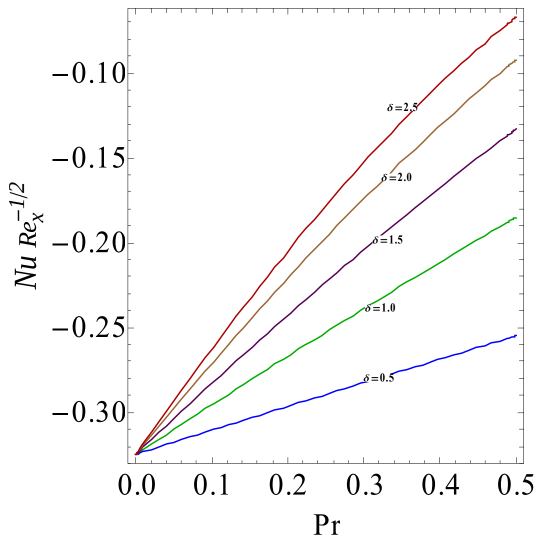

Fig. 9.17 : δ and Pr on Nu.

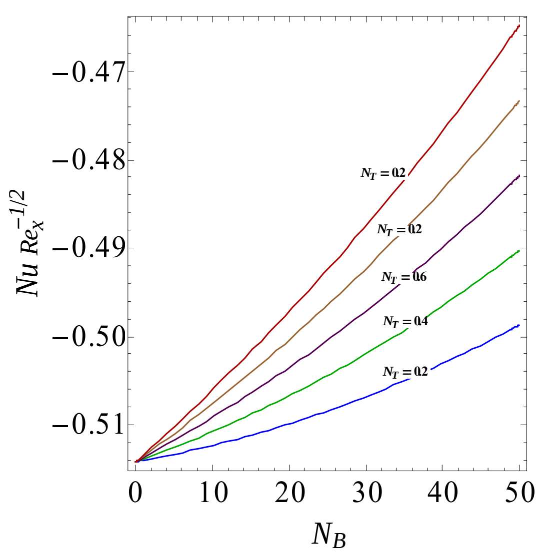

Fig. 9.18 : N_T and N_B on Nu.

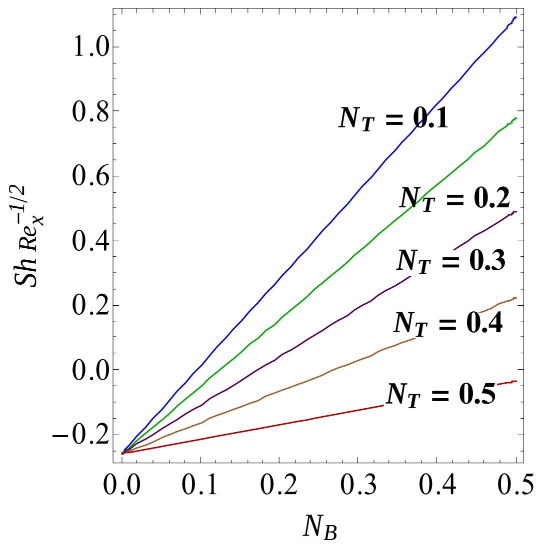

Fig. 9.19 : N_T and N_B on Sh.

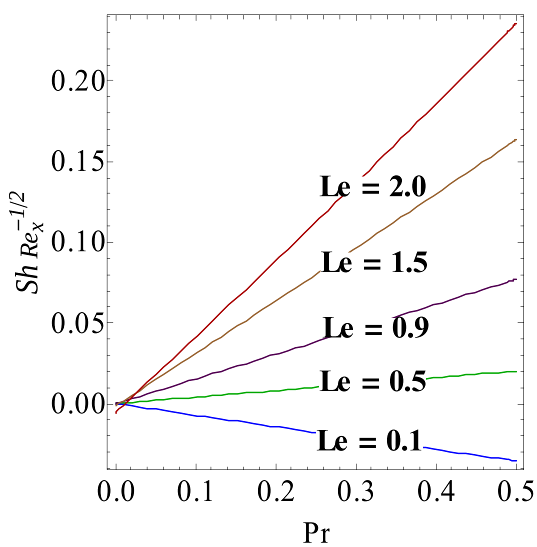

Fig. 9.20 : Pr and Le on Sh.

9.5 Concluding remarks

Key points are given below.

- Velocity increases for higher (K).
- Although $(t(\eta))$ is an increasing function of (δ) but it reduced for larger $(\Pr)$.

- Concentration gradient reduces for higher values of (Le) and (N_T) but it increases for (Mn).
- Shape and second grade parameters on skin friction coefficient have decreasing trend..
- Similar trend of (δ) and $(\Pr)$ is found for Nusselt number.
- Sherwood number shows increasing behavior for larger (Le) but result is opposite for (N_T).

Chapter 10

Impact of entropy generation on third grade nanofluid flow over a stretchable Riga wall with Cattaneo-Christov double diffusions

Flow of third grade nanofluid over a stretching Riga plate is addressed. Modeling is based through Cattaneo-Christov (CC) heat and mass fluxes. These considerations are entirely different than classical heat and mass fluxes by Fourier and Fick's laws. Formulation also consists of heat generation and mixed convection. Relevant transformations are used to develop ordinary differential system from partial differential equations. Optimal homotopy analysis technique is utilized to find the solution of differential equations. Total square residual error is computed.

10.1 Modelling

We analyze MHD two-dimensional mixed convective steady flow of third grade nanoliquid over a stretchable Riga wall. Analysis of heat and mass transport is studied through Cattaneo-Christov (CC) flux models. Here ($U_w = ax$) be the stretching velocity along ($x - axis$) and ($y - axis$) is perpendicular to ($x - axis$). Fig. $10.1(a, b)$ shows the flow diagram. The governing equations are

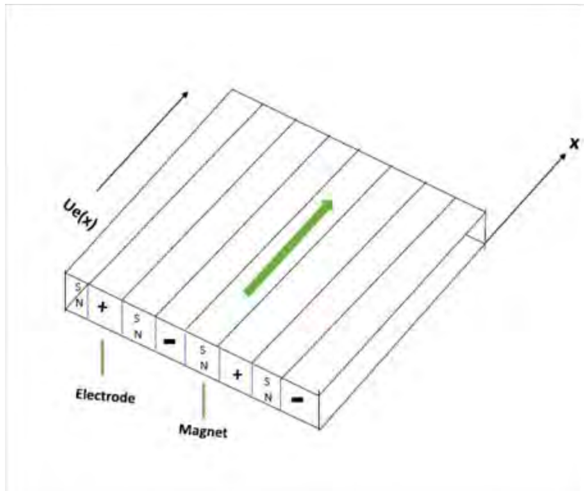

Fig. 10.1(a) : Structure of Riga wall

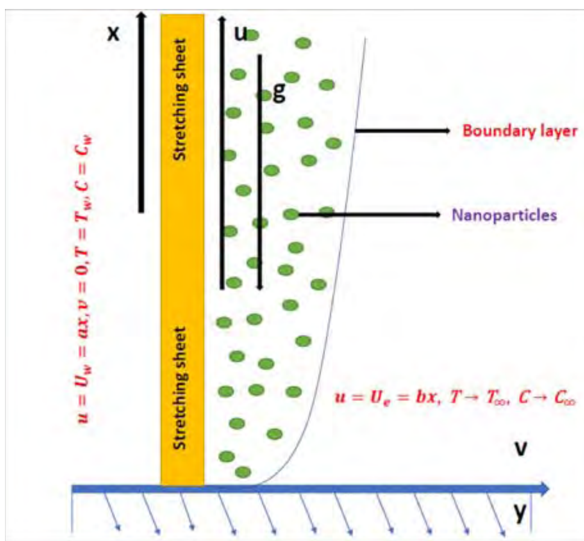

Fig. 10.1(b) : Flow geometry.

Continuity equation

$$\frac{\partial u}{\partial x} + \frac{\partial v}{\partial y} = 0, \tag{10.1}$$

The momentum equation

$$\left.\begin{array}{c} u\frac{\partial u}{\partial x}+v\frac{\partial u}{\partial y}=U_e\frac{\partial U_e}{\partial x}+\frac{\alpha_1}{\rho}\left(\frac{\partial u}{\partial x}\frac{\partial^2 u}{\partial y^2}+u\frac{\partial^3 u}{\partial x\partial y^2}+3\frac{\partial u}{\partial y}\frac{\partial^2 u}{\partial x\partial y}+v\frac{\partial^3 u}{\partial y^3}\right)\\ +\frac{\alpha_2}{\rho}\left(2\frac{\partial u}{\partial y}\frac{\partial^2 u}{\partial x\partial y}\right)+6\frac{\alpha_3}{\rho}\left(\left(\frac{\partial u}{\partial y}\right)^2\frac{\partial^2 u}{\partial y^2}\right)+\nu\frac{\partial^2 u}{\partial y^2}+\\ \frac{\pi J_o Q_o}{8\rho}Exp[-\frac{\pi}{a_1}y]+g\beta_t(T-T_\infty)\end{array}\right\}, \tag{10.2}$$

Corresponding boundary conditions are

$$\left.\begin{array}{c} u=U_w=ax,\quad v=0 \text{ at } y=0,\\ u=U_e=bx \text{ when } y\to\infty,\end{array}\right\}. \tag{10.3}$$

Skin friction coefficient is

$$C_{fx}=\left(\frac{\tau_w}{\rho_f\,(U_w)^2}\right), \tag{10.4}$$

where

$$\tau_w=\left(\mu\frac{\partial u}{\partial y}\right)_{y=0}+\left[\frac{\alpha_1}{\rho}\left(2\frac{\partial u}{\partial x}\frac{\partial u}{\partial y}+u\frac{\partial^2 u}{\partial x\partial y}+v\frac{\partial^2 u}{\partial y^2}\right)+2\frac{\alpha_3}{\rho}\left(\frac{\partial u}{\partial y}\right)^3\right]_{y=0}. \tag{10.5}$$

According to Cattaneo-Christove (CC) theory the heat flux for steady ($\frac{\partial q}{\partial t}=0$) and incompressible ($\nabla\cdot\mathbf{V}^*=0$) fluid satisfies

$$\mathbf{q}+\delta_E(\mathbf{V}^*\cdot\triangledown\mathbf{q}-\mathbf{q}\cdot\triangledown\mathbf{V}^*)=-k\triangledown\mathbf{T}, \tag{10.6}$$

temperature expression in current situation satisfies

$$\left.u\frac{\partial T}{\partial x}+v\frac{\partial T}{\partial y}=-\nabla.\mathbf{q}+\tau\left[D_B\frac{\partial C}{\partial y}\frac{\partial T}{\partial y}+\frac{D_T}{T_\infty}\left(\frac{\partial T}{\partial y}\right)^2\right]+\frac{Q}{\rho c_p}(T-T_\infty)\right\}. \tag{10.7}$$

annihilating $\mathbf{q}$ from Eqs. (10.6) and (10.7) yields to the following relation for the temperature field

$$u\frac{\partial T}{\partial x}+v\frac{\partial T}{\partial y}+\delta_E\left[\begin{array}{c} u\frac{\partial u}{\partial x}\frac{\partial T}{\partial x}+v\frac{\partial u}{\partial y}\frac{\partial T}{\partial y}+u\frac{\partial v}{\partial x}\frac{\partial T}{\partial y}+v\frac{\partial u}{\partial y}\frac{\partial T}{\partial x} \\ +2uv\frac{\partial^2 T}{\partial y\partial x}+u^2\frac{\partial^2 T}{\partial x^2}+v^2\frac{\partial^2 T}{\partial y^2}-\frac{Q}{\rho C_p}\left(u\frac{\partial T}{\partial x}+v\frac{\partial T}{\partial y}\right) \\ -\tau D_B\left(v\frac{\partial T}{\partial y}\frac{\partial^2 C}{\partial y^2}+v\frac{\partial C}{\partial y}\frac{\partial^2 T}{\partial y^2}+u\frac{\partial^2 C}{\partial x\partial y}\frac{\partial T}{\partial y}+u\frac{\partial C}{\partial y}\frac{\partial^2 T}{\partial x\partial y}\right) \\ +2\frac{\tau D_T}{T_\infty}\left(v\frac{\partial T}{\partial y}\frac{\partial^2 T}{\partial y^2}+u\frac{\partial T}{\partial y}\frac{\partial^2 T}{\partial x\partial y}\right)\end{array}\right]= \\ \alpha\frac{\partial^2 T}{\partial y^2}+\tau\left[D_B\frac{\partial C}{\partial y}\frac{\partial T}{\partial y}+\frac{D_T}{T_\infty}\left(\frac{\partial T}{\partial y}\right)^2\right]+\frac{Q}{\rho C_p}(T-T_\infty)\Bigg\}. \quad (10.8)$$

The imposed boundary conditions are

$$\left.\begin{array}{c} T\to T_w \text{ at } y=0, \\ T\to T_\infty \text{ when } y\to\infty, \end{array}\right\}. \quad (10.9)$$

According to Cattaneo-Christove model the mass flux for steady and incompressible fluid flow obeys following expression

$$\mathbf{j}+\delta_F(\mathbf{V}^*\cdot\nabla\mathbf{j}-\mathbf{j}\cdot\nabla\mathbf{V}^*)=-D_B\nabla\mathbf{C}, \quad (10.10)$$

Here concentration field satisfies

$$\left.u\frac{\partial C}{\partial x}+v\frac{\partial C}{\partial y}=-\nabla.\mathbf{j}+\frac{D_T}{T_\infty}\frac{\partial^2 T}{\partial y^2}\right\}. \quad (10.11)$$

Eliminating $\mathbf{j}$ from Eqs. (10.10) and (10.11) our arrives at

$$\left.\begin{array}{c} u\frac{\partial C}{\partial x}+v\frac{\partial C}{\partial y}+\delta_F\left[\begin{array}{c} u^2\frac{\partial^2 C}{\partial x^2}+u\frac{\partial u}{\partial x}\frac{\partial C}{\partial x}+u\frac{\partial v}{\partial x}\frac{\partial C}{\partial y}+ \\ 2uv\frac{\partial^2 C}{\partial x\partial y}\frac{\partial T}{\partial x}+v\frac{\partial u}{\partial y}\frac{\partial C}{\partial x}+v^2\frac{\partial^2 C}{\partial y^2}+v\frac{\partial v}{\partial y}\frac{\partial C}{\partial y} \\ -D_B\left(u\frac{\partial^3 C}{\partial x\partial y^2}+v\frac{\partial^3 C}{\partial y^3}\right)-\frac{D_T}{T_\infty}\left(v\frac{\partial^3 T}{\partial y^3}+u\frac{\partial^3 T}{\partial x\partial y^2}\right)\end{array}\right] \\ =D_B\frac{\partial^2 C}{\partial y^2}+\frac{D_T}{T_\infty}\frac{\partial^2 T}{\partial y^2}\end{array}\right\}. \quad (10.12)$$

The relevant boundary conditions are

$$\left.\begin{array}{c} C\to C_w \text{ at } y=0, \\ C\to C_\infty \text{ at } y\to\infty, \end{array}\right\}. \quad (10.13)$$

Dimensionless formulation

By considering transformations

$$u = axf'(\eta), \quad v = -\sqrt{a\nu}f(\eta), \quad t = \frac{T - T_\infty}{T_w - T_\infty}, \ J = \frac{C - C_\infty}{C_w - C_\infty}, \eta = \sqrt{\frac{a}{\nu}}y \Bigg\}, \tag{10.14}$$

the Eq. [10.1] is trivially satisfied while Eqs. [10.2, 10.3, 10.8, 10.9, 10.12, 10.13] becomes

$$\left. \begin{array}{c} f''' + f'' - f'^2 + \alpha_1^* \left(f'f''' - f'f'' - f''''f\right) + \left(\alpha_1^* + \alpha_2^*\right) f''f'' \\ +6\alpha_3^* \operatorname{Re} f''f''f''' + S^2 + MExp[-B\eta] + \lambda t = 0 \end{array} \right\}, \tag{10.15}$$

$$\left. \begin{array}{c} t'' + \Pr\gamma_1(ff't' + f'^2t'' - \delta ft' - 2ff't'') - \Pr\gamma_1 N_B(ft'J'' - fJ't') \\ - \Pr\gamma_1 N_t J''t' + N_B t'J' + N_t t'^2 + \Pr\delta t] + \Pr ft' = 0 \end{array} \right\}, \tag{10.16}$$

$$J'' + ScfJ' + \frac{N_B}{N_t}t'' - Sc\gamma_3[f^2J'' + ff'J'] - \gamma_3\frac{N_B}{N_t}t'' = 0 \Big\}, \tag{10.17}$$

$$\left\{ \begin{array}{c} f(0) = 0, \ f'(0) = 1, \ f^{'}(\infty) = S \\ t(0) = 1, \ t(\infty) = 0, \\ J(0) = 1, \ J(\infty) = 0 \end{array} \right\}. \tag{10.18}$$

Skin friction coefficient satisfies

$$\sqrt{\operatorname{Re}_x}C_{fx} = f''(0) + \alpha_1^* \left(3f'(0)f''(0) - f(0)f'''(0)\right) + \alpha_2^* \left(f''(0)\right)^3. \tag{10.19}$$

10.2 Entropy rate

Mathematical expression for Entropy generation rate is

$$N_{gen}^{'''} = \frac{k}{T_\infty^2}\left(\frac{\partial T}{\partial y}\right)^2 + \frac{R_D}{T_\infty}\left(\frac{\partial T}{\partial y}\frac{\partial C}{\partial y}\right) + \frac{R_D}{T_\infty}\left(\frac{\partial C}{\partial y}\right)^2 \Bigg\}. \tag{10.20}$$

Characteristic entropy $\left(N_0^{'''}\right)$ is given as

$$N_0''' = \frac{k(\nabla T)^2}{L^2 T_\infty^2}, \tag{10.21}$$

Entropy generation after utilizing transformations yields

$$N_G = \frac{N_{gen}'''}{N_0'''} = \operatorname{Re} t'^2 + \frac{\operatorname{Re}\chi\gamma_4}{\Omega} t' J' + \operatorname{Re}\chi\gamma_4 J'^2. \tag{10.22}$$

10.2.1 Dimensionless parameters

$$\left.\begin{array}{c} M\left(=\frac{\pi J_o M_o}{8\rho a^2}\right),\ Da^{-1}\left(=\frac{\nu\epsilon}{k}\right),\ \lambda\left(=\frac{g\beta_t(T_w-T_\infty)}{a}\right),\ B\left(=\frac{\pi}{a_1}\sqrt{\frac{\nu}{a}}\right), \\ \left[\alpha_1^*\left(=\frac{\alpha_1 a}{\mu}\right), \alpha_2^*\left(=\frac{\alpha_2 a}{\mu}\right),\ \alpha_3^*\left(=\frac{\alpha_3 a}{\mu}\right)\right],\ S\left(=\frac{b}{a}\right),\ \gamma_1\left(=a\delta_E\right), \\ \gamma_2\left(=\frac{h_f \nu}{a}\right),\ \gamma_3\left(=a\delta_F\right),\ \gamma_4=\left(\frac{\nabla C}{C_\infty}\right),\ N_B\left(=\frac{\tau D_B(C_w-C_\infty)}{\nu}\right), \\ N_T\left(=\frac{\tau D_T(T_w-T_\infty)}{\nu T_\infty}\right),\ Sc\left(=\frac{\alpha}{D_B}\right),\ \delta\left(=\frac{Q}{\rho C_p}\right),\ \Pr\left(=\frac{\mu C_p}{k}\right), \\ \left(Br=\left(\frac{\mu U_w^2}{k\nabla T}\right)\right),\ \chi=\left(\frac{R_D C_\infty}{k}\right),\ \operatorname{Re}_x\left(=\frac{U_w x}{\nu_f}\right),\ \left(\Omega=\left(\frac{\nabla T}{T_\infty}\right)\right), \end{array}\right\}. \tag{10.23}$$

10.3 Solutions methodology

The series solutions are obtained by using the Optimal method of homotopy analysis. The mathematical expressions for average squared residual errors are

$$\varepsilon_{k^*}^f(h_f) = \frac{1}{N+1}\sum_{j=0}^{N} * \left[\sum_{i=0}^{k}(f_i)_{\eta=j\Pi\eta}\right]^2, \tag{10.24}$$

$$\varepsilon_{k^*}^t(h_f,h_t,h_J) = \frac{1}{N+1}\sum_{j=0}^{N} * \left[\sum_{i=0}^{k^*}(f_i)_{\eta=j\Pi\eta}, \sum_{i=0}^{k^*}(t_i)_{\eta=j\Pi\eta}, \sum_{i=0}^{k^*}(J_i)_{\eta=j\Pi\eta}\right]^2, \tag{10.25}$$

$$\varepsilon_{k^*}^J(h_f,h_t,h_J) = \frac{1}{N+1}\sum_{j=0}^{N} * \left[\sum_{i=0}^{k^*}(f_i)_{\eta=j\Pi\eta}, \sum_{i=0}^{k^*}(t_i)_{\eta=j\Pi\eta}, \sum_{i=0}^{k^*}(J_i)_{\eta=j\Pi\eta}\right]^2, \tag{10.26}$$

$$\varepsilon_{k^*}^{t^*} = \varepsilon_{k^*}^f + \varepsilon_{k^*}^t + \varepsilon_{k*}^J, \tag{10.27}$$

in which $\left(\varepsilon_{k^*}^{t^*} = 0.0518763\right)$ denotes the total square residual error. Here $\alpha_1^* = 0.1, \alpha_2^* = 0.2, \alpha_3^* = 0.3, S = 0.1$, $M = 0.2$, $N_T = 0.1$, $\Pr = 1.2$, $N_B = 0.5$, $\operatorname{Re} = 0.1$, $\gamma_1 = \gamma_3 = 0.2$, $\chi = 0.1$ and $\Omega = 0.4$. The values of convergence-control parameters are $h_f = -0.8273$, $h_\theta = -0.1559$ and $h_g = -1.4712$. Fig. 9.2 shows the total residual error graph.

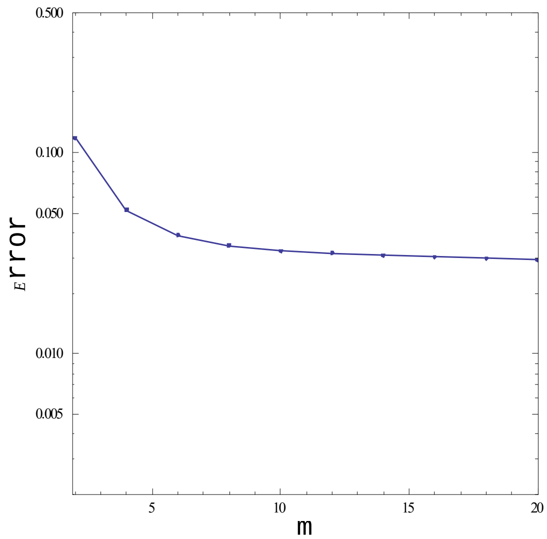

Fig. 10.2 : Total residual error

Table; 10.1

k^*	$\varepsilon_{k^*}^{f}$	$\varepsilon_{k^*}^{t}$	$\varepsilon_{k^*}^{J}$
2	0.0345265	0.00781397	0.0768611
6	0.0314574	0.00135282	0.00597602
8	0.0306576	0.000855484	0.00300873
10	0.030006	0.000623588	0.00203128
14	0.0289533	0.000424908	0.0015619
16	0.0285086	0.000377863	0.00147933
20	0.027728	0.000324747	0.00129755

10.4 Discussion

This section describes the consequences of different physical variables for the velocity $f'(\eta)$, temperature $t(\eta)$, concentration $J(\eta)$ and entropy N_G. The values selected in computations are $S = 0.1$, $M = 0.2$, $N_T = 0.1$, Pr =1.2, $N_B = 0.5$, $\mathrm{Re} = 0.1$, $\alpha_1^* = 0.1$,$\alpha_2^* = 0.1, \alpha_2^* = 0.1$, $\gamma_1 = \gamma_2$= 0.2, $\lambda = 0.2, S = 0.1, \gamma_3 = 0.3$, $\chi = 0.1$ and $\Omega = 0.4$.

10.5 Velocity profile

Figs. (10.3), (10.4) and (10.5) examine analysis by taking into account the effects of (α_1^*) , (α_2^*) and (α_3^*) respectively. With an increase of (α_1^*) the velocity of fluid is small near the plate i.s within the range $((0 = \eta = 1.0))$. Although it illustrates a reverse pattern followed by a transformation at $(\eta = 1.5)$. In facts the material parameters have inverse relation to viscosity. Thus for larger values of $(\alpha_2^* = 0.0, 1.0, 2.0, 3.0, 4.0, 5.0)$ and $(\alpha_3^* = 0.0, 1.0, 2.0, 3.0, 4.0, 5.0)$ thickness of fluid decreases and thus fluid motion enhances. This seems only meaningful argument behind this ascending progression of fluid velocity. Fig. (10.6) shows the variation of $(M = 0.0, 0.1, 0.2, 0.3, 0.4, 0.5)$ on $f'(\eta)$. For larger (M) the velocity enhances.

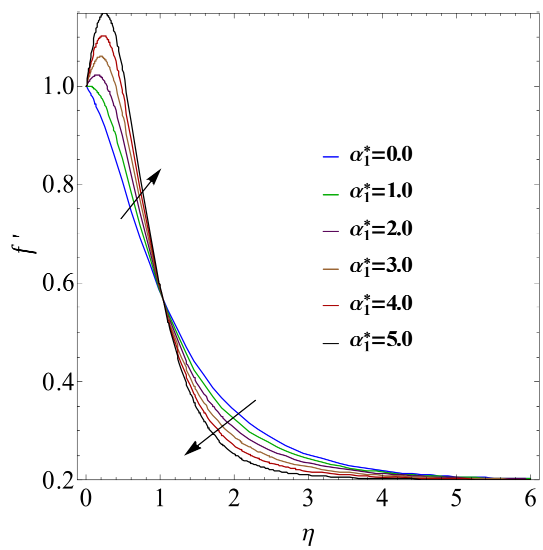

Fig. 10.3 : f' against α_1^*.

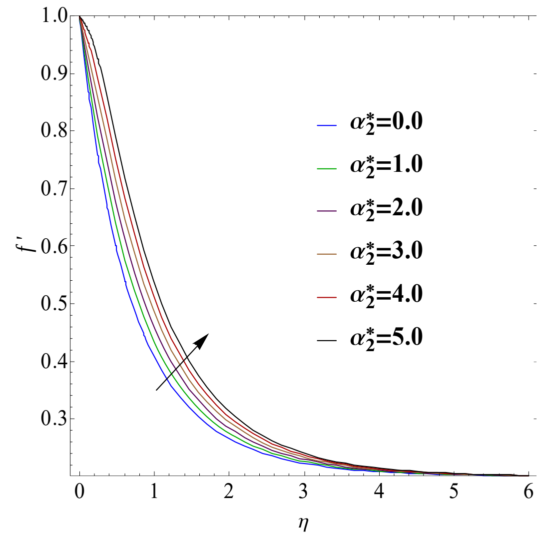

Fig. 10.4 : f' against α_2^*.

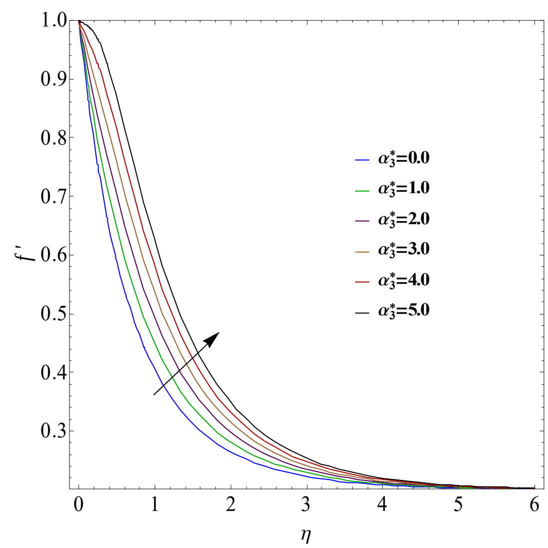

Fig. 10.5 : f' against α_3^*.

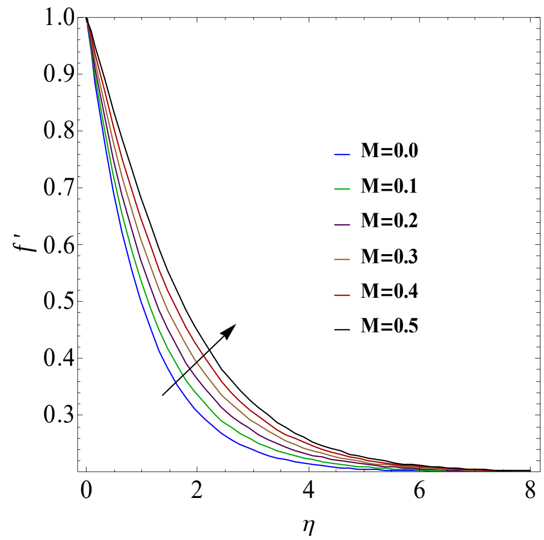

Fig. 10.6 : f' against M.

10.6 Temperature

Effect of (γ_1) on $t(\eta)$ is represented in Fig. (10.7). For larger (γ_1) fluid particles take extra time to move heat from the heated surface to the cold one. Therefore $t(\eta)$ decays for higher (γ_1). Fig. (10.8) displays that temperature decays for larger $(S = 0.0, 0.5, 1.0, 1.5, 2.0, 2.5)$. Fig. (10.9) exhibits that $(\Pr = 1.0, 2.0, 3.0, 4.0, 5.0, 6.0)$ leads to reduce $t(\eta)$. Influence of $(\delta = 0.1, 0.3, 0.6, 0.9.1.2, 1.5)$ on $t(\eta)$ is shown in Fig. (10.10). Higher (δ) yield more heat in fluid which enhances temperature. Influence of temperature $t(\eta)$ for (N_B) is plotted in Fig. 9.11. Here $t(\eta)$ upsurges for larger $(N_B = 0.1, 0.5, 1.0, 1.2, 2.0, 2.5)$. This is because an uplift in the base fluid thermal conductivity exists with greater (N_B). Therefore the boundary layer becomes thicker and temperatures rise.

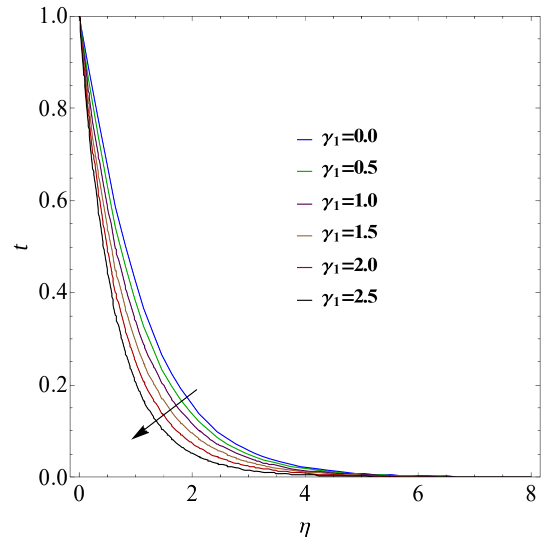

Fig. 10.7 : t against γ_1.

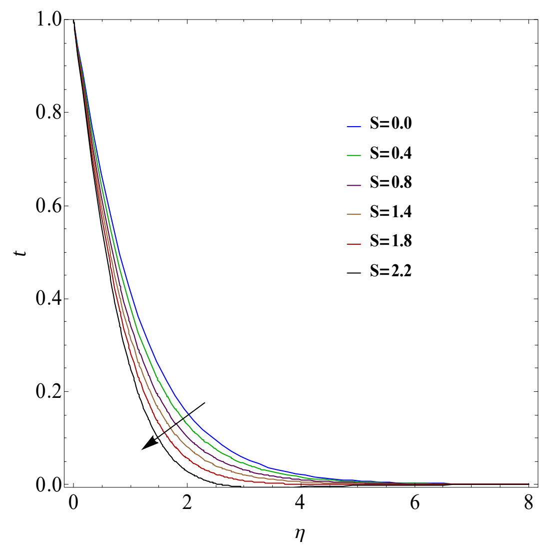

Fig. 10.8 : t against S.

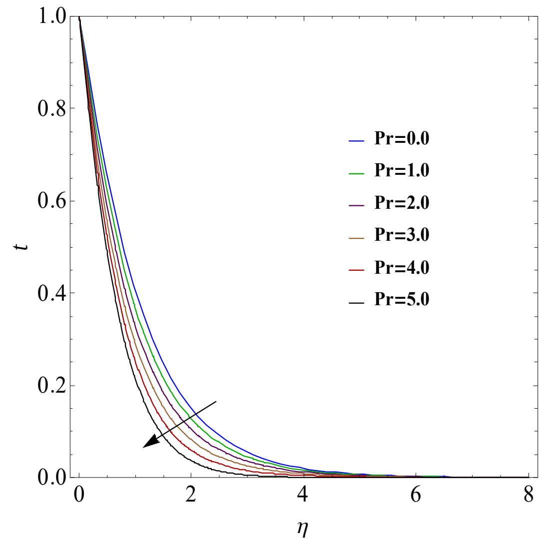

Fig. 10.9 : t against Pr.

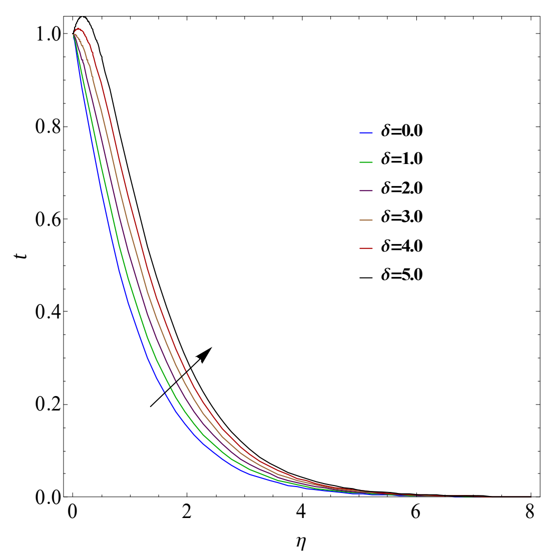

Fig. 10.10 : t against δ.

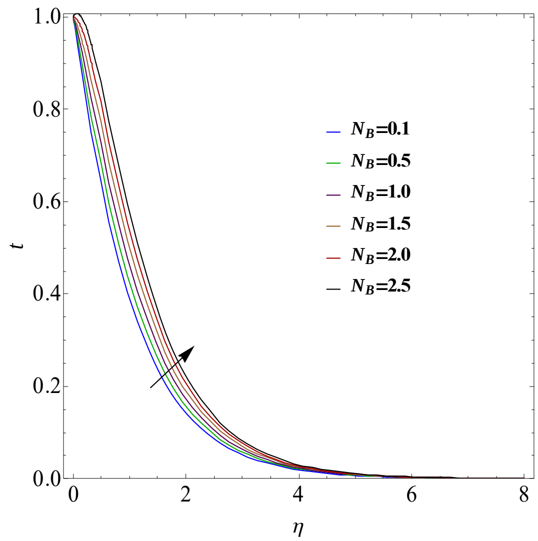

Fig. 10.11 : t against N_B.

10.7 Concentration

Fig. (10.12) illustrates the effect of (γ_2) on $J(\eta)$. Clearly $J(\eta)$ is reduced for larger ($\gamma_3 = 0.0, 0.2, 0.4, 0.6, 0.8, 1.0$). In fact higher ($\gamma_3$) mass transfer decreases from liquid to the surface. Fig. (10.13) shows for larger ($N_B = 0.1, 0.5, 1.0, 1.5, 2.0, 2.5$) reduces concentration. There is fast movement and collisions of nanoparticles with higher (N_B) and thus more heat is emitted and thus the concentration decreases. Fig. (10.14) evaluated impact of ($N_T = 0.1, 0.5, 1.0, 1.5, 2.0, 2.5$) on $J(\eta)$. Clearly concentration increases.

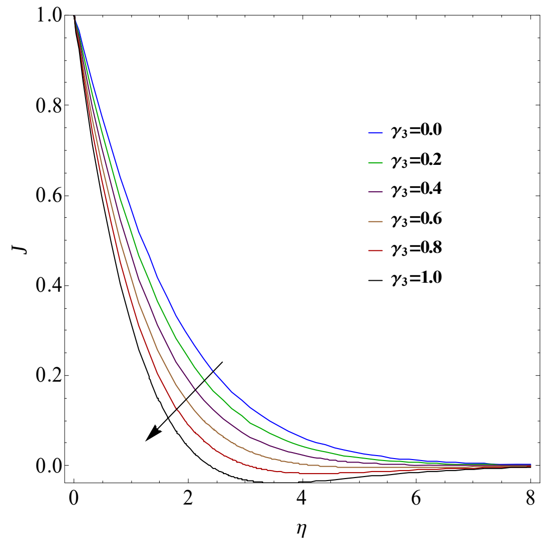

Fig. 10.12 : J against γ_3.

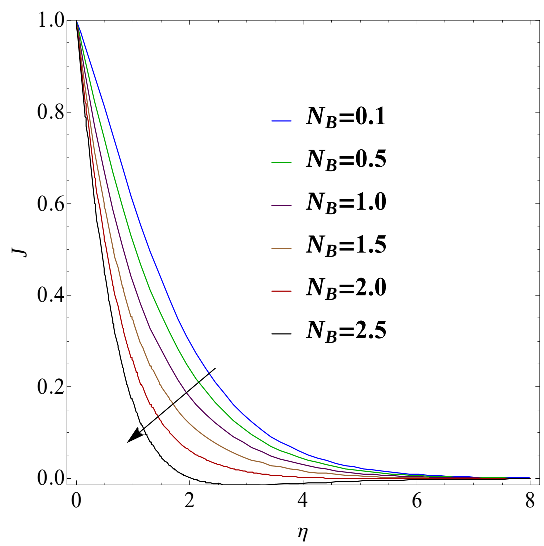

Fig. 10.13 : J against N_B.

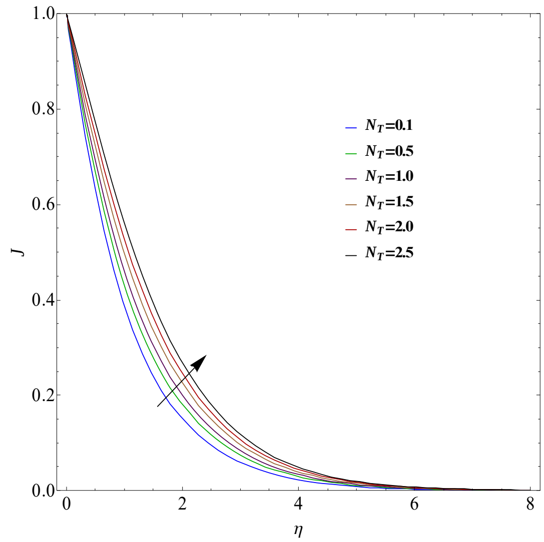

Fig. 10.14 : J against N_T.

10.8 Entropy

Fig. (10.15) shows the outcome of (χ) on N_G. For higher $(\chi = 0.1, 0.5, 1.0, 1.5, 2.0, 2.5)$ the N_G enhances. More disorderness occure in the fluid when diffusivity increases and thus entropy enhances. Fig. (10.16) shows that (N_G) increases for larger of $(\mathrm{Re} = 0.1, 0.2, 0.3, 0.4, 0.5, 0.6)$. Here inertial impacts dominate the fluid viscosity. Impact of $(\Omega = 0.1, 0.2, 0.3, 0.4, 0.5, 0.6)$ on entropy (N_G) is discussed in Fig. (10.17). Higher temperature difference parameter (Ω) entropy increases.

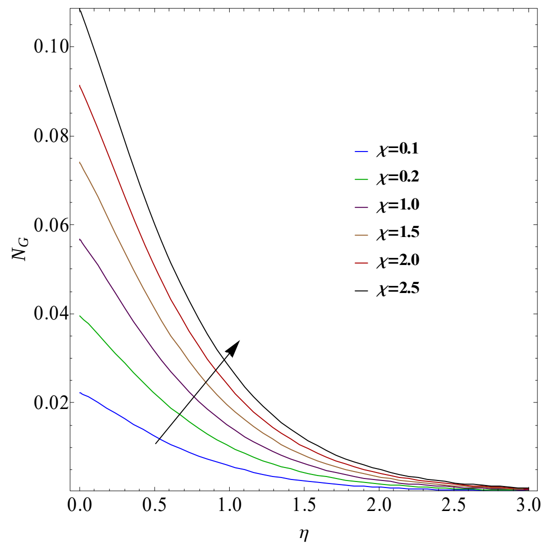

Fig. 10.15 : N_G against χ.

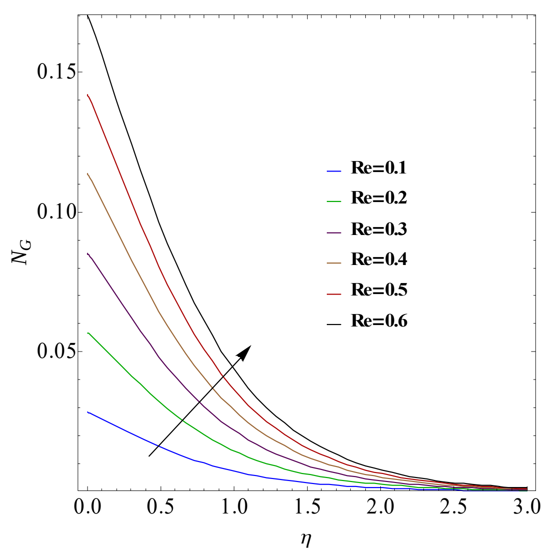

Fig. 10.16 : N_G against Re.

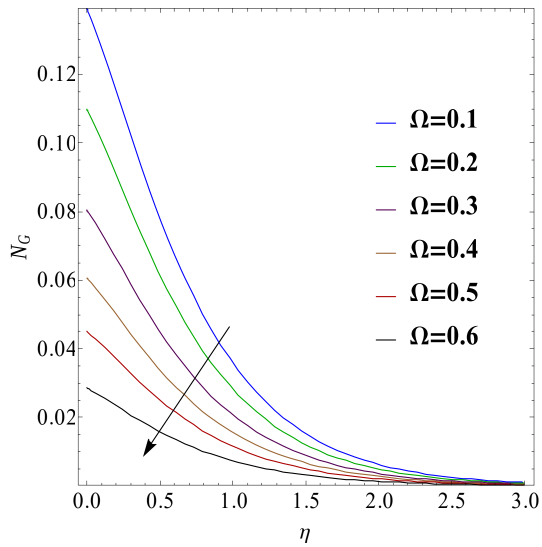

Fig. 10.17 : N_G against Ω.

10.9 Concluding remarks

Major conclusions include the points described below.

- Fluid velocity improves for larger (M) and third grade parameters.
- $(t(\eta))$ enhances for larger $(N_B), (N_T)$ and (δ) but opposite result is seen for (γ_1).
- Concentration is reduced via (γ_3) and (N_B).
- For higher (N_t) concentration enhances.
- Effects of (χ) and (Re) on (N_G) are opposite to that of (Ω).

Bibliography

[1] J. B. Fourier, J Theorie analytique. De La chaleur Paris, (1822) .

[2] C. Cattaneo, Sulla conduzione del calore. Atti Semin Mat Fis Univ Modena Reggio Emilia, 3(1948)83-101.

[3] C.I. Christov, On frame indifferent formulation of the Maxwell-Cattaneo model of finite-speed heat conduction. Mechanics Research Communications, 36(2009)481-486.

[4] M. Ciarletta and B. Straughan, Uniqueness and structural stability for the Cattaneo-Christov equations. Mechanics Research Communications, 37(2010)445 - 447.

[5] S.A.M. Haddad, Thermal instability in Brinkman porous media with Cattaneo-Christov heat flux. International Journal of Heat and Mass Transfer, 68(2014)659-668.

[6] T. Hayat, F. Haider, T. Muhammad and A. Alsaedi, Darcy-Forchheimer flow with Cattaneo-Christov heat flux and homogeneous-heterogeneous reactions. Plos one,12(2017)0174938.

[7] N. Acharya, K. Das and P.K. Kundua, Cattaneo-Christov intensity of magnetized upper-convected Maxwell nanofluid flow over an inclined stretching sheet: a generalized Fourier and Fick's perspective. International Journal of Mechanical Sciences, 130(2017)167-173.

[8] S. Han, L. Zheng, C. Li and X. Zhang, Coupled flow and heat transfer in viscoelastic fluid with Cattaneo-Christov heat flux model. Applied Mathematics Letters, 38(2014)87-93.

[9] M.N. Ozisik, Thermal radiation transfer and interactions with conduction and convection. Wiley, New York (1973).

[10] R.D. Cess, The interaction of thermal radiation in boundary layer heat transfer. In: Proceedings of the 3rd International Heat Transfer Conference, 5(1966)154–163.

[11] V.S. Arpaci, Effect of thermal radiation on the laminar free convection from a heated vertical plate. International Journal of Heat and Mass Transfer, 11(1968)871–881.

[12] M.W.A. Khan, M.I. Khan, T. Hayat and A. Alsaedi, Entropy generation minimization (EGM) of nanofluid flow by a thin moving needle with nonlinear thermal radiation. Physica B: Conden. Matter, 534(2018)113-119.

[13] R. Kumar, S. Sood, M. Sheikholeslami and S. A. Shehzad, Nonlinear thermal radiation and cubic autocatalysis chemical reaction effects on the flow of stretched nanofluid under rotational oscillations. Journal of Colloid and Interface Science, 505(2017)253-265.

[14] M.J. Babu and N. Sandeep, Effect of nonlinear thermal radiation on non-aligned bio-convective stagnation point flow of a magnetic-nanofluid over a stretching sheet. Alexandria Engineering Journal, 55(2016)1931-1939.

[15] T. Hayat, M.I. Khan, S. Qayyum, A. Alsaedi and M.I. Khan, New thermodynamics of entropy generation minimization with nonlinear thermal radiation and nanomaterials. Physics Letters A, 382(2018)749-760.

[16] F.A. Soomro, M. Usman, R.U. Haq and W. Wang, Melting heat transfer analysis of Sisko fluid over a moving surface with nonlinear thermal radiation via collocation method. International Journal of Heat and Mass Transfer, 126(2018) 1034-1042.

[17] S.S. Ghadikolaei, K. Hosseinzadeh, M. Hatami, D.D. Ganji and M. Armin, Investigation for squeezing flow of ethylene glycol ($C_2H_6O_2$) carbon nanotubes (CNTs) in rotating stretching channel with nonlinear thermal radiation. Journal of Molecular Liquids, 263(2018)10-21.

[18] G. Reda, A. Rahman, M.M. Khader and A.M. Megahed, Melting phenomenon in magneto hydro-dynamics steady flow and heat transfer over a moving surface in the presence of thermal radiation. Chinese Physics B, 22(2013)030202.

[19] L. Roberts, On the melting of a semi-infinite body of ice placed in a hot stream of air. Journal of Fluid Mechanics, 4 (1958)505-528.

[20] K. Das, Radiation and melting effects on MHD boundary layer flow over a moving surface. Ain Shams Engineering Journal, 5(2014)1207-1214.

[21] T. Hayat, M. Imtiaz and A. Alsaedi, Melting heat transfer in the MHD flow of Cu–water nanofluid with viscous dissipation and Joule heating. Advanced Powder Technology, 4(2016).

[22] S.U.S. Choi, Enhancing thermal conductivity of fluids with nanoparticles. ASME, FED 231/MD 66(1995)99-105.

[23] M. Usman, F.A. Soomro, R.U. Haq, W. Wang and O. Defterli, Thermal and velocity slip effects on Casson nanofluid flow over an inclined permeable stretching cylinder via collocation method. International Journal of Heat and Mass Transfer, 122(2018)1255-1263.

[24] M. Sheikholeslami, M.T. Mustafa and D.D. Ganji, Effect of Lorentz forces on forcedconvection nanofluid flow over a stretched surface. Particuology, 26(2016)108-113.

[25] B.J. Gireesha, B. Mahanthesh, G. T. Thammanna and P. B. Sampathkumar, Hall effects on dusty nanofluid two-phase transient flow past a stretching sheet using KVL model. Journal of Molecular Liquids, 256(2018)139-147.

[26] T. Hayat, A. Aziz, T. Muhammad, A. Alsaedi and M. Mustafa, On magnetohydrodynamic flow of second grade nanofluid over a convectively heated nonlinear stretching surface. Advanced Powder Technology, 27(2016)1992-2004.

[27] S.U. Khan, S.A. Shehzad, A. Rauf and N. Ali, Mixed convection flow of couple stress nanofluid over oscillatory stretching sheet with heat absorption/generation effects. Results in Physics, 8(2018)1223-1231.

[28] K.L. Hsiao, Micropolar nanofluid flow with MHD and viscous dissipation effects towards a stretching sheet with multimedia feature. International Journal of Heat and Mass Transfer, 112(2017)983-990.

[29] K.R. Rajagopal, T.Y. Na and A.S. Gupta, Flow of a viscoelastic fluid over a stretching sheet. Rheologica Acta 23(1984) 213-215.

[30] N. Riley, Magnetohydrodynamics free convection, Journal of Fluid Mechanics,18(1964)577-586.

[31] D.F. Fairbank and C.R. Wike, Diffusion and chemical reaction in an isothermal laminar flow along a soluble flat plate. Journal of Industrial and Engineering Chemistry, 42(1950)471-475.

[32] H.I. Andersson, O.R. Hansen and B. Holmedal, Diffusion of a chemically reactive species from a stretching sheet. International Journal of Heat and Mass Transfer, 37(1994)659-664.

[33] E. Magyari and B. Keller, Exact solutions for self-similar boundary-layer flows induced by permeable stretching walls. European Journal of Mechanics - B/Fluids, 19(2000)109–122.

[34] E. Magyari and B. Keller, A direct method to calculate the heat transfer coefficient of steady similar boundary layer flows induced by continuous moving surfaces. International Journal of Thermal Sciences, 44(2005)245–254.

[35] X.Y. Tian, B.W. Li and Z.M. Hu, Convective stagnation point flow of a MHD non- Newtonian nanofluid towards a stretching plate. International Journal of Heat and Mass Transfer, 127(2018)768-780.

[36] B. Mahanthesh, B.J. Gireesha, R.S.R. Gorla, F.M. Abbasi and S.A. Shehzad, Numerical solutions for magnetohydrodynamic flow of nanofluid over a bidirectional nonlinear stretching surface with prescribed surface heat flux boundary. Journal of Magnetism and Magnetic Materials, 417(2016)189–196.

[37] T. Hayat, M.I. Khan, M. Farooq, A. Alsaedi, M. Waqas and T. Yasmeen, Impact of Cattaneo-Christov heat flux model in flow of variable thermal conductivity fluid over a variable thicked surface. International Journal of Heat and Mass Transfer, 99(2016)702–710.

[38] M.I. Khan, M. Tamoor, T. Hayat and A. Alsaedi, MHD boundary layer thermal slip flow by nonlinearly stretching cylinder with suction/blowing and radiation. Results in Physics, 7(2017)1207–1211.

[39] T. Hayat, Y. Wang and K. Hutter, Hall effects on the unsteady hydromagnetic oscillatory flow of a second grade fluid. International Journal of Non-Linear Mechanics, 39(2004)1027-1037.

[40] K.R. Rajagopal, A note on unsteady unidirectional flows of a non-Newtonian fluid. International Journal of Non-Linear Mechanics, 17(1982)369-373.

[41] K.R. Rajagopal, On the creeping flow of a second grade fluid. Journal of Non-Newtonian Fluid Mechanics, 15(1984) 239-246.

[42] R. Bandelli, Unsteady unidirectional flows of a second grade fluid in domain with heated boundaries. International Journal of Non-Linear Mechanics, 38(1995)263-269

[43] C. Fetecau, A new exact solution for the flow of Maxwell fluid past an infinite plate. International Journal of Non-Linear Mechanics, 38(2003)423-427.

[44] Z. Abbas, M. Sajid and T. Hayat, MHD boundary-layer flow of an upper-convected Maxwell fluid in a porous channel. Theoretical and Computational Fluid Dynamics, 20(2006)229-238.

[45] R.L. Fosdick and K.R. Rajagopal, Thermodynamics and stability of fluids of third grade. Proceedings of the Royal Society of London Series A, 339(1980)351-377.

[46] A. Mastroberardino and U.S. Mahabaleswar, Mixed convection in viscoelastic flow due to a stretching sheet in a porous medium. Journal of Porous Media, 16(2013)483-500.

[47] S.O. Adesanya and O.D. Makinde, Thermodynamic analysis for a third grade fluid through a vertical channel with internal heat generation. Journal of Hydrodynamics, 27(2015)264-272.

[48] R. Ellahi and A. Riaz, Analytical solutions for MHD flow in a third-grade fluid with variable viscosity. Mathematical and Computer Modelling, 52(2010)1783-1793.

[49] T. Hayat, H. Nazar, M. Imtiaz, A. Alsaedi and M. Ayub, Axisymmetric squeezing flow of third grade fluid in presence of convective conditions. Chinese Journal of Physics, 55(2017)738-754.

[50] M. Sajid, M. Mughees and N. Ali, A theoretical analysis of blade coating for third-grade fluid. Journal of Plastic Film and Sheeting (2019) https://doi.org/10.1177/8756087919828417.

[51] T. Hayat, N. Naz, S. Asghar and A. Alsaedi, Soret-Dufour effects on three-dimensional flow of third grade fluid. Nuclear Engineering and Design, 243(2012)1-14.

[52] S.A. Shehzad, A. Alsaedi and T. Hayat, Three-Dimensional Flow of Jeffrey Fluid with Convective Surface Boundary Conditions. International Journal of Heat and Mass Transfer, 55(2012)3971-3976.

[53] M. Turkyilmazoglu, Extending the traditional Jeffrey-Hamel flow to stretchable convergent/divergent Channels. Computers and Fluids, 100(2014)196-203.

[54] R. Ellahi and F. Hussain, Simultaneous Effects of MHD and partial slip on peristaltic flow of Jeffrey fluid in a rectangular duct. Journal of Magnetism and Magnetic Materials, 393(2015)284-292.

[55] T. Hayat, M.I. Khan, M. Farooq, M. Waqas, A. Alseadi and T. Yasmeen, Impact of Cattaneo–Christov heat flux model in flow of variable thermal conductivity fluid over a variable thicked Surface. International Journal of Heat and Mass Transfer, 99 (2016)702-710.

[56] T. Hayat, T. Hussain, S.A. Shahzad and A. Alseadi, Thermal and concentration stratifications effects in radiative flow of Jeffrey fluid over a stretching sheet. Plos One, 10(2014)107858.

[57] P. Forchheimer, Wasserbewegung durch boden, Z Ver D Ing. 45(1901)1782-1788.

[58] M.A. Seddeek, Influence of viscous dissipation and thermophoresis on Darcy-Forchheimer mixed convection in a fluid saturated porous media. Journal of Colloid and Interface Science, 293(2006)137–142.

[59] M. Muskat, The flow of homogeneous fluids through porous media. Physics, 7(1936)346.

[60] R. Tsai and J.S. Huang, Heat and mass transfer for Soret and Dufor's effects on Hiemenz flow through porous medium onto a stretching surface. International Journal of Heat Mass Transfer, 52 (2009)2399-2406

[61] T. Hayat, F. Shah, A. Alsaedi and Z. Hussain, Outcome of homogeneous and heterogeneous reactions in Darcy-Forchheimer flow with nonlinear thermal radiation and convective condition. Results in Physics, 7(2017) 2497-2505.

[62] T. Hayat, M. Waqas, M.I. Khan, A. Alsaedi and S.A. Shehzad, Magnetohydrodynamic flow of Burgers fluid with heat source and power law heat flux. Chinese Journal of Physics, 55(2017)318-330.

[63] M.H. Ahmadi, M.A. Ahmadi, A.H. Mohammadi, M. Mehrpooya and M. Feidt, Thermodynamic optimization of Stirling heat pump based on multiple criteria. Energy Conversion and Management, 80(2014)319-328.

[64] R.S. Doohan, P.K. Kush and G. Maheshwari, Exergy based optimization and experimental evaluation of plate fin heat exchanger. Applied Thermal Engineering, 102(2016)80-90.

[65] H. Hajabdollahi, Economic optimization of shell and tube heat exchanger using nanofluid. World Academy of Science, Engineering and Technology International Journal of Mechanical and Mechatronics Engineering, 11(2017)1350-1354.

[66] T. Tharakeshwar, K. Seetharamu and B.D. Prasad, Multi-objective optimization using bat algorithm for shell and tube heat exchangers. Applied Thermal Engineering, 110(2017)1029-1038.

[67] M.B.R. Rodríguez, J.L.M. Rodríguez and C.H. De. O. Fontes, Thermo ecological optimization of shell and tube heat exchangers using NSGA II. Applied Thermal Engineering, 156(2019)91-98.

[68] M. Amidpour and A.V. Azad, Economic optimization of shell and tube heat exchanger based on constructal theory. Proceed. ASME 2010 4^{th} International Conference. Energy Sustain. ES2010 May 17-22, Phoenix, Arizona, USA.

[69] A.V. Azad and M. Amidpour, Economic optimization of shell and tube heat exchanger based on constructal theory. Energy, 36(2011)1087-1096.

[70] A. Hadidi and A. Nazari, Design and economic optimization of shell-and-tube heat exchangers using biogeography-based (BBO) algorithm. Applied Thermal Engineering, 51(2013)1263-1272.

[71] A. Ghanei, E. Assareh, M. Biglari, A. Ghanbarzadeh and A. R. Noghrehabadi, Thermal-economic multi-objective optimization of shell and tube heat exchanger using particle swarm optimization (PSO). Heat and Mass Transfer, 50(2014) 1375-1384.

[72] S.V. Dhavle, A.J. Kulkarni, A. Shastri and I. R. Kale, Design and economic optimization of shell-and-tube heat exchanger using cohort intelligence algorithm. Neural Computing and Applications, 30(2018)111-125.

[73] A. Bejan, Fundamentals of exergy analysis, entropy generation minimization and the generation of flow architecture. International Journal of Energy Research, 26(2002)545-565.

[74] A. Bejan, Models of power plants that generate minimum entropy while operating at maximum power. American Journal of Physics, 64(1996)1054-1059.

[75] P. Salamon, K.H. Hoffmann, S. Schubert, R.S. Berry and B. Andresen, What conditions make minimum entropy production equivalent to maximum power production. Journal of Non-Equilibrium Thermodynamics, 26(2001)73-83.

[76] Y. Haseli, Optimization of regenerative Brayton cycle by maximization of a newly defined second law efficiency. Energy Conversion and Management, 68(2013)133-140.

[77] Y. Haseli, Efficiency of irreversible Brayton cycles at minimum entropy generation. Applied Mathematical Modelling, 40(2016)8366-8376.

[78] M. Torabi, Z. Zhang and G. Peterson, Interface entropy generation in micro porous channels with velocity slip and temperature jump. Applied Thermal Engineering, 111(2017)684-693.

[79] D. Das and T. Basak, Role of distributed/discrete solar heaters for the entropy generation studies in the square and triangular cavities during natural convection, Applied Thermal Engineering, 113(2017)1514-1535.

[80] M.A. Abdous, H. Saffari, H.B. Avval and M. Khoshzat, Investigation of entropy generation in a helically coiled tube in flow boiling condition under a constant heat flux. International Journal of Refrigeration, 60(2015)217-233.

[81] M.M. Rashidi, N.Vi. Ganesh, A.K.A. Hakeem, B. Ganga and G. Lorenzini, Influences of an effective Prandtl number model on nano boundary layer flow of $\gamma Al_2O_3 - H_2O$ and $\gamma Al_2O_3 - C_2H_6O_2$ over a vertical stretching sheet, International Journal of Heat and Mass Transfer, 98 (2016) 616-623.

[82] S. Lee, S.U.S.Choi, S. Li, and J.A. Eastman, Measuring thermal conductivity of fluids containing oxide nanoparticles. Journal of Heat transfer, 121(1999)280-289.

[83] X. Wang, X. Xu and S. U. S. Choi, Thermal conductivity of nanoparticles-fluid mixture. Journal of Thermophysics and Heat Transfer, 13(1999)474-480.

[84] R.L. Hamilton and O.K. Crosser, Thermal conductivity of heterogeneous two component systems. Industrial & Engineering Chemistry Fundamentals, 1(1962)187-191.

[85] S.E.B. Maiga, C.T. Nguyen, N. Galanis and G. Roy, Heat transfer behaviors of nanofluids in a uniformly heated tube. Superlattices and Microstructures, 35(2004)543-557.

[86] C.V. Pop, S. Fohanno, G. Polidori and C.T. Nguyen, Analysis of laminar-to-turbulent threshold with water$-\gamma Al_2O_3$ and ethylene glycol$-\gamma Al_2O_3$ nanofluids in free convection. In Proceedings of the 5th IASME/WSEAS International Conference on Heat Transfer, Thermal Engineering and Environment, Athens, Greece, 188, 25 - 27(2017).

[87] A. Ishak, R. Nazar and I. Pop, Boundary layer flow and heat transfer over an unsteady stretching vertical surface. Meccanica 44(2009)369–375.

[88] M.M. Rashidi and M.A. Abbas, Effect of slip conditions and entropy generation analysis with an effective Prandtl number model on a nanofluid flow through a stretching sheet, Entropy 19(2017)2–15.

[89] T. Hayat, T. Muhammal, S.Al Mezal and S.J. Liao, Darcy-Forchheimer flow with variable thermal conductivity and Cattaneo-Christov heat flux. International Journal of Numerical Methods for Heat & Fluid Flow, 26(2016)2355–2369.

[90] M.I. Khan, F. Shah, M. Waqas, T. Hayat and A. Alsaedi, The role of $\gamma Al_2O_3 - H_2O$ and $\gamma Al_2O_3 - C_2H_6O_2$ nanomaterials in Darcy-Forchheimer stagnation point flow: an analysis using entropy optimization. International Journal of Thermal Sciences, 140(2019)20-27.

[91] A. Jamaludin, R. Nazer and I. Pop, Three-dimensional magnetohydrodynamic mixed convection flow of nanofluids over a nonlinearly permeable stretching/shrinking sheet with velocity and thermal slip. Applied Sciences, 8(2018)1128.

[92] S. Liao, Notes on the homotopy analysis method: Some definitions and theorems. Communications in Nonlinear Science and Numerical Simulation, 14(2009)983-997.

Turnitin Originality Report

Analysis of Mathematical Models with Different Aspects of Heat Transfer by Faisal Shah .

turnitin

From DRSM (DRSM L)

- Processed on 31-May-2021 08:38 PKT
- ID: 1597509080
- Word Count: 27872

Focal Person (Turnitin)
Quaid-i-Azam University
Islamabad

Similarity Index
15%
Similarity by Source
Internet Sources:
11%
Publications:
9%
Student Papers:
6%

02 June 2021

sources:

1 1% match (Internet from 15-Apr-2015)
http://www.mdpi.com/1099-4300/15/6/2081/pdf

2 1% match (Internet from 26-Nov-2020)
https://researchportal.port.ac.uk/ws/files/10951028/1_s2.0_S0167732218321615_main_1_.pdf

3 < 1% match (student papers from 24-Jun-2019)
Submitted to Higher Education Commission Pakistan on 2019-06-24

4 < 1% match (student papers from 18-Feb-2019)
Submitted to Higher Education Commission Pakistan on 2019-02-18

5 < 1% match (student papers from 17-Jan-2014)
Submitted to Higher Education Commission Pakistan on 2014-01-17

6 < 1% match (student papers from 26-Aug-2011)
Submitted to Higher Education Commission Pakistan on 2011-08-26

7 < 1% match (student papers from 13-Feb-2011)
Submitted to Higher Education Commission Pakistan on 2011-02-13

8 < 1% match (student papers from 19-Oct-2019)
Submitted to Higher Education Commission Pakistan on 2019-10-19

9 < 1% match (student papers from 22-Nov-2012)
Submitted to Higher Education Commission Pakistan on 2012-11-22

10 < 1% match (student papers from 08-Feb-2013)
Submitted to Higher Education Commission Pakistan on 2013-02-08

11 < 1% match (student papers from 27-Sep-2015)
Submitted to Higher Education Commission Pakistan on 2015-09-27

12 < 1% match (student papers from 11-Feb-2013)
Submitted to Higher Education Commission Pakistan on 2013-02-11

13 < 1% match (student papers from 10-Jun-2013)
Submitted to Higher Education Commission Pakistan on 2013-06-10